UNIVERSITY OF CALIFORNIA SAN DIEGO

Lagrangian analyses of ichthyoplankton: insights into transport processes in the Southern California Bight

A Dissertation submitted in partial satisfaction of the requirements
for the degree Doctor of Philosophy

in

Oceanography

by

Lucinda Anna Quigley

Committee in charge:

Peter Franks, Chair
Sarah Giddings
James Nieh
Colleen Petrik
Andrew Thompson

2025

The Dissertation of Lucinda Anna Quigley is approved, and it is acceptable in quality and form for publication on microfilm and electronically.

University of California San Diego

2025

DEDICATION

This dissertation is dedicated to Dr. Joel Llopiz,
who introduced me to the world of oceanography.

TABLE OF CONTENTS

LIST OF FIGURES

LIST OF TABLES

ACKNOWLEDGEMENTS

Firstly, thank you to my advisor, Peter Franks, for your mentorship and support. I am incredibly grateful that I snuck in as your last graduating PhD student, following in the footsteps of so many other accomplished scientists that all had the great privilege of having you as their advisor. It is difficult to fully express the impact that you had on my time at Scripps, though I can say with confidence that your unwavering support, critical thinking, and compassion has made me the scientist and person I am today. I hope to one day have as much of an impact on others as you have had on me.

Thank you to my committee and all my coauthors who provided helpful feedback on my chapters and broadened by perspective. This dissertation was improved by every one of your suggestions. I must extend a big thank you to Andrew Thompson. Your enthusiasm and genuine care for my success is evident, and I am fortunate to have you as a mentor.

To my BO cohort and friends Ella and Dante, I am grateful to have shared this journey with you. Throughout my PhD, you have both grounded me and provided me with encouragement. To all my other Scripps friends, colleagues, and professors, thank you for supporting me and teaching me - I have learned so much through my time at Scripps, in ways that extend beyond just becoming a scientist.

Thank you to Anela and the Choy Lab for introducing me to the world of sea-going oceanography. Your work ethic and dedication to research is admirable, and I will always be appreciative of the support you gave me.

Lastly, thank you to my family, especially my parents, for always encouraging me to follow my dreams, no matter how wild they may sound. All of my accomplishments are as much mine as they are yours.

Chapter 1, in part is currently being prepared for submission for publication of the material. The dissertation author was the primary investigator and author of this material.

Chapter 2, in full, is a reprint of the material as it appears in: Quigley L. A., Franks, P. J. S., Thompson, A. R., Field, J. C., Santora J. A. (2024). Quantifying the fates and retention of larval rockfish through Lagrangian analyses. Marine Ecology Progress Series. The dissertation author was the primary investigator and author of this paper.

Chapter 3, in full, has been submitted for publication of the material as it may appear in: Quigley L. A., Franks, P. J. S., Thompson, A. R., Ben-Aderet, N., Fennie, H. W., Morales, M. M., Santora J. A., Bjorkstedt, E. P. (2025). Larval transport pathways reveal critical habitat and benefits of a marine protected area to fisheries. Fisheries Oceanography. The dissertation author was the primary investigator and author of this paper.

VITA

2020	Bachelor of Science in Environmental Science, Brown University
2022	Master of Science in Marine Biology, University of California San Diego
2025	Doctor of Philosophy in Oceanography, University of California San Diego

ABSTRACT OF THE DISSERTATION

Lagrangian analyses of ichthyoplankton:
insights into transport processes in the Southern California Bight

by

Lucinda Anna Quigley

Doctor of Philosophy in Oceanography

University of California San Diego, 2025

Professor Peter Franks, Chair

Physical dynamics in the ocean play critical roles in the early life stages of fish. Larvae and eggs of many species behave as passive drifters in the upper water column, making dispersal to or from favorable habitats an important process in their survival to the juvenile stage. Traditional fisheries oceanography is often focused on the Eulerian perspective – comparing ichthyoplankton abundances with environmental and oceanographic indexes where the fish were sampled to understand what conditions drive survival, and ultimately, lead to recruitment to the

adult population. This perspective is useful for fisheries management and predicting how changing ocean conditions may affect commercially important fish. However, the Eulerian perspective is a "snapshot" view in space and time and lacks information regarding ichthyoplankton transport pathways and the associated oceanographic conditions experienced by the individual along their drifting trajectories. Here, I leverage Lagrangian methods to investigate ichthyoplankton dispersal patterns in the Southern California Bight.

In Chapter 1, I used high-resolution glider-measured velocities to assess the utility of satellite-derived geostrophic currents for understanding upper ocean transport processes. I found that satellite-derived geostrophic velocities perform well at resolving ocean circulation patterns in the upper 200 m of the California Current. In Chapter 2, I leveraged a 25-year record of satellite-derived geostrophic velocities to assess transport and retention of virtual particles representing rockfish. Spatial patterns of advection revealed high retention regions in the Southern California Bight. Interannual variability in retention was correlated with the abundance of pelagic juvenile rockfish collected months later, underscoring the importance of physical processes in the early life stages of rockfish. Lastly, in Chapter 3, I built on the previous two chapters by combining measured satellite-derived velocities with *in situ* collections of larval rockfish and associated otolith measurements to predict regions of spawning and dispersal. Backward-in-time particle tracking revealed that high quality rockfish were born offshore of Point Conception, while forward-in-time particle trajectories highlighted the role of the Cowcod Conservation Areas in sourcing larvae to nearby regions accessible to fishing. Overall, this dissertation demonstrates the utility of satellite-derived geostrophic velocities for understanding transport processes and emphasizes the importance of mesoscale circulation patterns on the early life stages of fish.

INTRODUCTION

The California Current System (CCS) is an eastern boundary upwelling system, characterized by dynamic physical oceanographic conditions and biological productivity (Checkley and Barth 2009). The surface-intensified California Current flows equatorward approximately 300-400 km offshore, bringing, fresh, cool water southward (Lynn and Simpson 1987). Near the coast (typically within 150 km), the California Undercurrent is centered between 0-200 m deep, and flows poleward, transporting higher salinity, warm water northward (Hickey 1979, Lynn and Simpson 1987, Rudnick et al. 2017a, Zaba et al. 2021). Coastal wind-driven upwelling brings deep, cold, saline, nutrient-rich waters to the surface, enhancing primary production. At Point Conception, the California Current bifurcates and forms the Southern California Eddy, a semi-persistent cyclonic eddy in the Southern California Bight (SCB; Lynn and Simpson 1987, Owen 1980).

The SCB is a region within the CCS, bounded by a curved coastline that extends from south of San Diego, CA to Point Conception. In the SCB, upwelling is weaker than the northern region of the CCS and varies seasonally, with the most intense upwelling occurring in the spring and lasting through the fall (Lynn and Simpson 1987, Checkley and Barth 2009). The bathymetry in the SCB, including the Channel Islands, along with submarine canyons and basins, contributes to complex circulation patterns and the formation of mesoscale features such as eddies and fronts (Caldeira et al. 2005, Dong et al. 2009).

The high productivity of the SCB supports economically and ecologically important fisheries. Since 1950, the California Cooperative Oceanic Fisheries Investigations (CalCOFI) program has been conducting fisheries-related oceanographic research in the CCS. The initial motivation for the CalCOFI program was to understand the cause of sharp declines in the Pacific

sardine fishery that occurred in the 1930s and 1940s (McClatchie 2014). Since its inception, CalCOFI has expanded to focus on long-term hydrographic and biological sampling of the CCS. This consistent, long-term sampling effort has proved essential for understanding drivers of fish recruitment in the SCB.

Quantifying the roles that ocean circulation processes play in the early life stages of fish is essential for fisheries management. Fish eggs and larvae have weak swimming abilities and therefore are highly susceptible to transport by ocean currents. Advection to or from favorable habitats may modulate their survival, and ultimate recruitment, to the adult population. Successful recruitment is driven by larval survival – the larval stage is associated with the highest mortality rate (Hjort 1914, Houde 2008, Hare 2014). The CCS is associated with strong offshore transport, driven largely by westward propagating eddies that pinch off filaments, which entrain trap larvae and advect them offshore to unfavorable habitats (Fiedler 1986, Chenillat et al. 2015, Nagai et al. 2015, Amos et al. 2019, Chabert et al. 2021). Conversely, mesoscale features can also retain larvae and may facilitate survival through local upwelling and increased productivity (Bjorkstedt et al. 2002, Bakun 2006, McGillicuddy 2016). Understanding and predicting fish recruitment is dependent on resolving spatiotemporal variability in ocean circulation patterns and the associated impacts on ichthyoplankton dispersal and survival.

Fisheries research typically focuses on the Eulerian perspective – correlating discrete environmental and oceanographic properties with measures of fish biomass and abundance (Bakun 2006). Through long-term sampling such as the CalCOFI program, these analyses can provide critical insights into ecological patterns. However, the Eulerian approach is a "snapshot" view, and it is limited by the static nature of sampling. Conversely, Lagrangian analyses take a dynamic approach by following trajectories of particles through space and time. This perspective

enhances our ability to identify physical-biological interactions that underlie the Eulerian observations.

Advances in satellite altimetry have made global measurements of ocean currents and mesoscale physical dynamics widely available. Combining measurements of ocean circulation with ichthyoplankton distributions can provide insights into the critical roles that physical forcings play in the early life stages of fish. This dissertation leverages satellite-derived geostrophic velocities to address foundational questions regarding the physical-biological interactions driving ichthyoplankton abundances, distributions, and survival. The SCB is an ideal region for these analyses, given its complex circulation patterns and productive fisheries, along with long-term sampling efforts that provide robust data. Focusing on physical processes from a Lagrangian perspective enables us to understand not just correlations of fish distributions with their environment, but also the underlying mechanisms and dynamics responsible.

Chapter 1 : Assessing the depths that satellite-derived ocean currents represent using high resolution glider data

1.1 Introduction

Satellite-derived ocean currents are used widely in oceanographic research due to their spatial and temporal coverage. Geostrophic velocities derived from satellite altimetry are used for a range of applications, including search and rescue, oil spill remediation, and tracking the transport of water masses and particles such as plastics and plankton. Lagrangian particle tracking using satellite-derived currents, forward and backward-in-time, has been shown to be effective at revealing the transport and distributions of biological particles such as phytoplankton and larvae, leading to a better understanding of dispersal (forward-in-time) and origins (backward-in-time) (d'Ovidio et al. 2010, Gangrade and Franks 2023, Quigley et al. 2024, Strub et al. 2024). Satellite-derived geostrophic velocities have also been used to show the importance of currents in the movement of larger marine animals (Luschi et al. 2003, Gasper et al. 2006). Walker et al. (2011) used satellite-derived velocities to track surface oil released from the 2010 Deepwater Horizon Gulf of Mexico oil spill. Satellite-derived geostrophic velocities were used by Castelao et al. (2023) and Furey et al. (2023) to investigate freshwater pathways. Similarly, Onink et al. (2019) used satellite-derived geostrophic + Ekman currents to assess microplastic accumulation.

In spite of the frequent use of satellite-derived horizontal velocities, there is an unresolved underlying issue with the data: what do the remotely sensed velocities actually represent? They are often referred to as "surface geostrophic velocities" (e.g., Wunsch and Gaposchkin 1980, Mork and Skagseth 2010, Kosempa and Chambers 2014), but what is the "surface"? How deep in the ocean do we find flows that are the same speed and direction as the satellite-derived geostrophic velocities? In an analysis of how ocean velocities influence

leatherback turtle movement, Gaspar et al. (2006) used satellite-derived geostrophic velocities to represent surface currents, assuming the surface currents were relatively similar to currents experienced by leatherback turtles that spend most of their time in the upper 50 m of the water column. Conversely, Della Penna et al. (2015) assessed satellite-derived geostrophic velocities in relation to elephant seal diving behavior, and interpreted these velocities as being well representative of the entire water column in the Southern Ocean, where the mixed layer is deep. From these examples, it is evident that there are varying assumptions about the depths that satellite-derived geostrophic velocities represent.

Geostrophic flows result from the balance of the pressure gradient force and the Coriolis force. The geostrophic balance is achieved over time scales greater than the inertial period (~days) and horizontal scales of 10-100s of km (the mesoscale). Horizontal velocities (*u,v*) are derived from the equations:

$$v = \frac{1}{f\rho}\frac{\partial p}{\partial x} \tag{1.1}$$

$$u = -\frac{1}{f\rho}\frac{\partial p}{\partial y} \tag{1.2}$$

Where f is the Coriolis parameter, ρ is density, and p is pressure, given by:

$$p = \int_{-z}^{\eta} g\,\rho(z)dz \tag{1.3}$$

Here z is depth, and η is the sea surface height (SSH) - the height of the sea surface above the geoid where z=0. Substituting Equation 1.3 into Equations 1.1 and 1.2, and separating the pressure integral into the ranges [-z, 0] and [0, η] we find:

$$v = \frac{1}{f\rho}\frac{\partial}{\partial x}\int_{-z}^{0}\rho\,(z)dz + \frac{g}{f}\frac{\partial \eta}{\partial x} \tag{1.4}$$

$$u = -\frac{1}{f\rho}\frac{\partial}{\partial y}\int_{-z}^{0}\rho\,(z)dz - \frac{g}{f}\frac{\partial \eta}{\partial y} \tag{1.5}$$

The first terms in Equations 1.4 and 1.5 can be thought of as the relative geostrophic velocities, while the second terms are often called the "surface velocities" (e.g., Wunsch and Gaposchkin 1980, Mork and Skagseth 2010). The relative velocities are depth-dependent and driven by subsurface horizontal density gradients. The surface velocities are depth-independent, driven by variations in SSH. The combination of the relative and surface velocities is the absolute geostrophic velocity.

Altimetry-derived geostrophic currents typically use the second term of Equations 1.4 and 1.5 to calculate geostrophic velocities through measurements of SSH. As such, it is common to refer to satellite-derived geostrophic velocities as "surface velocities." However, SSH is influenced by subsurface density gradients; geostrophic currents derived from SSH also reflect the contributions of density gradients within the water column below the surface (Wunsch 1997, Morrow et al. 2017). Desbruyères et al. (2021) showed that altimetry-derived SSH anomalies in the North Atlantic tracked decadal temperature anomalies down to 2000 m, illustrating the potential contribution of deep, subsurface dynamics to SSH. At scales < 30 days, SSH and bottom pressure show strong coherence, consistent with a barotropic response of SSH to atmospheric forcing (Vinogradova et al. 2007). Raj et al. (2018) found high correlations between monthly anomalies of satellite-derived geostrophic currents and current-meter observations at 100 m depth, further illustrating the connections between SSH-derived geostrophic currents and subsurface velocities. Additionally, surface currents are likely to be strongly affected by wind stress and other ageostrophic components that may not be well captured by satellite-derived geostrophic velocities. The total velocity at the surface is a sum of the geostrophic and ageostrophic components, including currents driven by wind, friction, and tides (Wunsch and Gaposchkin 1980).

Given the potential of SSH altimetry to reflect subsurface dynamics, and the inability of most remote platforms to measure surface-intensified ageostrophic flows, it is important to understand what depths the satellite-derived geostrophic currents best represent. The lack of consistent terminology (i.e., "surface currents", "near-surface currents") can make it difficult for researchers to understand what part of the water column their remotely sensed velocity products reproduce, and thus, what applications to are most appropriate for their use. Previous work has compared satellite-derived geostrophic velocities to modeled velocities, high frequency radar, as well as drifter and glider trajectories (e.g. Strub et al. 1997, Morrow et al. 2017, Hart-Davis et al. 2018, Dagested and Röhrs 2019, Borrione et al. 2019, Barcello-Llull et al. 2023, Furey et al. 2023). Strub et al. (1997) found correlations between satellite-derived geostrophic velocities and *in situ* measurements of velocities at depths of 48-100 m in the CCS. Dagested and Röhrs (2019) found that the satellite-derived geostrophic currents performed well compared to ocean models at predicting drifter trajectories at the surface and 1 m deep. Altimetry data validation has also been performed by calculating geostrophic velocities from glider measurements of temperature and salinity, and comparing them to co-located altimetry measurements (e.g. Morrow et al. 2017, Borrione et al. 2019).

Here, we quantify how satellite-derived geostrophic currents relate to subsurface horizontal velocities by comparing them to velocities derived from a large database generated by *in situ* gliders. Using a multi-year dataset of Spray glider observations in the California Current System (CCS) from the California Underwater Glider Network (CUGN), we compare three satellite-derived geostrophic velocity products to glider-measured, depth-dependent velocities from the surface to 500 m. Our objective is to identify the depths that satellite-derived geostrophic currents most accurately represent, and examine how this relationship changes

vertically through the water column, and spatially within the CCS. Our work provides insights into the measurement of currents by satellite altimetry and provides a more complete understanding of the ocean properties that these products estimate. Understanding the depths that satellite-derived geostrophic currents represent is essential for studies across a wide range of disciplines that commonly use these products to assess upper ocean circulation dynamics.

1.2 Materials and Methods

Study region

Data for the analyses performed in this study came from the CCS. The CCS is an eastern boundary upwelling system, associated with high biological productivity. The surface-intensified California Current flows south offshore of the coast, bifurcating at Point Conception, where part of it continues south and the other part forms the cyclonic Southern California Eddy in the Southern California Bight (Hickey 1979, Owen 1980, Checkley and Barth, 2009; Figure 1.1). The California Undercurrent is a subsurface current that flows north along the coast, with a center around 50-150 m deep (Rudnick et al. 2017a). Surface, wind-driven Ekman transport is significant in the CCS, influenced by strong equatorward winds and intensified by promontories such as Point Conception (Chereskin 1995, Pickett and Paduan 2003).

Horizontal velocities were obtained from Spray gilders, part of the CUGN (Rudnick 2016). The CUGN has been operating sustained glider measurements of the CCS since 2005. Gliders transit four of the California Cooperative Oceanic Fisheries Investigation (CalCOFI) cross-shore lines (Figure 1.1). In the south, Line 90 extends westward from Dana Point, California. Moving northward, Line 80 begins at Point Conception, Line 66 at Monterey Bay, and Line 56 at Bodega Bay (Figure 1.1).

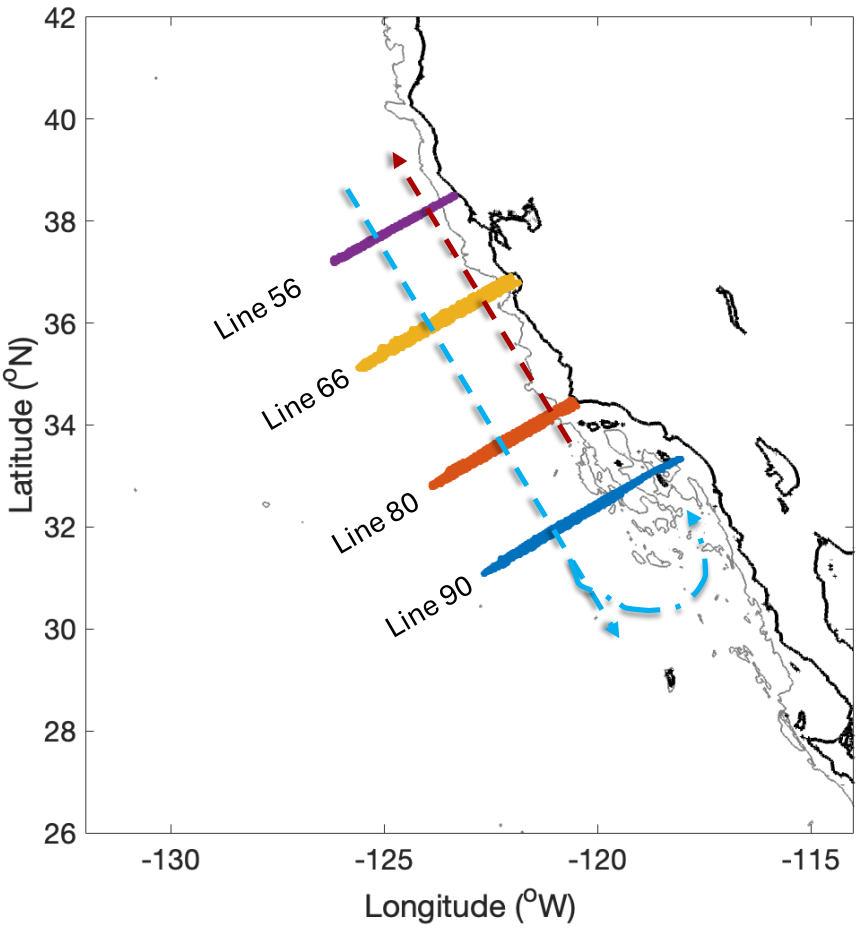

Figure 1.1: Study region off California showing locations of CUGN glider measurements, along Lines 90, 80, 66, and 56. The 1000 m isobath is shown in light gray. The California Current is illustrated by the blue dashed arrow, with the Southern California Eddy shown in with the blue dot-dash arrow. The California Undercurrent is depicted by the red dashed arrow.

Glider velocities

Spray gliders are autonomous underwater vehicles that move obliquely through the water column by changing their buoyancy (Sherman et al. 2001). The gliders perform dives from the surface to 500 m and back repeatedly along a transect. Spray moves vertically at approximately 0.1 m s^{-1} and horizontally at 0.24 m s^{-1}, at a pitch of 17° (Todd et al. 2017). Spray gliders are equipped with sensors to measure temperature, salinity, pressure, acoustic backscatter, fluorescence, and velocity.

Beginning in 2015, the 750-kHz Sontek acoustic doppler current profilers (ADCPs) that had previously been flown on the Spray gliders were replaced with 1-MHz Nortek instruments to measure velocities (Todd et al. 2017). The Nortek is a broadband instrument with four transducers mounted at the rear of the glider, facing downward when the glider is directed upward at a 17.4° angle (Todd et al. 2017). For consistency of velocity measurements, we use data from only gliders equipped with the Nortek ADCP. Horizontal velocities are obtained by referencing the vertical shear measured by the ADCP to the vertically averaged velocity of the glider during the dive. The vertically averaged velocity is calculated as a dead-reckoning, by comparing the displacement of the glider predicted by a model based on the glider's pressure, pitch and heading, to the actual displacement measured by a GPS (Rudnick and Cole 2011). Vertical shear is measured during the ascent of the glider dive. Horizontal velocities are calculated in 10 m bins from the surface to 500 m. We used only the glider data from the cross-shore CalCOFI lines; we removed glider missions that went outside of the core region encompassing the transect lines. This resulted in a total of 64,311 glider observations at 50 depth bins: 8,083 on Line 56.7, 17,663 on Line 66.7, 17,913 on Line 80, and 20,652 on Line 90.

Satellite-derived geostrophic velocities

Satellite-derived geostrophic velocities were obtained from the Copernicus Marine Environment Monitoring Service. We used three Level 4 gridded velocity products: geostrophic, geostrophic + Ekman surface, and geostrophic + Ekman 15 m (https://doi.org/10.48670/moi-00148; https://doi.org/10.48670/mds-00327). The Level 4 products merge along-track measurements from several altimeter missions. The geostrophic velocities are interpolated to daily intervals with a 0.125° spatial resolution. The geostrophic + Ekman surface and Ekman 15

m are daily geostrophic velocities with a tidal component, and an Ekman component at 0 m or 15 m. Ekman currents are wind-driven; the Coriolis effect causes surface currents to be deflected 45° to the right of the wind vector in the Northern Hemisphere. Vertical shear of the surface current with depth creates an Ekman spiral, whereby the depth-integrated velocity over the spiral is 90° to the right of the wind direction. Ekman currents are modeled using European Centre for Medium-Range Weather Forecasts ERA5 wind stress (Rio et al. 2014). These data are available at a 0.25° resolution.

Velocity comparisons

We matched the spatial and temporal locations of each glider observation to satellite-derived geostrophic velocities, by selecting satellite-derived geostrophic horizontal velocities (u, v) at the nearest date, latitude, and longitude of the gilder data. We analyzed glider data from each of the four CalCOFI lines separately. At each of the 64,311 glider times and locations, we compared the satellite-derived horizontal (u,v) geostrophic velocities to the glider (u,v) velocities at each of the 50 depth bins from the surface to 500 m, and for each of the three different satellite products. We also calculated a vertical average of CUGN glider velocities in slabs extending from the surface to a specified depth. We then compared these depth-averaged slab CUGN velocities to the local satellite-derived geostrophic velocities to assess how deep below the surface the water column was most strongly correlated with the satellite-derived geostrophic velocities.

To quantify the relationships between satellite-derived geostrophic velocities and glider velocities, we used both the Pearson correlation coefficient and the Concordance Correlation Coefficient (CCC). The Pearson correlation coefficient measures the linear correlation between

two variables regardless of whether they lie on a 1:1 line, while the CCC is a measure of how close the two variables are to a 1:1 line. In other words, the CCC is effective at assessing how well individual observations of the same quantity align with each other (Lin 1989). To assess cross-shore differences in correlation, we calculated the CCC in longitude bins defined by the spatial resolution of the satellite data.

We used the CUGN climatology product to quantify subsurface temperature and density distributions (Rudnick et al. 2017a,b). The CUGN climatology provides mean variables calculated from glider transects over the entire time period (2005-present; Rudnick et al. 2017a,b). These data are available for Lines 66, 80, and 90. From the climatology data, we calculated horizontal and vertical density gradients of potential density along each of the three CalCOFI lines. We then compared depths of maximum horizontal and vertical density gradients to the depths of the maximum CCC value within each longitude bin.

1.3 Results

Geostrophic velocities

Pearson correlation coefficients and CCC between satellite-derived geostrophic velocities and CUGN velocities both revealed subsurface maxima (Figure 1.2). Correlations peaked between 50-200 m depth, then decreased with increasing depth, with the exception of Line 56, which showed a second subsurface peak around 300 m, most apparent in the u (cross-shore) velocities. Pearson correlation coefficients ranged from 0.26 (at 500 m on Line 90) to 0.67 (at 70 m on Line 80), and all p-values were <0.001. Concordance correlation coefficients ranged from 0.25 (at 500 m on Line 90) to 0.66 (at 80 m on Line 80). Line 80 had the highest peak correlation coefficients.

Maximum CCC values ranged from 0.54 to 0.66 across all lines. The average depth of the maximum CCC for *u* and *v* combined occurred at 97.5 m; at 65 m for *v*, and at 130 m for *u*. Pairwise comparisons of the geostrophic velocities and the CUGN velocities at different depths can be found in the Supplemental Material (Supplemental Figures 1.1-1.3).

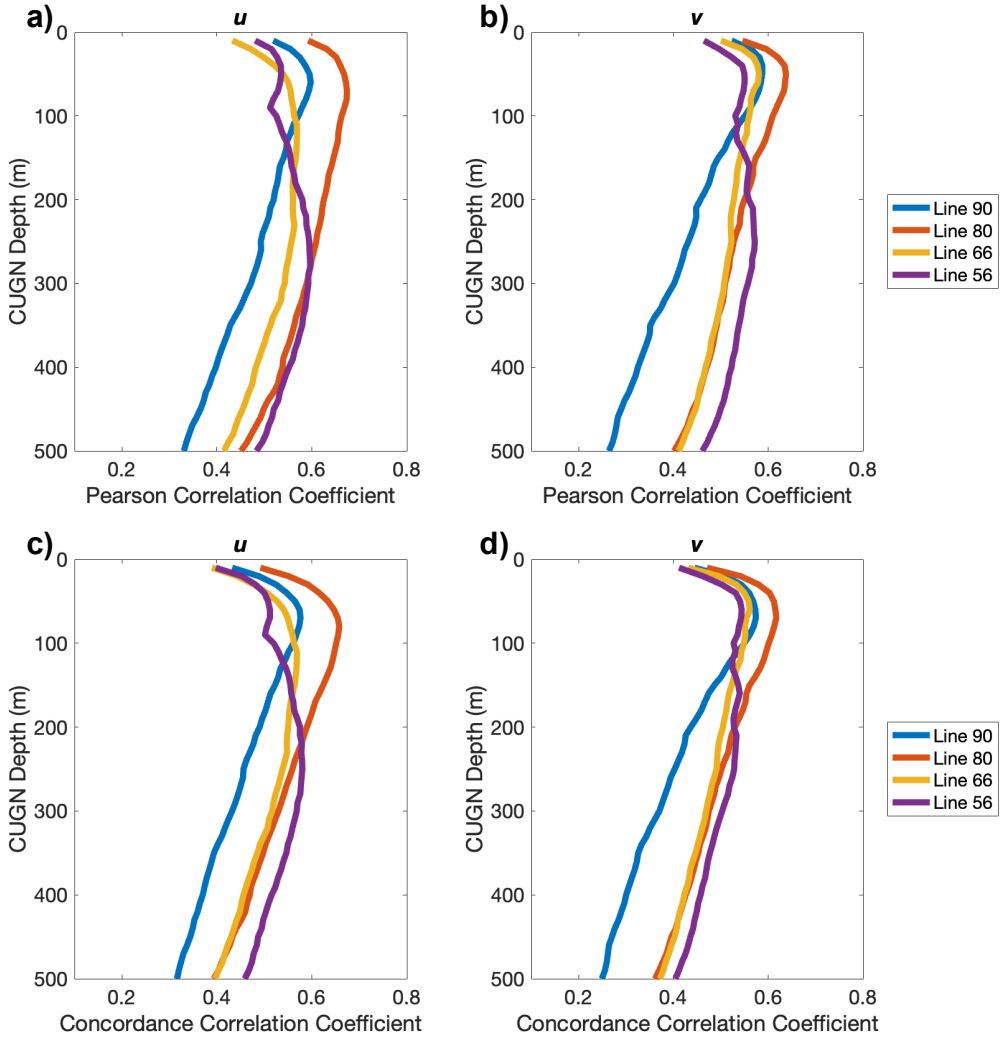

Figure 1.2: Pearson correlation coefficient (a, b) and concordance correlation coefficients (c, d) between satellite-derived geostrophic velocities (*u, v*) and CUGN velocities (*u, v*) from the surface to 500 m.

Integrated depth profiles of CUGN velocities also revealed subsurface maxima of correlations with satellite velocities (Figure 1.3). Velocities averaged from the surface to 170 m

had the highest CCC on average across all the lines. The maximum CCC for *v* occurred when comparing CUGN velocities averaged from 0-140 m for Line 90, 0-150 m for Line 80, 0-120 m for Line 66, and 0-140 m for Line 56. For *u*, the maximum CCC was obtained for the average of 0-190 m for Line 90, 0-200 m for Line 80, 0-170 m for Line 66, and 0-270 m for Line 56. Line 80 had the highest CCC of integrated velocities, followed by Line 90, Line 66, and Line 56.

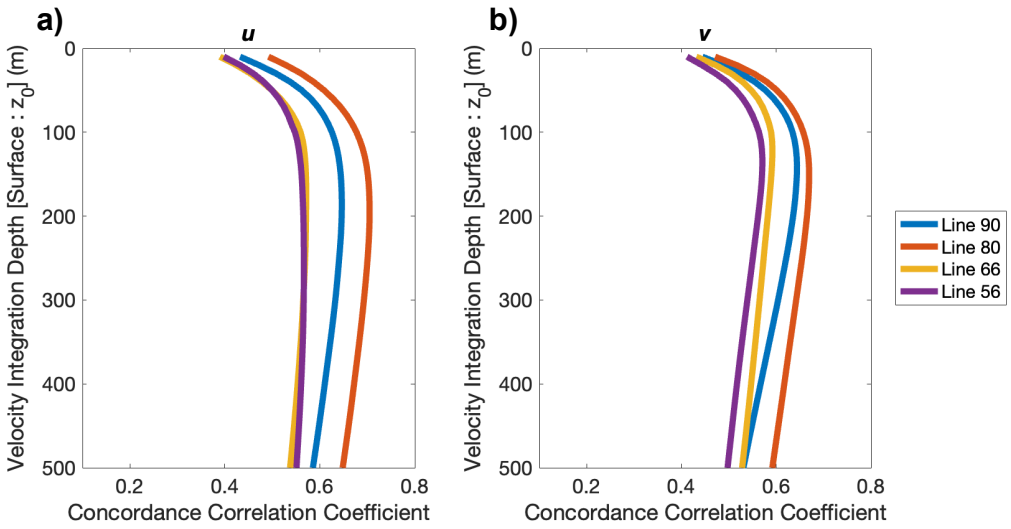

Figure 1.3: Concordance correlation coefficients of the integrated depth profiles for *u* (a) and *v* (b). The x-axis is the concordance correlation coefficient associated with the averaged glider velocities integrated over the surface to the defined depth. Glider velocities were averaged from the surface to the y-axis depth.

Longitudinal transects reveal spatial patterns of correlations between CUGN velocities and satellite-derived geostrophic velocities. Across all lines, the highest CCC values were found offshore (Figure 1.4). A strong cross-shore pattern is seen on Line 90, where nearshore correlations are relatively low, and increase moving west of -120° (Figure 1.4g and 1.4h). Strong subsurface correlations are also evident in the offshore regions.

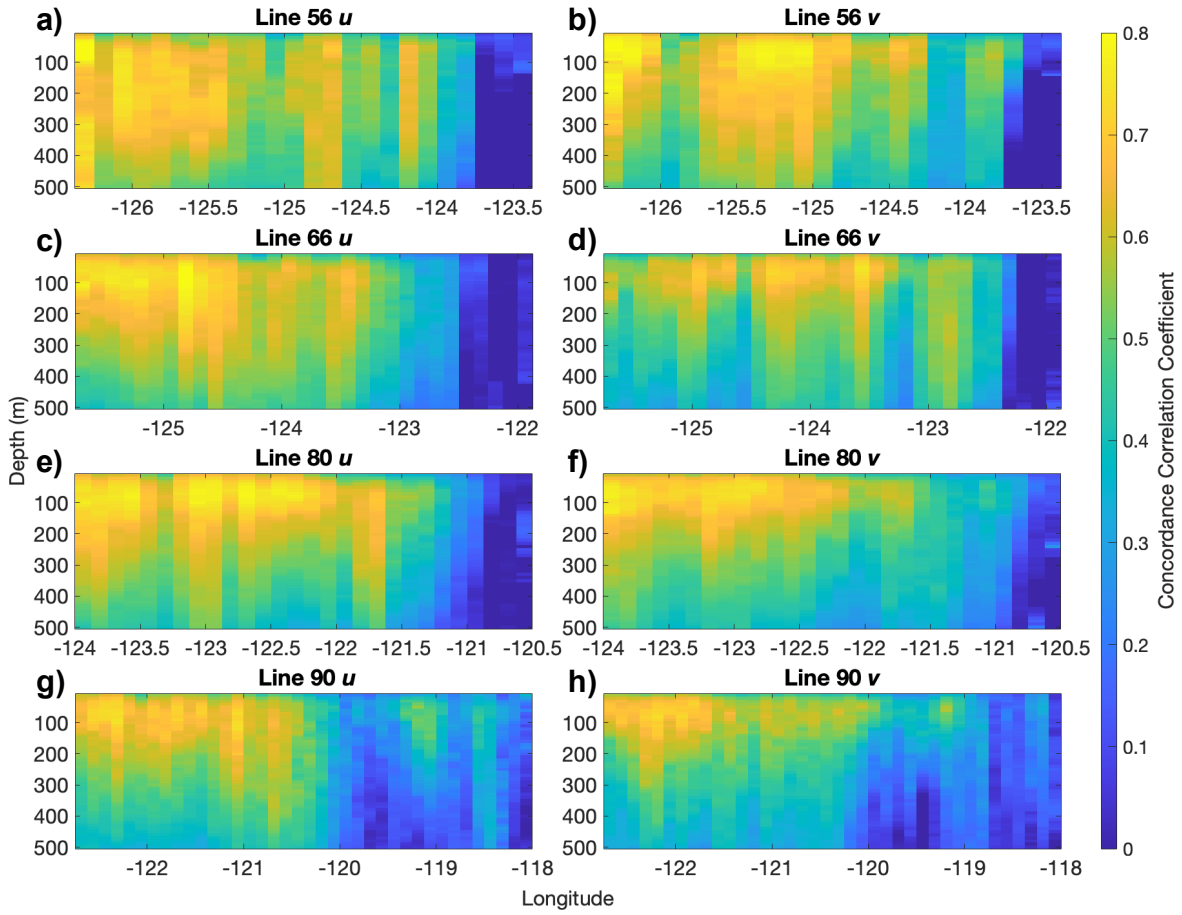

Figure 1.4: Concordance correlation coefficient by depth and longitude. Concordance correlation coefficients at each depth were binned into 0.125° longitudinal bins and averaged. Note the different x-axis scales.

Cross-shore sections of potential density and temperature reveal subsurface patterns along Lines 90, 80, and 66. The mean temperature profiles closely resemble the potential density profiles (Figure 1.5a and 1.5b). Across all of the CalCOFI lines, the isopycnals and isotherms in the upper 200 m deepen offshore. The maximum vertical gradient of potential density reveals the depth of the pycnocline centered around approximately 100 m offshore, and the pycnocline shoals toward the coast (Figure 1.5c), consistent with a southward mean geostrophic flow. The depth of the maximum vertical density gradient is similar to the depth of the maximum horizontal density gradient (Figure 1.5c and 1.5d). Horizontal density gradients drive the

subsurface relative velocity component of geostrophic velocities (Equation 1.4 and 1.5). Horizontal gradients of the mean potential density also reveal the shoaling of the pycnocline near the coast, with the highest absolute value of the gradient also centered around 100 m across each transect (Figure 1.5d). The depths that produced the maximum CCC values align closely with the depths of the maximum horizontal and vertical potential density gradients (Figure 1.5c and 1.5d). This alignment weakens near the coast and increases offshore.

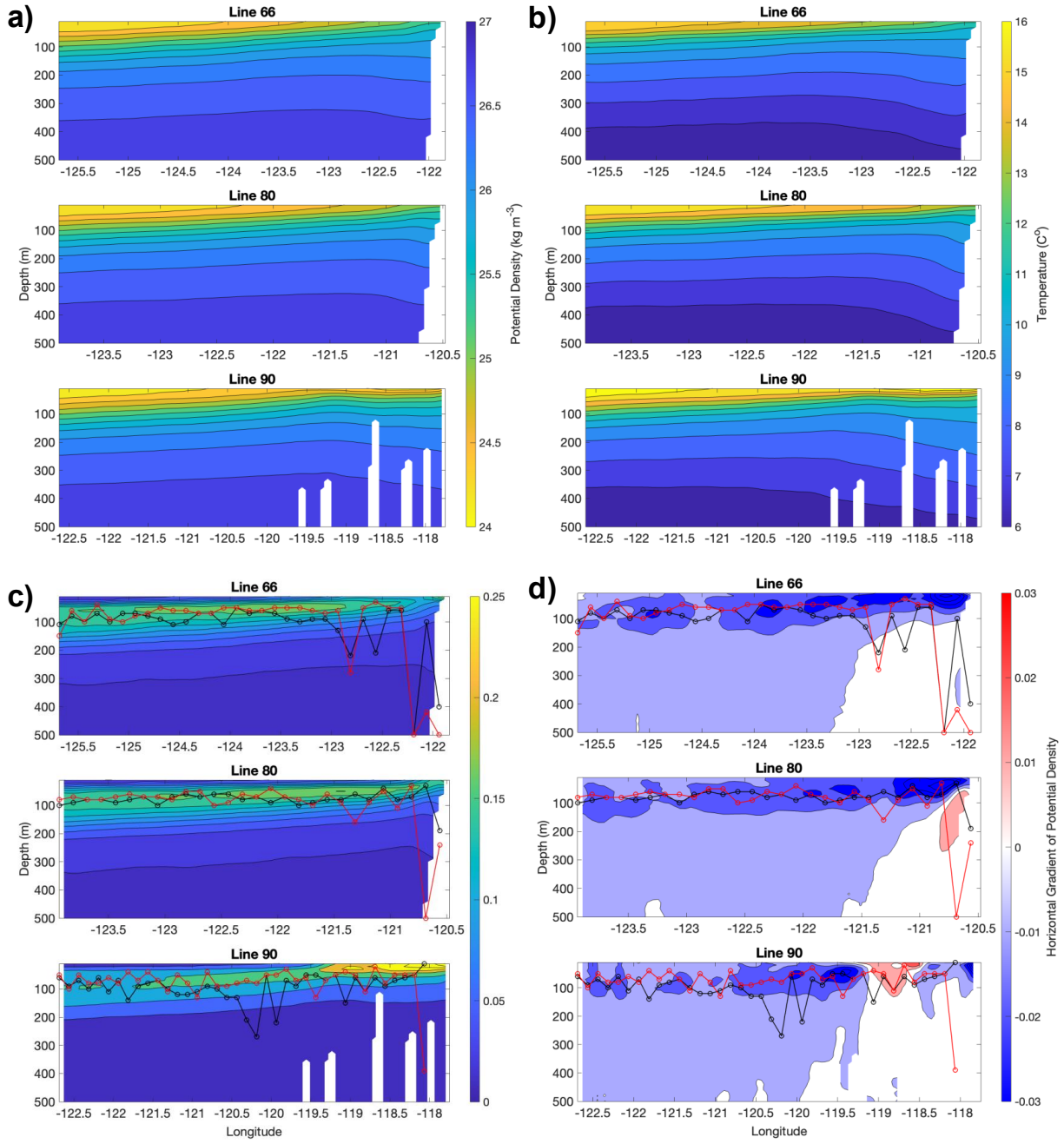

Figure 1.5: a) Mean potential density, b) mean temperature, c) vertical gradient of mean potential density, and d) horizontal gradient of mean potential density along Lines 66, 80, and 90. The maximum depth of the CCC within each longitudinal bin is plotted for *u* (black) and *v* (red) on top of the gradients in panels c and d.

Ekman velocities

Satellite-derived geostrophic velocities with Ekman components (surface and 15 m) show correlation patterns with CUGN velocities similar to the geostrophic velocities. For *u* velocities of both Ekman products, the CCC had an average subsurface maximum of 145 m across all lines (Figure 1.5a and 1.5c). The profiles of the surface Ekman *v* do not follow this pattern, and the correlations peak at or near the surface and decrease with depth (Figure 1.5b). The average depth of the maximum CCC for Ekman 15 m *v* was 50 m. The profiles of *u* for both the Ekman surface and Ekman 15 m have similar shapes and CCC values. These patterns are also consistent with the profiles of CCC for the geostrophic *u* (Figure 1.2).

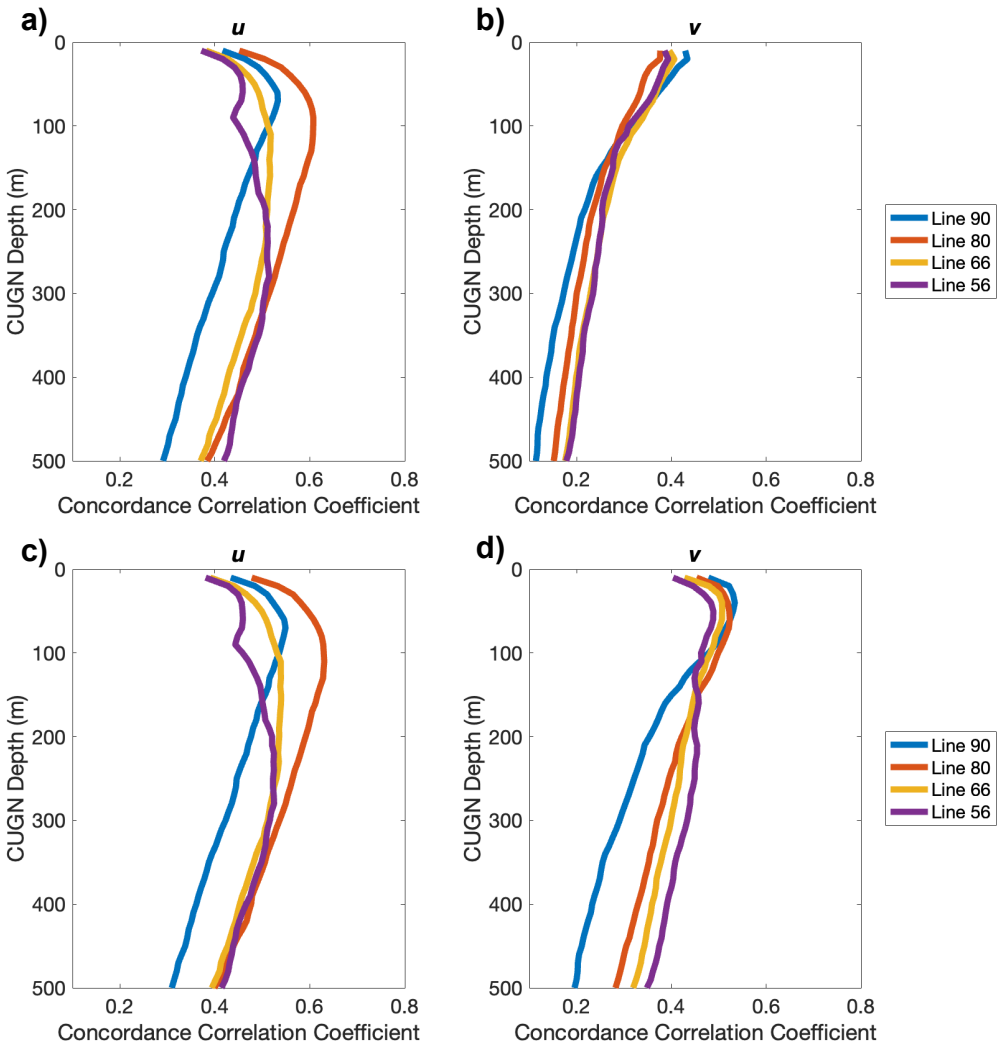

Figure 1.6: Concordance correlation coefficients between CUGN velocities (*u, v*) from the surface to 500 m and satellite-derived geostrophic + Ekman surface (a, b) and geostrophic + Ekman 15 (c, d).

The integrated depth profiles of CUGN velocities also show correlations of the satellite-derived geostrophic + Ekman surface and Ekman 15 m velocities similar to the geostrophic velocities (Figure 1.7). For *u*, highest CCC values occurred between the satellite-derived geostrophic velocities and CUGN velocities averaged from the surface to 200 m. These results are consistent with the results of the geostrophic velocities, with Line 80 having the highest correlations, followed by Line 90, Line 66, and Line 56 (Figure 1.3). There are differences in the

profiles of CCC for the integrated depth comparisons for *v* between the satellite-derived geostrophic + Ekman velocity products. For the surface Ekman, overall CCC were low, peaking at the 0-40 m average (Figure 1.7a). For the geostrophic product with Ekman 15 m, the best correlation occurred between the satellite-derived geostrophic velocities and the 0-110 m averaged CUGN *v* velocities (Figure 1.7d). Overall, Line 90 showed the strongest CCC of the integrated velocities for both Ekman *v* velocities (Figure 1.7b and 1.7d).

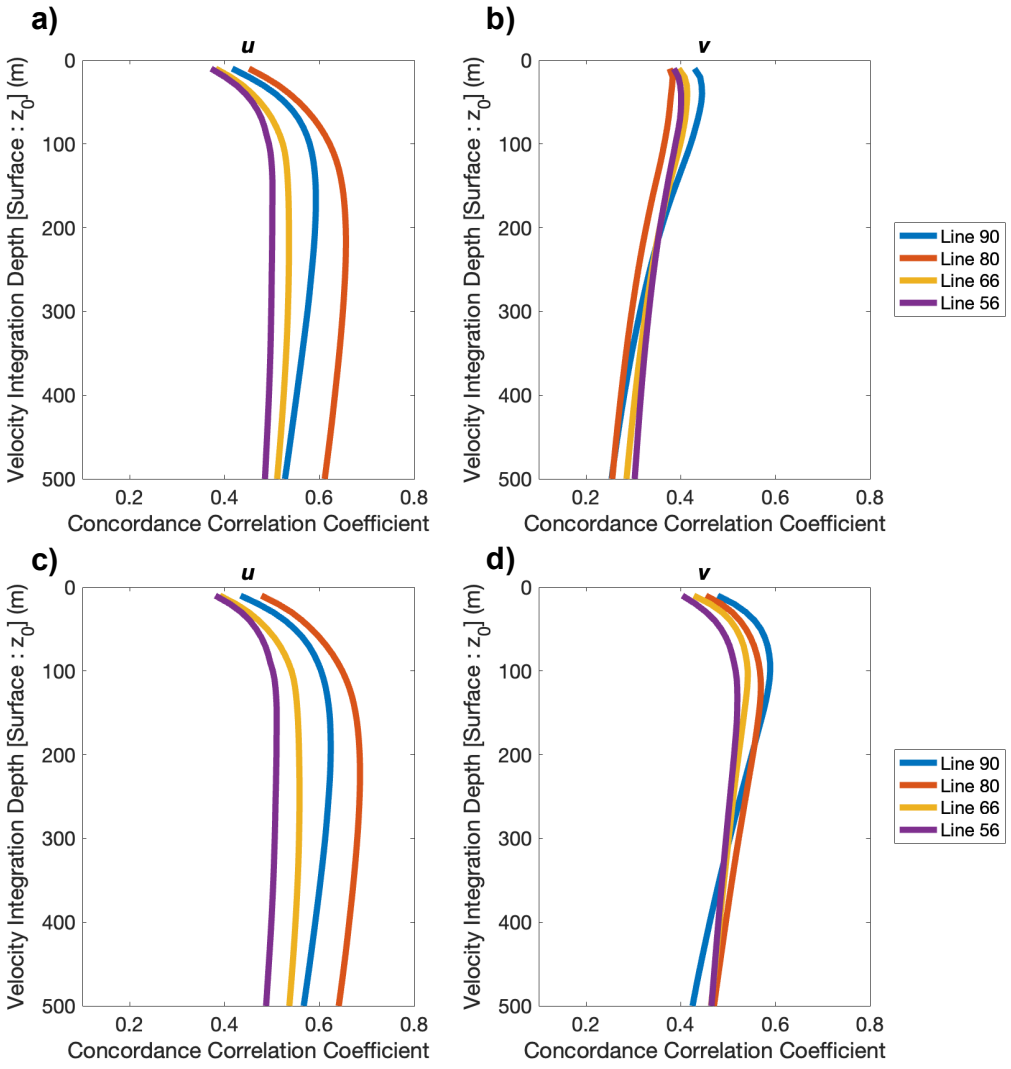

Figure 1.7: Concordance correlation coefficients of the integrated depth profiles (*u, v*) for geostrophic + Ekman surface (a, b) and geostrophic + Ekman 15 m (c, d). The x-axis is the concordance correlation coefficient associated with the averaged glider velocities integrated over the surface to the defined depth. Glider velocities were averaged from the surface to the y-axis depth.

1.4 Discussion

Satellite-derived geostrophic velocities are often termed "surface" velocities, and thus, researchers may interpret these velocities as representing ocean circulation in some thin surface layer of the ocean water column. Satellite-derived geostrophic velocities do measure differences

in SSH which vary within the upper meter or less of the water column; therefore, calling these velocities “surface” is not unfounded.

Some researchers have implemented satellite-derived geostrophic velocities for applications related to transport in the upper water column, not just the surface (e.g., Della Penna et al. 2015, Furey et al. 2023, Strub et al. 2024). Desbruyères et al. (2021) showed that altimetry-derived geostrophic velocities capture large-scale circulation patterns from the surface to the pycnocline. Our results align with this perspective, showing that satellite-derived geostrophic velocities, both with and without an Ekman component included, are most strongly correlated with glider velocities averaged from approximately 0-170 m in the CCS. Below 200 m, the vertical shear of glider-derived velocities is small – this leads to relatively consistent CCC values with increasing depth below 200 m when comparing the integrated depth CUGN velocities with the satellite-derived geostrophic velocities (Figures 1.3 and 1.7). It is important to note that this 0-170 m layer average, while much deeper than the surface deviations in SSH, could still be thought of as the “surface” velocities, as this section is the upper water column. Here, we have refined our understanding of satellite-derived surface geostrophic velocities by showing that these velocities are representative of a layer extending 50-200 m deep into the water column.

The strongest correlations of satellite-derived geostrophic velocities with vertical profiles of CUGN velocities in 10 m depth bins were found at subsurface depth bins (Figure 1.2 and 1.6). All satellite-derived geostrophic velocity products, both with and without an Ekman component included, showed maximum correlations subsurface, at depth bins in the upper 300 m – primarily between 50 and 150 m. The depth of maximum correlation between satellite-derived geostrophic velocities and CUGN velocities are likely driven by cross-shore shifts in pycnocline depth in the CCS. The pycnocline, driven largely by vertical temperature gradients, shoals near the coast and

deepens offshore, resulting in cross-shore horizontal density gradients (Figure 1.5). The thermal wind equations state that the vertical shear of geostrophic currents is proportional to the horizontal density gradient. In regions with a well-mixed upper layer above the pycnocline, horizontal and vertical density gradients can be minimal. Minimal horizontal density gradients lead to a small relative velocity term, making the absolute geostrophic velocities similar to the surface geostrophic velocities measured by the altimeter (Equation 1.4 and 1.5). Chereskin (1995) illustrated that the vertical shear of geostrophic flow is minimal in the upper 60 m of the CCS. This finding is consistent with our observation of horizontal density gradients being weaker near the surface offshore, and maximal between 50 and 100 m depth, corresponding with the depth of the pycnocline (Figure 1.5). The mixed layer depth varies seasonally and spatially throughout the CCS, but is typically within the upper 100 m of the water column (Kara et al. 2000). The depth of the maximum horizontal density gradient corresponds with the depth of the maximum CCC values we observed, especially offshore, where geostrophy is most relevant (Figure 1.5). Our results support the notion that altimetry-derived geostrophic currents are representative of the water column above the pycnocline.

Conceptually, our findings are consistent with the theory of geostrophy: in an upper layer that is well mixed, weak horizontal and vertical density gradients result in minimal shear of geostrophic velocities. In other words, the relative velocity term is consistent with depth, or small compared to the surface velocity term in Equations 1.4 and 1.5. Where horizontal density gradients are maximum, there is a strong vertical shear of geostrophic currents, and the relative velocity term becomes more important in the calculation of the absolute geostrophic velocity. This occurs at the pycnocline in the CCS. Wind-driven components of flow not detected by altimetry but measured by glider ADCPs are strongest at the surface and decrease in magnitude

with depth. The ageostrophic component of velocity is generally confined to an upper layer, approximately 100 m at mid-latitudes (Wunsch and Gaposchkin 1980). This leads to maximum correlations between glider-derived velocities and satellite-derived geostrophic velocities at the depths where the vertical shear of geostrophic flow is still minimal, and the surface-intensified wind-driven flows have dissipated. Pairwise comparisons of satellite-derived geostrophic velocities and CUGN velocities support this hypothesis – at 10 m below the surface, the range of CUGN velocities is high, and this range decreases with depth, illustrating the influence of surface-intensified flows evident in the CUGN data (Supplemental Figures 1.1-1.3).

We found that all the satellite-derived geostrophic velocity products we analyzed had similar, significant correlation patterns with the CUGN velocities, with the exception of geostrophic + Ekman surface *v* velocity whose correlations were low, and decreased almost monotonically from the surface (Figure 1.6b). Chereskin (1995) observed the Ekman spiral in the northern CCS to occur in the upper 48 m. In the CCS, alongshore winds drive Ekman transport, resulting in southwestward depth-integrated velocities, and surface velocities 45° to the right of the southeast wind direction (Hickey 1979). Co-located comparisons of velocities revealed CUGN-measured velocities at all depths in the north/south (*v*) direction were primarily stronger than the remotely sensed geostrophic + Ekman surface velocities (Supplemental Figure 1.2). This shift in velocity magnitude resulted in low CCC values (Figure 1.6b). The geostrophic + Ekman surface *v* velocities are primarily negative (southward) velocities, while the CUGN *v* velocities are more evenly distributed around 0 (north and south). Using Argo floats and drouged drifters, Rio et al. (2014) constructed the global model of Ekman currents used in the satellite products in this study and found the best fit angle of Ekman currents responding to wind stress was 20-40° at the surface and 40-60° at 15 m depth (Rio et al. 2014). Modeled angle response to wind stress

changes seasonally, driven by seasonal stratification (Rio et al. 2014). The modeled Ekman currents are consistent with the conceptual Ekman spiral, but the model predicts smaller angles than Ekman theory posits. This may help explain the predicted strong southward geostrophic + Ekman surface velocities, which are reflective of the surface-intensified flow 20-40° to the right of the primarily southeastward wind stress. The Ekman spiral causes the velocities to shift westward and decrease in magnitude with increasing depth through the water column, thereby giving a weaker southward (v) signal in the 15 m modeled Ekman velocities. This weaker Ekman velocity component may have led to the stronger correlations of the geostrophic + 15 m Ekman velocities with the CUGN v velocities than the geostrophic + surface Ekman velocities (Supplemental Figure 1.3). In other words, the predicted surface Ekman velocities reduce the fidelity of the remotely sensed velocities in reproducing the CUGN measured velocities by potentially overestimating the southward Ekman component.

We found differences in the glider and satellite-derived geostrophic velocity correlations between geographic areas (CalCOFI lines). In most of our analyses, Line 80 was associated with the highest correlations, and Line 56 consistently had the lowest correlations. One potential explanation for this is the difference in glider sampling efforts between lines. Glider sampling on Line 56 began in 2019, while the other lines have been locations of continued glider sampling since the early 2000s. For our analyses, Line 56 was associated with fewer glider observations than the other 3 lines. The relatively short time series and smaller dataset on Line 56 may lead to less-robust statistics. Indeed, we suspect that the second subsurface CCC maximum around 300 m in the Line 56 correlations may be spurious, as it is not observed in the other lines. Revisiting these analyses in the future when the time series is extended is recommended.

The regional oceanography of the CCS can be used to gain insight into our observed spatial trends. Along all CalCOFI lines, nearshore correlations between satellite-derived geostrophic velocities and CUGN velocities were relatively low, while high correlations were found offshore (Figure 1.4). The transition from low to high CCC values aligns spatially with the transition from the California Undercurrent to the California Current, especially for Lines 80 and 66 where that transition is well defined near the shelf break (Figure 1.4; Rudnick et al. 2017a). Cross-shore trends of the CCC revealed a distinct shift in correlation strength around -120° W along Line 90 (Figure 1.4g and 1.4f). This shift corresponds with Point Conception, which marks the transition of the Southern California Bight to offshore waters. Within the Southern California Bight, correlations are strongest around -119° W, coinciding with the positive horizontal density gradient, and associated northward flow characteristic of the California Undercurrent (Rudnick et al. 2017a). Mesoscale stirring is weaker in the Southern California Bight (Giddings et al. 2022), and correlations between glider-derived velocities and satellite-derived geostrophic velocities are relatively poor in this region. Most satellite altimetry is not able to detect smaller, submesoscale features (Chavanne and Klein 2010). The satellite-derived geostrophic velocities may be more accurate offshore of the Southern California Bight, where altimeters can resolve larger-scale mesoscale flows such as the California Current, which are weaker near the coast. Similarly, Doglioni et al. (2023) found the highest correlations between altimetry-derived geostrophic velocities and mooring velocities in regions of stable flow (e.g. boundary currents) compared to regions with weaker flows and dominated by eddy activity. Recent developments in satellite technology (e.g., Surface Water Ocean Topography; Morrow et al. 2019) have focused on increasing the spatial resolution of remotely sensed data, allowing detection of finer-scale circulation patterns and submesoscale features by satellite. Additional comparative analyses

should be performed to discern whether the spatial limitations we identified can be overcome using newer satellite-derived geostrophic velocity products.

Limitations

The California Current is a coastal geostrophic current, easily accessible to the CUGN glider paths. Our analyses revealed the strong connection between the depth of maximum correlation and the depth of maximum horizontal density gradient and the depth of dissipation of ageostrophic velocities. This association could enable the extrapolation of our results to other regions where the local hydrographic patterns are known. Correlations between glider-measured velocities and satellite-derived geostrophic velocities may not be as high in locations dominated by submesoscale features and ageostrophic flow, as others have found, and as evidenced by our CCC values in the Southern California Bight (Figure 1.4; Sudre and Morrow 2008). Additional comparative analyses of glider-derived velocities and satellite-derived geostrophic velocities should be performed in other regions to explore if these correlations change under different circulation conditions.

The vertical shear of the glider's velocity is measured on the ascent of the dive, while the depth-averaged velocity is measured across the entire descent-ascent of the vehicle. This may lead to error through the spatiotemporal mismatch of the velocity measurements; however, this error is minimal over scales greater than 30 km (Todd et al. 2011). Additionally, the midpoint of the ascent is used as the time and location for depth-based velocity measurements. Spray covers approximately 3 km horizontally in a dive cycle, meaning potential error arising from location imprecision is less than 1 km. This imprecision is unlikely to make a difference in the correlations with satellite-derived geostrophic velocities, as the resolution of satellite-derived

geostrophic velocities is significantly lower (~14-28 km). Additionally, instrument error may play a role in the correlations we observed. Spray gliders perform poorly in the upper few meters of the water column, which could affect correlations between satellite-derived geostrophic velocities and the shallowest depth bin of the glider data (Todd et al. 2017). Individual glider profiles are subjected to high-frequency velocity perturbations such as inertial oscillations, internal waves, and tides (Todd et al. 2017, Sudre and Morrow 2008). Nevertheless, we chose to use individual glider profiles rather than temporally averaged profiles to best align with daily geostrophic velocity fields from altimetry and to assess how well the geostrophic velocities capture instantaneous velocities.

1.5 Conclusions

Given the wide range of applications and accessibility of satellite-derived geostrophic velocities, it is important to understand what these velocities actually measure in the water column. We compared satellite-derived geostrophic velocities to depth-resolved glider measurements of velocities to generate vertical profiles of satellite-glider velocity correlations. We found significant correlations between satellite-derived geostrophic velocities and glider-derived velocities, with distinct spatial patterns, both vertically through the water column, and horizontally with distance from shore. Our results provide insights into the depth horizons that satellite-derived geostrophic velocities most accurately represent in the CCS. We found that correlations were strongest at approximately 100 m depth, and with velocities of slabs averaged from the surface to approximately 170 m. The strongest correlations were observed offshore, in the California Current. These results serve as a foundational basis and guidance for researchers in fields that use these products to assess ocean circulation, transport, and dispersal processes. We caution against assuming satellite-derived geostrophic velocities are representative of the

total sea surface velocities, but recommend use of these products for understanding circulation patterns of the integrated upper water column.

1.6 Acknowledgements

Thank you to Dan Rudnick for assistance with the CUGN data.

Chapter 1, in part is currently being prepared for submission for publication of the material. The dissertation author was the primary investigator and author of this material.

1.7 Supplemental Material

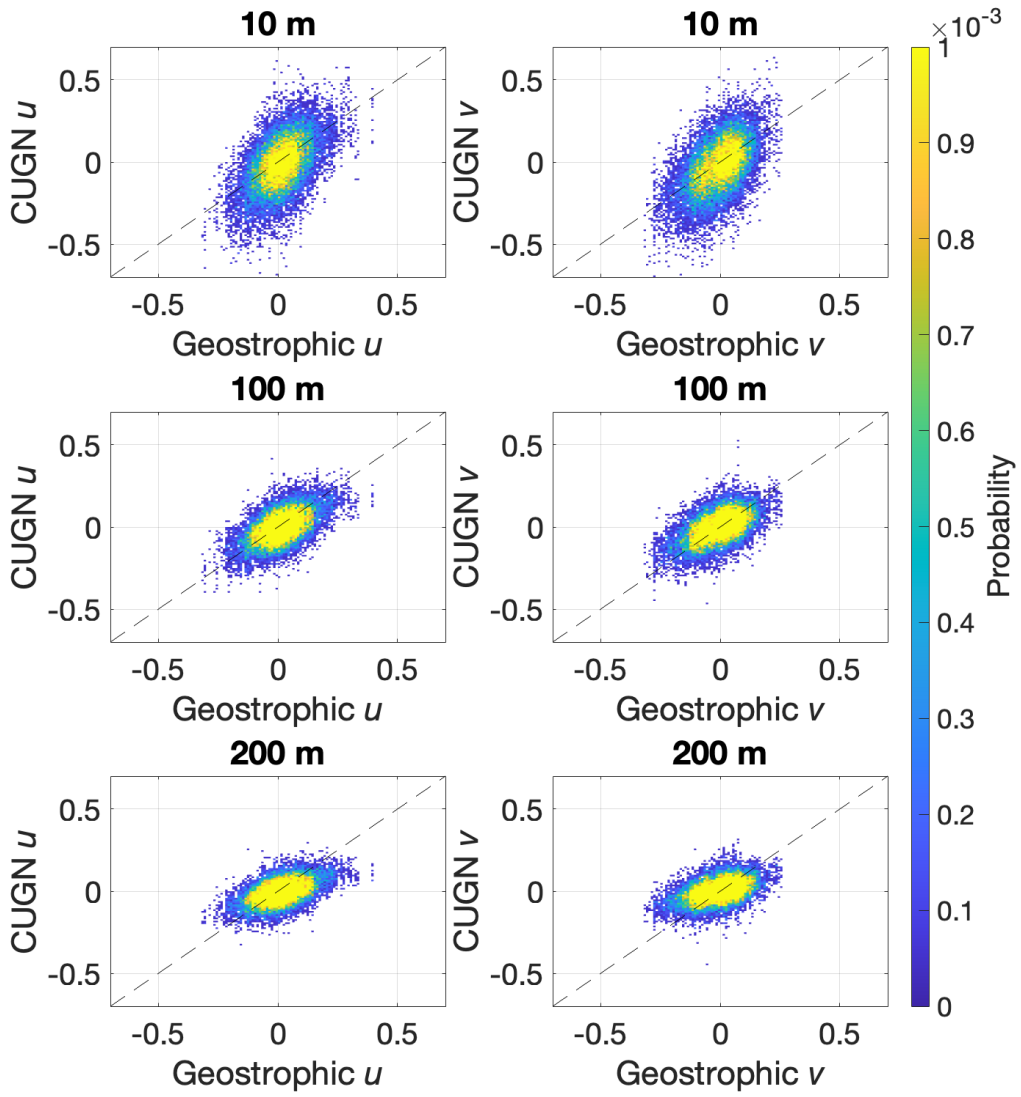

Supplemental Figure 1.1: Comparisons between geostrophic velocities and CUGN velocities at 3 depth bins (10 m, 100 m, and 200 m) along Line 90. The color corresponds to the relative probability, equal to the number of observations in each bin relative to the total number of observations. The dashed black line is the 1:1 line.

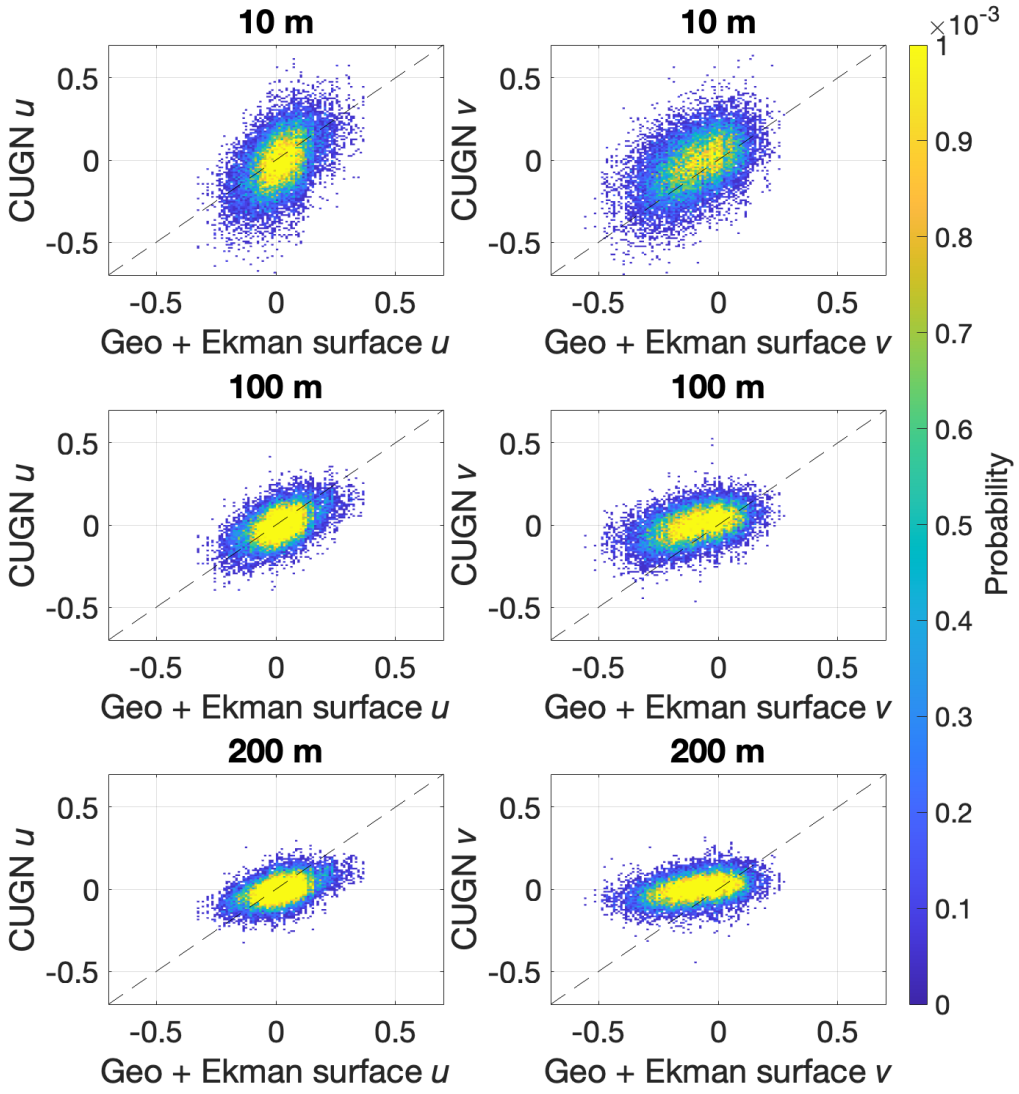

Supplemental Figure 1.2: Same as above, but for geostrophic + Ekman surface velocities.

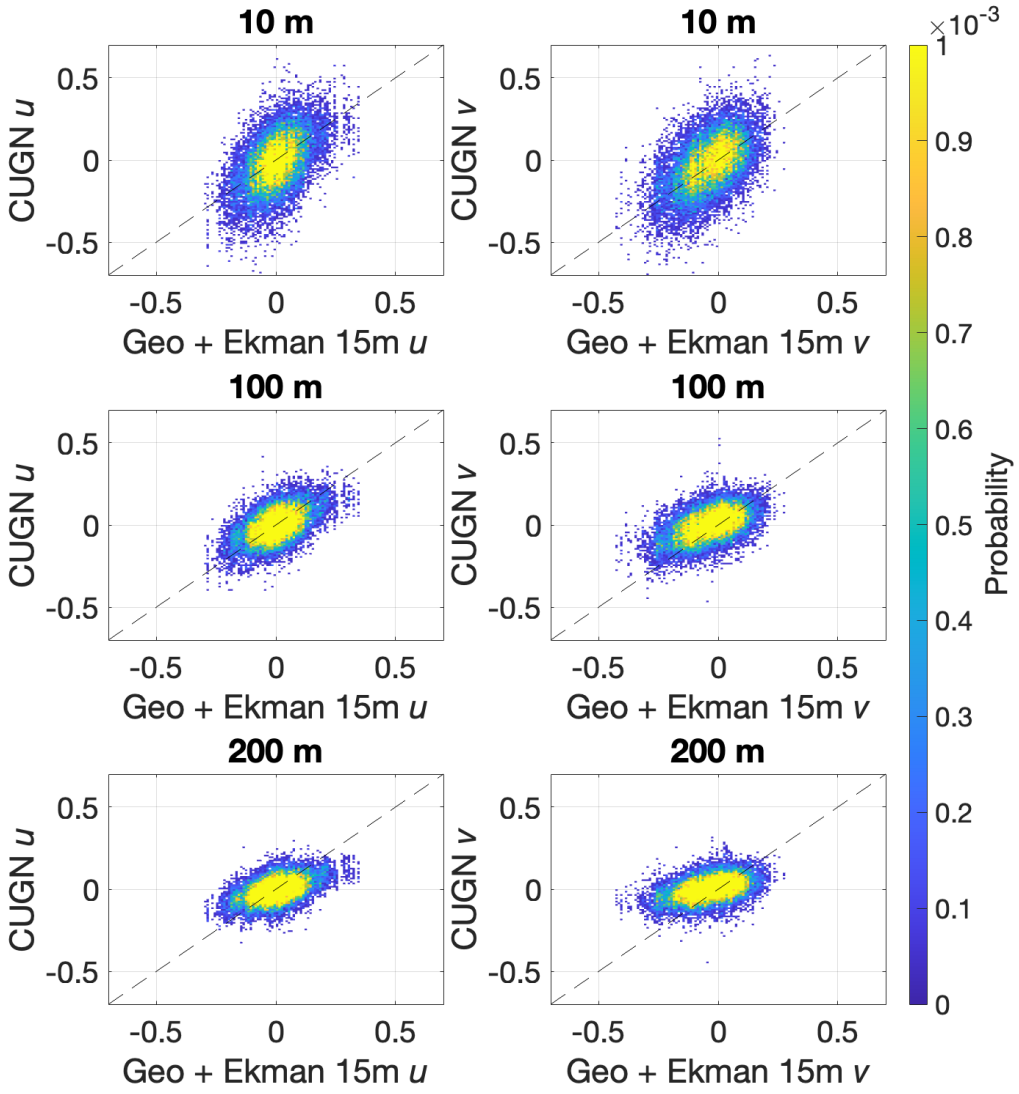

Supplemental Figure 1.3: Same as above, but for geostrophic + Ekman 15 m velocities.

Chapter 2 : Quantifying the fates and retention of larval rockfish through Lagrangian analyses

2.1 Abstract

Understanding larval transport pathways and retention is important for fisheries management and predicting recruitment variability. We investigated how mesoscale circulation patterns influence the retention and dispersal of larval rockfish (*Sebastes* spp.) within the California Current System off the western coast of the United States. Using a 25-year record of satellite-derived geostrophic and Ekman velocity fields, Lagrangian particle tracking simulations were implemented to find pathways of passively drifting virtual particles representing rockfish larvae. Statistical fates of particles were averaged to reveal mean spatial and temporal patterns in retention and distance traveled. Yearly retention values were compared to observed pelagic juvenile rockfish abundance collected on annual surveys. Retention patterns varied spatially throughout the region, with the Southern California Bight emerging as a highly retentive region. Interannual variability in overall retention was positively related to the abundance of pelagic juvenile rockfish collected in the same year. Our analyses provide evidence supporting the successful implementation of the geographic placement of the Cowcod Conservation Areas, which were spatial closures implemented in the early 2000s to rebuild overfished rockfishes, and illustrate the utility of numerical simulations for understanding retention and transport of pelagic larvae such as rockfish.

2.2 Introduction

Understanding the suite of drivers that affect fish recruitment requires knowledge of the roles that physical mechanisms play in larval survival. Successful recruitment generally requires greater relative larval survival, as the larval stage of fishes is typically the life stage with the

highest mortality rate (Hjort 1914, Houde 2008, Hare 2014). Due to weak swimming abilities of the early life history stages of fishes, spatiotemporal variability of ocean currents can impact the distribution and survival of ichthyoplankton. Consequently, resolving larval transport is an important step toward understanding the influence of hydrodynamics on larval survival, in order to better predict fish distributions and recruitment.

Rockfish (*Sebastes* spp.) are ecologically and commercially important fishes found in the Northeast Pacific. There are more than 65 Sebastes species present along the western coast of the United States, with the greatest number of species found in the vicinity of the Southern California Bight (SCB; Love et al. 2002). Female rockfishes release internally hatched larvae (primitively viviparous). The majority of species (including the more abundant species) spawn during the winter, with larvae developing into pelagic juveniles after approximately 1–2 months (Love et al. 2002). During their early larval period, rockfish exhibit weak swimming abilities and do not vertically migrate, essentially acting as passive particles drifting in the upper mixed layer, making their positioning highly susceptible to the influence of ocean currents (Moser and Boehlert 1991, Sakuma et al. 1999, Love et al. 2002, Stockhausen and Hermann 2007, Kashef et al. 2014). Following their larval stage, winter-spawning rockfish typically remain in the water column as pelagic juveniles for several months before settling out to either nearshore or shelf habitats, at which point they are typically referred to as "settled juveniles." Depending on the species, this juvenile stage typically will last for several to many years, with adult life spans ranging from approximately a decade to up to a century or more for some species (Love et al. 2002).

During the late 1990s and early 2000s, seven rockfish species were declared overfished, with expected recovery times ranging several decades due to species slow growth, late maturity,

high longevity, and generally low productivity (Berkeley et al. 2004a). This led to management responses to reduce fishing mortality, including spatial habitat closures. Marine protected areas called Cowcod Conservation Areas (CCAs) were established in the SCB with the intent of protecting habitat for cowcod (*Sebastes levis*). The CCAs, comprised two separate areas encompassing a total surface area of approximately 11,138 km^2. While the CCAs were implemented primarily to help rebuild cowcod, other rockfish species benefited from the reserves (Hitchman et al. 2012, Thompson et al. 2016, Thompson et al. 2017, Fennie et al. 2024). These conservation areas were established based on historical catch records of cowcod and prohibited bottom contact fishing at depths greater than 20 to 40 fathoms (~36-73 m; depth closure regulations were modified slightly over time) to minimize cowcod fishing mortality (Butler et al. 2003, Dick et al. 2019). These closures, coupled with a broad suite of additional management measures implemented to rebuild depleted populations were highly successful, as the cowcod stock was declared rebuilt in 2019, following earlier rebuilding success of five of the initial seven rockfish species declared to be overfished. Consequently, most regulations that implemented spatial closures to protect overfished rockfishes were removed in 2023, including most protections within the CCAs. As of January 2024, commercial trawling is prohibited within the CCAs, while fixed gear and recreational fisheries are allowed.

While the CCAs were recognized as critically important for the recovery of the cowcod population, it is important to recognize that high adult catch records alone do not necessarily coincide with locations or habitats conducive for larval survival (Shen et al. 2017) and subsequently, recruitment, which is needed to maintain population growth. Marine protected areas that are located in regions where larvae are produced but are then advected to unfavorable habitats, may be less effective than if the protected areas were located in zones where locally

produced larvae are transported to ecologically favorable areas (White et al. 2014). Marine reserves should also supply larvae to zones accessible to fishing (Pelc et al. 2010, Hitchman et al. 2012). Thus, determining the placement of marine reserves benefits from the identification of transport pathways of larvae and retention hotspots (Stockhausen and Hermann 2007, Petersen et al. 2010, Hitchman et al. 2012, Andrews et al. 2021).

Larval transport models are useful tools for fisheries management and marine reserve planning (Lett et al. 2006, Stockhausen and Hermann 2007, Petersen et al. 2010, Andrews et al. 2021, Mori et al. 2022). Petersen et al. (2010) used numerical simulations of particle transport to investigate larval rockfish transport patterns in a narrow coastal region in central California. Their work illustrated the utility of simple numerical simulations in understanding transport pathways of rockfish in the California Current System (CCS). More recently, Morales (2023) used particle tracking to show that ocean current patterns can facilitate recruitment of shortbelly rockfish (*S. jordani*) in central California.

The CCS is an eastern boundary upwelling system, characterized by high biological production and dynamic oceanographic conditions (Checkley and Barth 2009; Bograd et al. 2019). The California Current brings cool, low salinity, high oxygen and high nutrient water from the north, equatorward. Warmer, higher salinity water forms the California Undercurrent, which flows northward near shore and is centered at a depth of ~100 m although its depth can range from 500 m to the surface (Zaba et al. 2021). Coastal wind-driven upwelling brings deep, cold, saline, low oxygen, and nutrient-rich waters to the surface at the coast, enhancing primary production along the coast. Surface Ekman transport is directed offshore, driving coastally upwelled waters into waters that are more oligotrophic and associated with lower production. In the CCS, the physical environment varies with both seasonal wind-driven upwelling and

interannual climate variations such as the El Niño Southern Oscillation and the Pacific Decadal Oscillation (Checkley and Barth 2009).

Ichthyoplankton distributions are impacted by temporal variability in upwelling and ocean circulation, coupled with the timing of fish spawning. Spawning in the winter, when wind-driven offshore Ekman transport is weakest, is one strategy to minimize advection offshore (Parrish et al. 1981, Giddings et al. 2022). Cross-shore transport of larvae to offshore oligotrophic regions may have negative consequences for fish survival and recruitment (Nieto et al. 2014; Morales 2023). Nearshore retention of rockfish larvae may facilitate survival through increased prey availability and delivery of larvae to viable adult habitats, including marine protected areas (Caselle et al. 2010, Petersen et al. 2010).

Our objective is to quantify the fates of rockfish larvae released in central and southern California – the epicenter of rockfish diversity (Love et al. 2002). Lagrangian particle tracking simulations, forced by a 25-year record of remotely sensed geostrophic and Ekman velocity fields, were used to track passively drifting virtual particles representing rockfish larvae. Spatial and temporal patterns of larval rockfish transport were quantified by metrics including the fraction of larvae retained inshore of the 2000 m isobath, net distance traveled, gross distance traveled, and the net-to-gross displacement ratio. We also examined particle advection into and away from the CCAs in the SCB and investigated connectivity of the CCAs. Finally, we examined the relationship between simulated interannual larval retention and observed annual pelagic juvenile abundance patterns derived from a fisheries-independent ecosystem assessment survey. Our analyses provide novel insights into rockfish larval transport and retention, with important implications for ongoing management of these commercially and ecologically important species.

2.3 Materials and Methods

Study location

Virtual particles representing rockfish larvae were randomly seeded throughout the study domain, and placements on land were avoided. The domain was defined by the coastline and the 2000 m isobath, and spanned from the SCB (~30.5° N) in the south to Monterey Bay (~37°N) in the north, with the northern and southern boundaries of the domain constructed approximately perpendicular to the coastline (Figure 2.1). Although the highest densities of most winter spawning rockfishes are in benthic habitats between approximately 100 and 500 m depth, the offshore extent of the domain was chosen based on observations of high abundances of rockfish larvae out to the 2000 m isobath (Moser and Boehlert 1991, Thompson et al. 2016). Bathymetry data was obtained from the ETOPO Global Relief Model (NOAA National Centers for Environmental Information 2022).

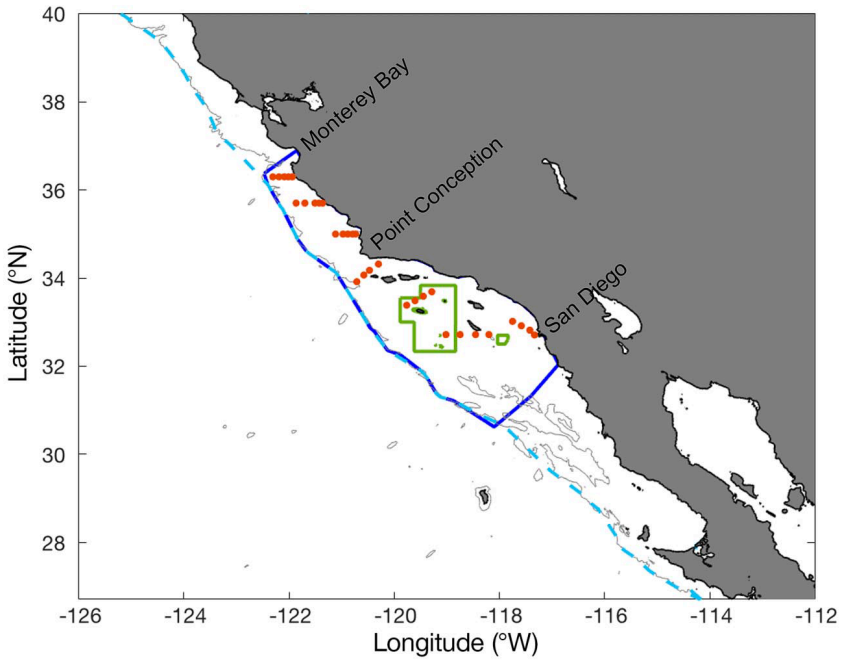

Figure 2.1: Study region in California. Dark blue line: domain where rockfish larval particles were seeded; light blue dashed line: offshore boundary that defines retention for the final locations; light gray lines: 2000 m isobath; green boxed outlines: Cowcod Conservation Areas; orange markers: Rockfish Recruitment and Ecosystem Assessment Survey sampling locations used in this study. The high-resolution coastline in all figures is for visualization purposes only.

Particle tracking

On each day from January 1 to January 31, 1,000 virtual particles were seeded at random locations within the defined domain (Figure 2.1). Particles were tracked forward in time for 30 days using a time step of 1 day. The simulations were performed every year for 25 years (1998-2022), resulting in a total of 775,000 particle trajectories. Although most rockfish have a spawning season that may span several months during late fall, winter, and sometimes early spring, January typically represents the month of greatest larval release for most species (Moser and Boehlert 1991).

We chose a simulation duration of 30 days based on rockfish larval stage duration. Larval and pelagic juvenile stage duration varies among rockfish species, but for winter-spawning

species, the larval stage typically lasts 1-2 months, with the pelagic juvenile stage lasting another 3-4 months, after larvae have undergone flexion and adopted meristic counts associated with adult stages (Love et al. 2002, Ralston et al. 2013, Kashef et al. 2014). Pre-flexion rockfish larvae are characterized by poor swimming ability (0.5 to 1.8 cm s^{-1}); however, swimming ability increases rapidly with body size, with pelagic juveniles capable of swimming 8.6 to 53.5 cm s^{-1} (Kashef et al. 2014). Pelagic juveniles are thus capable of outswimming some horizontal surface currents, suggesting that implementing forward-in-time particle tracking on rockfish older than 30 days may not be suitable. We conservatively defined a larval period of 30 days and assumed that rockfish within 30 days of parturition act as passively drifting particles, as other works have done (Petersen et al. 2010, Nishimoto et al. 2019).

Eulerian velocity fields at a given location were linearly interpolated from 0.25° gridded velocity data to estimate the particle's velocity at any arbitrary location. Given initial locations (x,y) at time (t), new particle locations (forward in time) can be found by the first-order Euler scheme. A random walk term representing horizontal diffusivity was added (Batchelder 2006), so the equation for forward-in-time particle tracking with spatially constant diffusivity was:

$$x(t + \Delta t) = x(t) + u(x, y, t) * \Delta t + \sqrt{2K_H \Delta t} * Q \quad (2.1)$$

$$y(t + \Delta t) = y(t) + v(x, y, t) * \Delta t + \sqrt{2K_H \Delta t} * Q$$

where Q is a Gaussian random variable with a zero mean and unit variance, and K_H is the horizontal diffusivity. A value of 26 m^2 s^{-1} was selected for K_H, where, where $K_H = (2.06 \times 10^{-4}) \times L^{1.15}$, with L referring to the length scale of diffusion, in our case, the ~28 km resolution of the velocity data used (Okubo 1970, Matsuzaki and Fujita 2017).

The velocity fields used to force the simulations do not resolve coastal flows well, so we assume that particles that were advected close to shore would become controlled predominantly

by finer-scale coastal dynamics that are outside the scope of this work. We implemented a boundary at the coastline where velocities become 0 m s^{-1} and used a "re-drifting operation," as defined by Kataoka et al. (2013). If a particle ended up on land during the simulation, the particle was returned to its location from the previous time step, and this operation was repeatedly performed in each time step (Kataoka et al. 2013). As a sensitivity analysis, we also conducted simulations using a time step of 1 hour, but found no significant difference in particle advection, so we opted to use daily time steps for computational efficiency. Further, we compared simulations releasing 1,000 and 10,000 particles per day and found no significant differences between yearly mean retention or spatial distribution of final particles, so we chose 1000 particles. Figures illustrating the results of the sensitivity analyses can be found in the Supplemental Material (Supplemental Figures 2.1 and 2.2).

Satellite-derived velocity fields

Geostrophic velocity fields used to generate larval trajectories were derived from satellite-estimated sea surface height (SSH) anomalies through the Copernicus Marine Environment Monitoring Service (https://doi.org/10.48670/mds-00327). We used daily geostrophic velocities with a wind-driven Ekman component at 15 m, available at a 0.25° (~28 km) resolution. Ekman currents were modeled using European Centre for Medium-Range Weather Forecasts ERA5 wind stress (Rio et al. 2014). We also performed simulations using only geostrophic velocity fields to assess the role of Ekman currents in our particle trajectories. Although the 2-dimensional geostrophic and Ekman currents do not completely resolve the fine scale complexity of currents, geostrophic and Ekman flows are the dominant components at the larger spatial and temporal scales we investigated (Parrish et al. 1981, Dong et al. 2021). We did

not investigate vertical motions in our analyses. Rockfish larvae are found in the upper 80 m of the water column and show no evidence of vertical migration, making them well suited for simulations that are forced by horizontal geostrophic and Ekman velocity fields (Moser and Boehlert 1991, Sakuma et al. 1999, Love et al. 2002).

The satellite-derived velocities are based on measurements of SSH anomalies. The SSH anomalies are a result of the vertical distribution of density throughout the water column below. The SSH anomalies are used to generate horizontal geostrophic surface currents from the horizontal pressure gradients and Coriolis. Using the satellite-derived geostrophic and 15-m Ekman velocities gives velocity fields representative of the upper ~100 m of the water column, with a weak contribution from the wind. We opted to use satellite-derived velocities instead of a hydrodynamic model: models can accurately reproduce average ocean properties such as eddy kinetic energy. However, in comparisons of regional ocean models and satellite data we found that the models we investigated did not accurately reproduce the locations and intensities of individual mesoscale features – and it is those features that are central to our investigations of larval transport. For the focus of this paper, which is recreating specific dispersal pathways of larvae, we determined that satellite-derived velocities were the best tool for exploring the influences of horizontal advection of rockfish larvae in mesoscale circulations in the Southern California Bight.

Rockfish fates

We classified each particle as "retained" based on whether its final location was inshore of the 2000 m isobath (Figure 2.1). Habitats shallower than 2000 m bottom depth are likely to be within swimming distance of habitat suitable for the settlement of pelagic juveniles, while

habitats deeper than 2000 m bottom depth represent distant offshore areas from which pelagic juveniles would unlikely to reach their adult habitat closer to shore. Particles that traveled north or south out of the seeding domain but remained inshore of the 2000 m isobath were thus included in the retained category.

For each particle, we computed the gross distance traveled (distance calculated over every daily time step and summed) and net distance traveled (distance calculated from seeding to final location). The net-to-gross displacement ratio, calculated as net distance divided by gross distance, was used to understand the degree of linearity of the particle trajectories. High net-to-gross displacement ratios indicate linear paths, while low net-to-gross displacement ratios indicate more meandering trajectories, potentially indicative of eddies.

We calculated time-averaged geostrophic and geostrophic + Ekman 15 m velocities by computing the mean velocity magnitude and direction for each 0.25° x 0.25° grid cell throughout the months of January and February across all 25 years to assess mean flow and differences between the two velocity products. We also calculated average wind speed at 1000 hPa during January and February across all 25 years to illustrate the role of the wind-driven Ekman velocity component. Wind data were obtained from ECMWF Reanalysis v5 (ERA5) monthly averaged data (Hersbach et al. 2023).

To assess temporal variability in retention, we calculated the fraction of particles that remained inshore of the 2000 m isobath after 30 days for each year and across all years combined. As a model evaluation exercise, we compared predicted yearly retention to observed pelagic juvenile rockfish abundance to assess the relationship between retention and survival to the pelagic young-of-the-year (YOY) stage. We used YOY rockfish abundance indices derived from the Rockfish Recruitment and Ecosystem Assessment Survey (RREAS; Figure 2.1). This

fixed-station survey collects 3-4 month old pelagic YOY rockfish off California using a midwater trawl (target depth of 30-40 m), and has been conducted in the late spring each year since 1983 (Ralston et al. 2013). Importantly, this is the time frame when larvae spawned in the winter would become pelagic juveniles. Since 2004, the survey effort expanded to include the entire U.S. West coast, including the SCB (Field et al. 2021). We used RREAS data from the years 2004 to 2022, and analyzed pelagic YOY rockfish abundances from stations between 36.3° N and 32.7° N, the region encompassing the south-central and southern regions of the survey (Figure 2.1). For each year, we calculated the arithmetic mean YOY rockfish abundance among all stations. We then performed Z-score normalization to standardize abundances to a mean zero and unit standard deviation. We compared rockfish yearly retention with abundance for the years 2004-2022, excluding 2011 and 2020 due to reduced RREAS sampling in those years (Santora et al. 2021).

To investigate spatial variability in retention, we calculated the number of particles seeded within each 0.25° x 0.25° grid cell that were subsequently retained inshore of the 2000 m isobath, divided by the total number of particles seeded within that grid cell. To visualize results, we mapped rockfish particle distributions. To account for varying shelf width throughout the study region, we computed the least-cost distance to shore for each grid cell (shortest distance from each grid cell to the nearest coastline grid cell). If distance to the coast explained the spatial patterns of retention, then we would expect that particles seeded farther from shore would be less likely to end up retained inshore of the 2000 m isobath, and particles seeded close to shore would be more likely to be retained. We multiplied the fraction of particles retained by the least-cost distance to shore for each grid cell to determine whether proximity to the coast could explain the spatial variability in the fraction retained. If the retention fraction was inversely related to the

distance to coast, then we would expect to see a relatively homogeneous distribution of the multiplication product, as small retention fractions would be multiplied by large distances, and large retention fractions would be multiplied by small distances. Similarly, we performed the same analysis using distance to the 2000 m isobath instead of distance to the coast. For this case, we divided retention by distance to the 2000 m isobath, as locations close to the boundary would likely have low retention, and locations far from the boundary would have high retention.

We also explored the transport pathways of particles that were seeded specifically within the CCAs. We examined both the final distributions of particles seeded in the CCAs as well as the seeding locations of particles that ended up in the CCAs. The fraction of particles retained was calculated as the number of particles that were seeded within the CCAs that remained inshore of the 2000 m isobath, divided by the total number of particles that were seeded within the CCAs.

2.4 Results

Velocity product evaluation

Temporally averaged geostrophic and geostrophic + Ekman 15 m velocities over 25 years (1998-2022) were similar (Figure 2.2a and 2.2b). While the Ekman component was minimal in winter in the CCS due to weak winds, it added a weak southwest flow component to the geostrophic velocities (Figure 2.2c). At equilibrium, surface Ekman currents are directed 45° to the right of the wind vector in the northern hemisphere, and total Ekman transport is directed 90° to the right of the wind vector. Ekman currents at 15 m were directed between 45-90° to the right of the wind vector. The southwestern flow attributed to the Ekman 15 m velocity component aligned with expectations, given the mean wind vectors which were strongly directed to the southeast (Figure 2.2d).

North of Point Conception (~34° N), there was strong northward flow along the coast that was part of a cyclonic circulation pattern. South of Point Conception, in the center of the SCB, flows appeared more chaotic and weaker in and around the Channel Islands. Off San Diego (-117° W, 32.5° N), the temporally averaged velocities appeared strong and directed southward. We opted to analyze the particle tracking simulations forced by geostrophic + Ekman 15 m velocities: the focus of our work is to determine offshore transport, and the Ekman currents can play a large role in advecting particles offshore. The particle distributions were similar between both velocity products, with the simulations using geostrophic + Ekman 15 m velocities resulting in particle distributions shifted southeast compared to the simulations forced by geostrophic velocities (Supplemental Figure 2.3). We include the results of the particle tracking simulations using geostrophic currents in Supplemental Figures 2.4 – 2.6 and Supplemental Table 2.1 in the Supplementary Material.

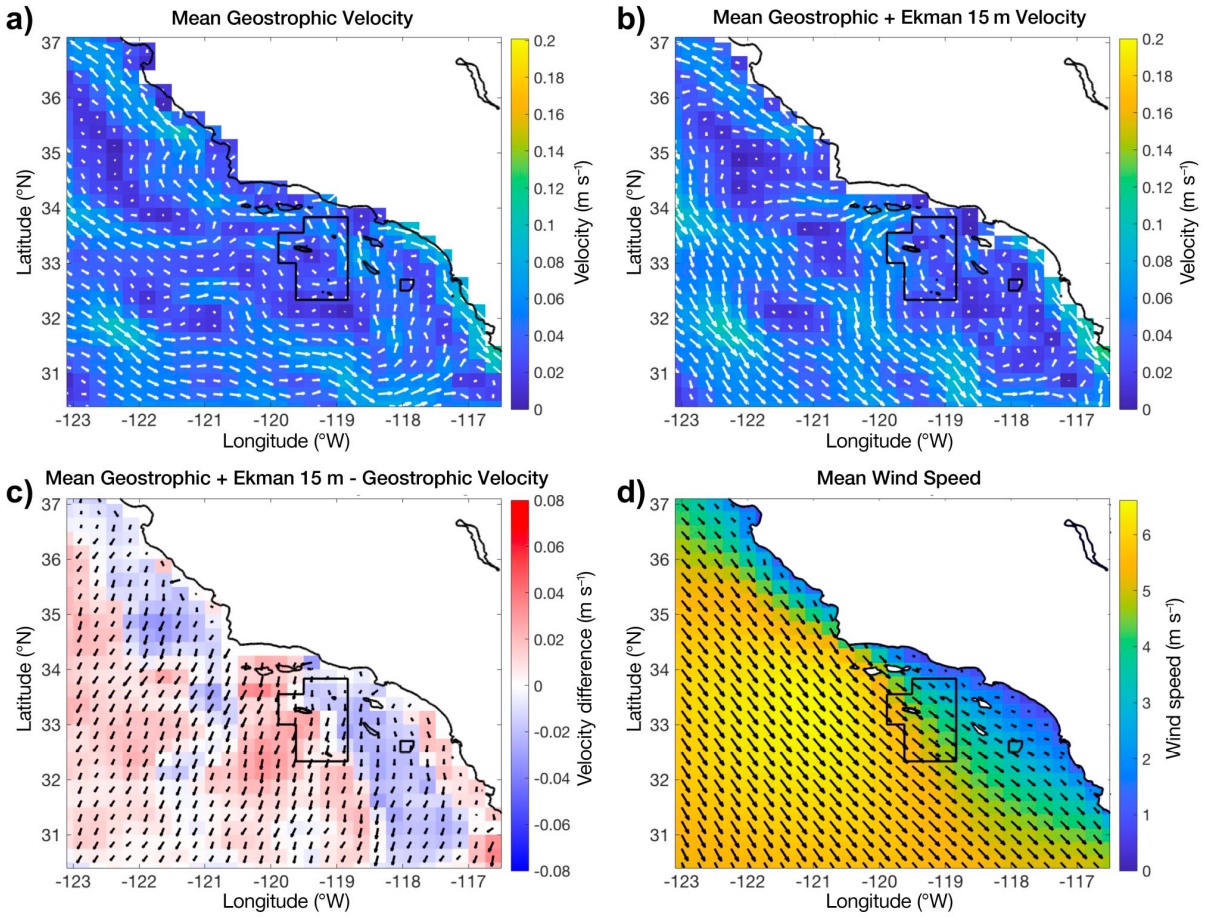

Figure 2.2: Average velocities over 25 yr during January and February for (a) geostrophic velocities; (b) geostrophic + Ekman 15 m velocities; (c) average geostrophic + Ekman 15 m velocities minus average geostrophic velocities (b – a); and (d) 25 yr average wind speed during January and February at 1000 hPa. Black boxed outlines: Cowcod Conservation Areas. Arrows are scaled according to the magnitude represented in the colors.

Particle tracking and rockfish fates

The final locations of particles after 30 days spanned from 27° N to 40° N, and from the coast to well offshore of the 2000 m isobath, up to 570 km from the coast. Particles spread relatively evenly northward and southward, with the farthest particle extending beyond the seeding domain 385 km north and 398 km south. Maps of the final locations reveal greater

concentrations of particle final locations within the seeding region, and enhanced concentrations in the SCB (Figure 2.3).

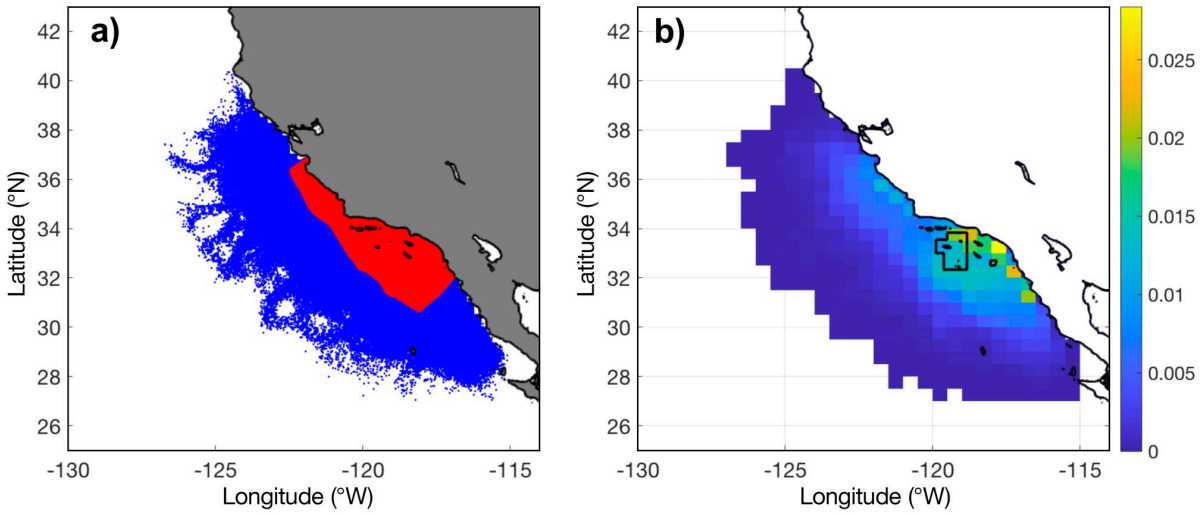

Figure 2.3: (a) Seed locations of all rockfish larval particles (red) and final locations of all particles after 30 d advection (blue); (b) distributions of final locations of all particles; color corresponds to the percentage of total particles found in that grid cell.

Spatial patterns of mean net and gross distance traveled by particles were similar. Particles seeded near the 2000 m isobath were advected farther in terms of both net and gross distance traveled. Minimum distances traveled were found near the coast and within the SCB (Figure 2.4a and 2.4b). The mean net-to-gross displacement ratio was highest in the SCB, along the coast near San Diego (Figure 2.4c). This high net-to-gross displacement is consistent with particles seeded in this region traveling relatively linearly. In contrast, other regions in the interior of the SCB showed lower net-to-gross displacement ratios, consistent with more tortuous trajectories.

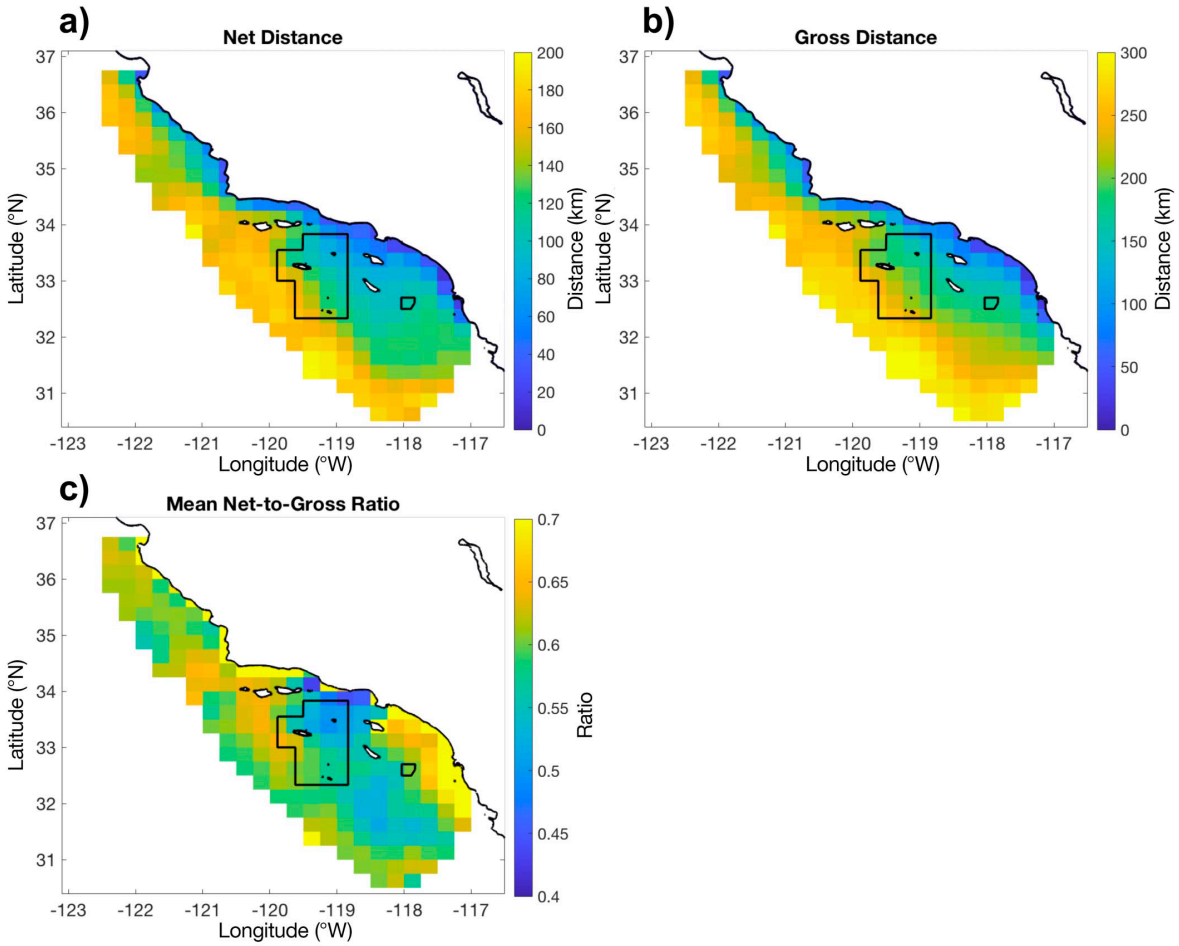

Figure 2.4: Mean (a) net, (b) gross, and (c) net-to-gross displacement ratio of distance traveled of rockfish larval particles seeded within each grid cell.

The fraction of larvae retained was highest in the SCB, close to the coast (Figure 2.5). The spatial patterns of the fraction retained were not perfectly inversely related to the distance to the coast or to the 2000 m isobath (Figure 2.5). In general, retention was highest close to the coast and far from the 2000 m isobath (Figure 2.6). For a given distance both to the coast and to the 2000 m isobath, there was a range of retention values associated with that distance (Figure 2.6). Distance to the 2000 m isobath explained more of the variability in retention than distance to coast, with a trend of increasing retention with increasing distance to the 2000 m isobath. The

R^2 values of a cubic polynomial fit to retention and distance to shelf, and retention and distance to coast were 0.84 and 0.22, respectively. However, right at the boundary of the 2000 m isobath (0 km away), there was still a range of 0.39 in retention values, indicating that proximity to geographic boundaries does not explain all of the variability in retention.

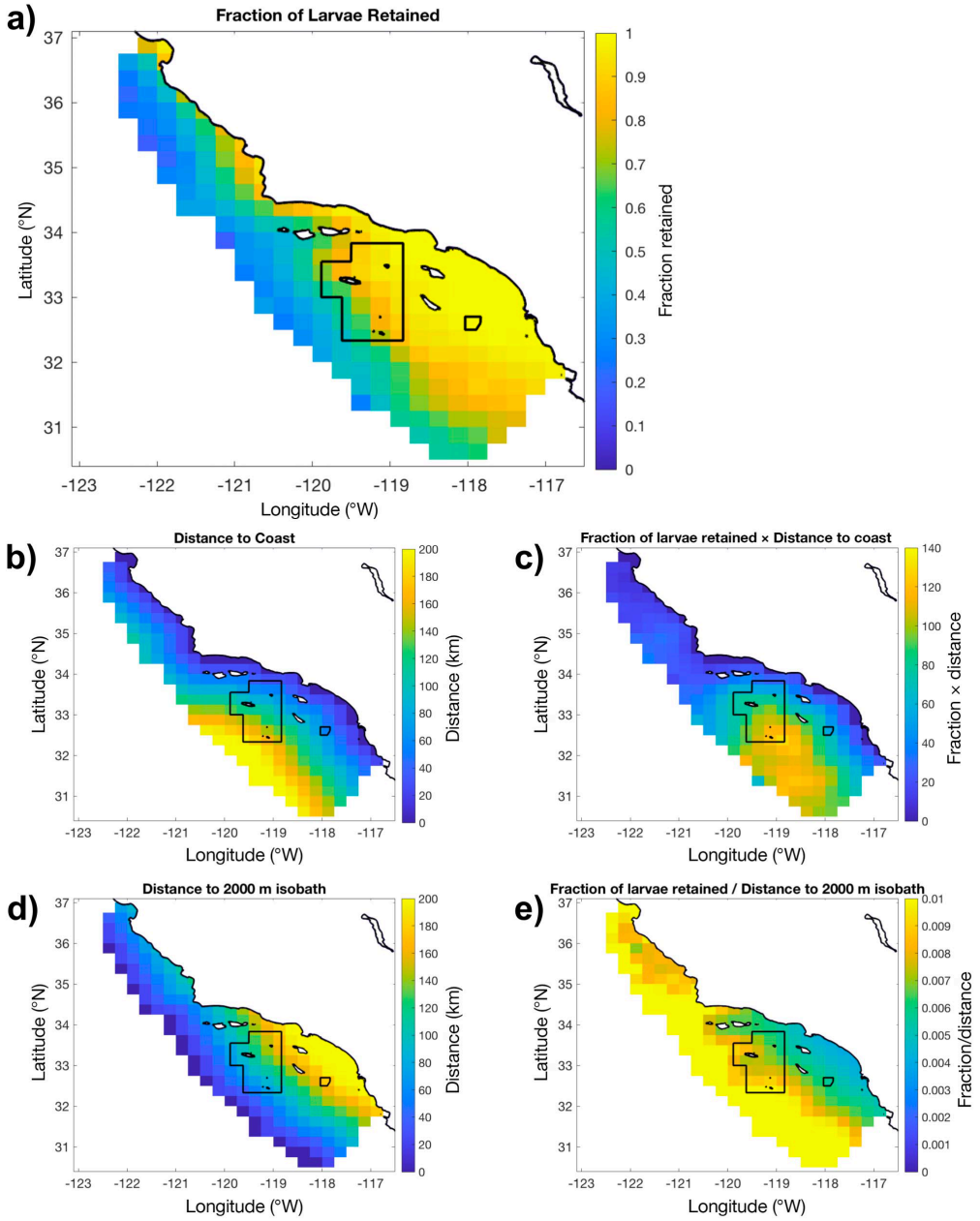

Figure 2.5: (a) Fraction of rockfish larvae seeded within each 0.25° × 0.25° grid cell that were retained inshore of the 2000 m isobath; (b) distance to coast for each 0.25° × 0.25° grid cell; (c) fraction of larvae retained multiplied by distance to coast; (d) distance to 2000 m isobath for each 0.25° × 0.25° grid cell; and (e) fraction of larvae retained divided by distance to 2000 m isobath.

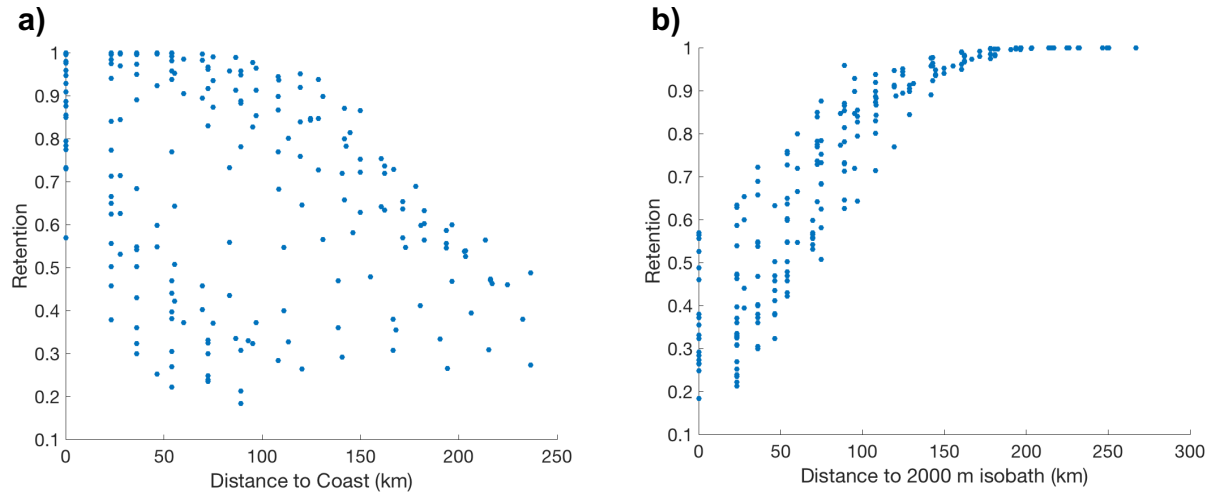

Figure 2.6: Retention of rockfish larval particles vs. (a) distance to the coast and (b) distance to the 2000 m isobath.

Table 2.1: Fraction of larvae retained inshore of the 2000 m isobath for each year and all years combined. Geostrophic + Ekman 15 m velocity fields were used to force the simulations.

Year	**Fraction Retained**
1998	0.82
1999	0.71
2000	0.86
2001	0.77
2002	0.67
2003	0.68
2004	0.69
2005	0.75
2006	0.65
2007	0.71
2008	0.76
2009	0.76
2010	0.75
2011	0.74
2012	0.64
2013	0.71
2014	0.71
2015	0.74
2016	0.73
2017	0.80
2018	0.65
2019	0.79
2020	0.58
2021	0.62
2022	0.51
All years	**0.71**

The fraction of particles retained across all years was 0.71 (Table 2.1). Interannual variability in retention ranged from 0.51 to 0.86. Distributions of particles that started or ended in the CCAs revealed specific patterns of transport associated with these regions. Particles seeded in the CCAs were primarily transported southeast (Figure 2.7a), although there was also a relatively high fraction of particles that were transported north and northeast to coastal habitats. Across all years combined, 19 percent of particles seeded in the CCAs ended up in the CCAs after 30 days. Of particles seeded outside of the CCAs, five percent of them were advected into the CCAs. Particles that ended in the CCAs after 30 days originated most frequently within the CCA and SCB (Figure 2.7b). Regions south of the CCAs sourced particles to the CCAs more than regions north of the CCAs, with minimal contributions (0.1% of the particles that ended up within the CCAs) originating from north of Point Conception (Figure 2.7b). These observations align with the patterns of mean flow; Point Conception delineates a boundary in flow, with particles that originated north of this topographic feature likely to be advected north or west, but not south (Figure 2.2).

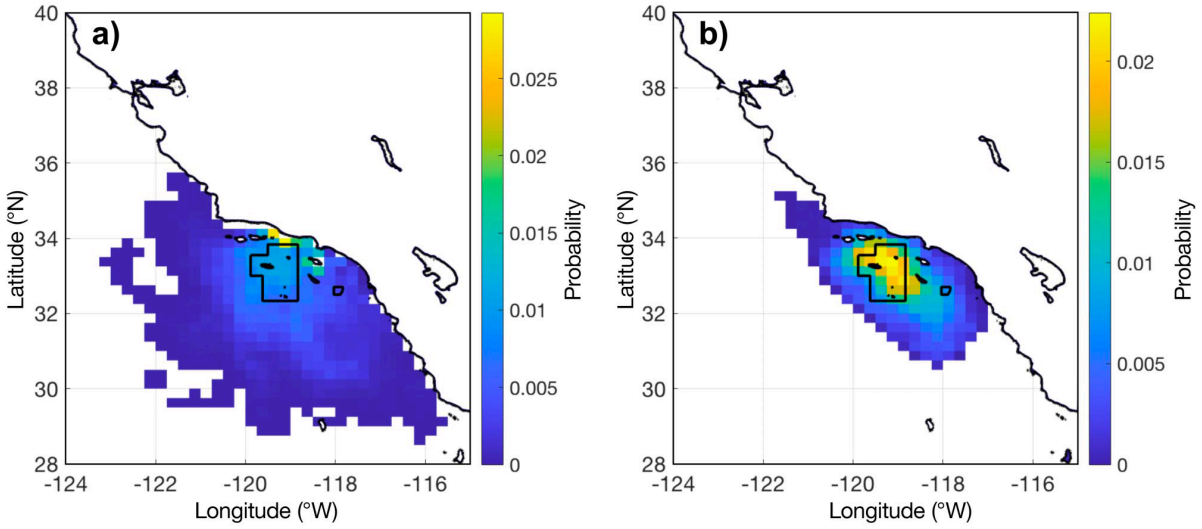

Figure 2.7: Distributions of (a) final locations of rockfish larval particles that started in the Cowcod Conservation Areas and (b) seed locations of particles that ended in the Cowcod Conservation Areas.

Yearly larval retention values were higher during observed high YOY abundance years (mean standardized abundances greater than 0) than during low YOY years (mean standardized abundances less than 0; Figure 2.8). High YOY abundance years occurred during 2005, 2010, and 2013-2017 (Figure 2.8a). Years of high YOY abundances were only associated with high retention values, while years of low YOY abundances corresponded to a wider range of retention values, including lower values. High YOY abundance years had retention fractions ranging from 0.71 to 0.80, while low juvenile abundance years corresponded to retention values ranging from 0.51 to 0.79 (Figure 2.8b). Retention values were significantly different between years of high and low juvenile abundance (*t*-test, $t = -2.213$, $p = 0.047$).

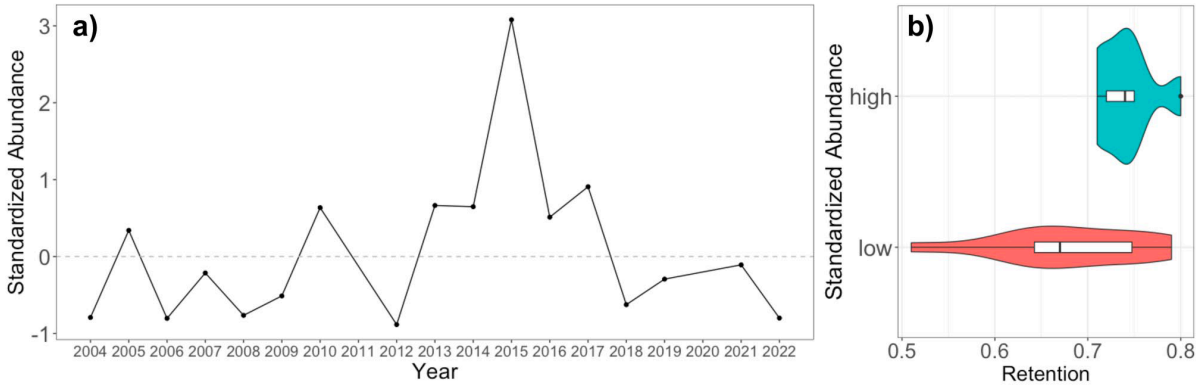

Figure 2.8: (a) Rockfish pelagic young-of-the-year standardized abundance over 2004–2022; (b) violin plots with inset boxplots illustrating retention values for high versus low abundance years. Boxplots display the 25th, median, and 75th percentiles. High and low abundances are defined by mean standardized abundances greater than 0 and less than 0, respectively.

2.5 Discussion

We investigated the spatial and temporal variability of larval rockfish transport and retention using a Lagrangian particle tracking model to assess scales of variability over 25 years. We evaluated our model with fishery independent observations of juvenile rockfish abundance and found higher recruitment coincides with higher retention rates. The numerical simulations and summary statistics illustrate potential dynamics of rockfish larval transport during winter, revealing differences across biogeographic provinces that are separated by a coastal promontory, and highlighting the importance and success of previous conservation and fishery management areas. Our simulations and analyses serve as relatively simple tools to increase our understanding of the role of mesoscale ocean circulation and retention patterns on larval success, and ultimately, recruitment.

Temporal patterns of transport

Larval survival and recruitment are functions of hydrodynamic and biological factors across many temporal and spatial scales (Houde 1987, Houde 2008, Hare 2014). The dominant

components of flow relevant to our study of month-long passive advection of larvae were geostrophic and Ekman velocities (Parrish et al. 1981). Although wind-driven upwelling and Ekman transport is minimal in the winter in the CCS (Chelton et al. 2007), Ekman velocities still contribute a flow component directed to the southwest (Figure 2.2). One life history strategy to minimize advection offshore is spawning during the winter, when upwelling and offshore transport is weak (Parrish et al. 1981, Taylor et al. 2004, Giddings et al. 2022). Even with the inclusion of Ekman velocities, our simulations suggest a high degree of overall retention of larvae in the winter; this suggests the effect of Ekman flow is not strong enough during January and February to counteract the geostrophic currents. Retention varied interannually, and in all years a majority of larvae released were retained inshore of the 2000 m isobath after 30 days. The years with the lowest retention (2020 and 2022) had mean velocities within the study region with a significant westward component: northwest and southwest, respectively (294°, 0.025 m s^{-1} and 241°, 0.024 m s^{-1}; Figure 2.9). The highest retention years (1998 and 2000) had weak mean velocities or eastward components: southeast and south (142°, 0.030 m s^{-1} and 180°, 0.00064 m s^{-1}; Figure 2.9). A strong offshore component leads to less retention due to the offshore transport of larvae.

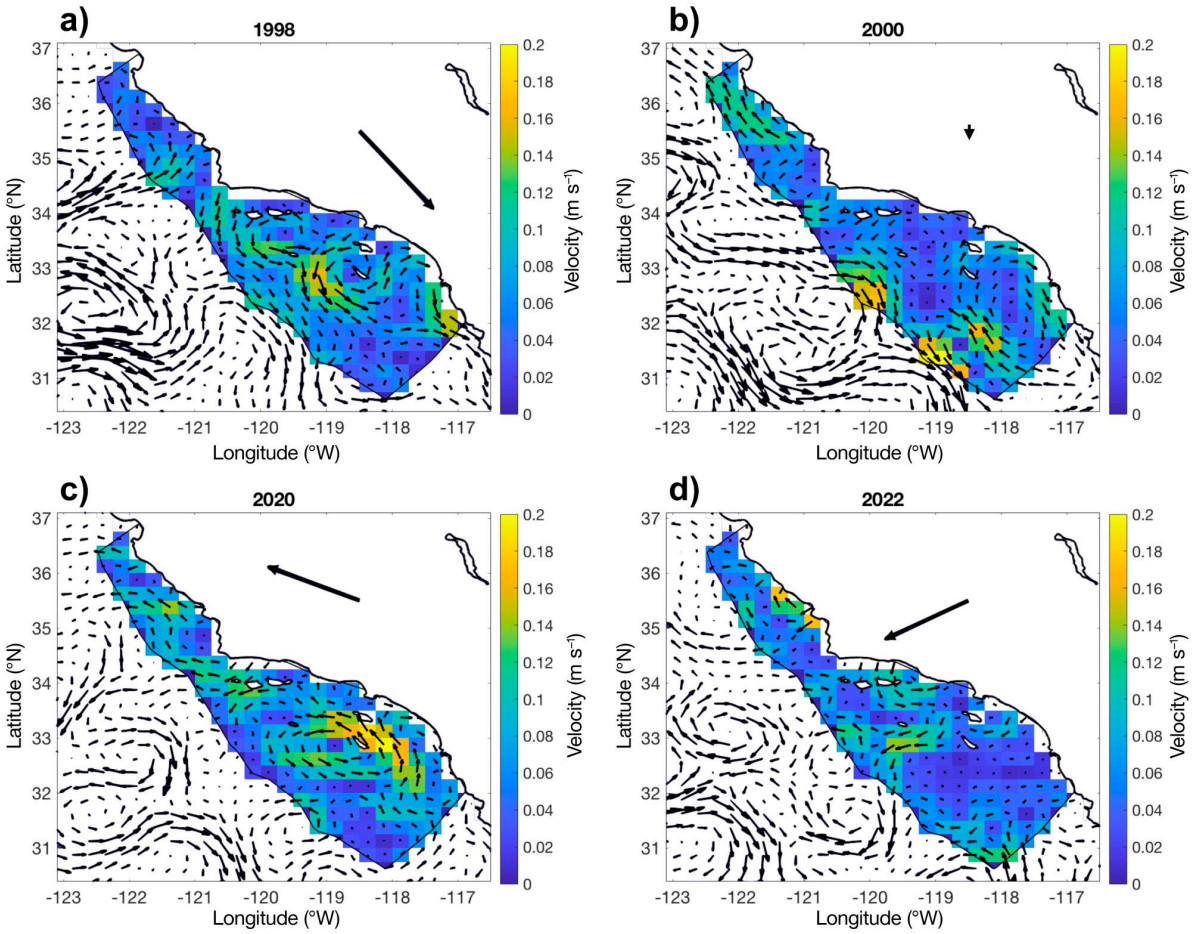

Figure 2.9: Mean geostrophic + Ekman 15 m currents from the first 61 d of each year, (corresponding with the days used in the rockfish larval particle tracking simulations) for (a,b) the 2 years with the highest retention, and (c,d) the 2 years with the lowest retention. Black arrows: direction of the mean velocity in the study region, scaled by magnitude.

Spatial patterns of transport

Our analyses support the idea that the SCB is a highly retentive region within central and southern California waters (Taylor et al. 2004). The retention and transport of larvae depended on the location of the initial release site. The spatial patterns of the net-to-gross displacement ratio reflect patterns observed in the time-averaged current velocities. The region with the highest mean net-to-gross displacement ratio was found along the coast of San Diego (between -118° W to -119° W and 31° N to 33° N), where strong mean flows were directed persistently to

the south. High net-to-gross displacement ratios were also observed southeast of Point Conception (~34° N), where strong, westward flows dominated the mean velocity field, as well as along the coast north of Point Conception, where northward velocities were strong and relatively free of eddies and meanders. In the interior of the SCB, the low net-to-gross displacement ratios corresponded to the weak and chaotic flow patterns characteristic of the interior of the Southern California Eddy. The Southern California Eddy is a semi-persistent feature in the SCB. It is present July through January, and is less prominent February through May, with periodic dissolution of the eddy most frequently occurring in April (Owen 1980, Lynn and Simpson 1987). Eddies can retain larvae (Owen 1980, Fiedler 1986, Nishimoto and Washburn 2002, Bakun 2006, Nishimoto et al. 2019). Thus, the Southern California Eddy may facilitate larval retention (Taylor et al. 2004), as evidenced by the low net-to-gross displacement ratios and high retention of particles seeded in the interior of the SCB. Conversely, the high net-to-gross displacement ratios off San Diego may be attributed to its mean southward transport and being located outside of the Southern California Eddy (Mitarai et al. 2009). In addition to Ekman transport being weakest in the winter, our analyses suggest that the stability of the Southern California Eddy in the winter is another characteristic of the hydrodynamic field that makes spawning in the winter advantageous.

The variability in the fraction of particles retained was not explained solely by the distance to the coast or distance to the 2000 m isobath, suggesting that interannual spatial variability in ocean circulation patterns influenced the resulting retention patterns. Fennie et al. (2024) found that rockfish larvae that were collected farther from fishing ports and in years when mothers were exposed to Pacific Subarctic (California Current) water were born larger – an indicator of larval condition. Larvae that are born farther from fishing ports, such as those in the

CCAs, may be in better condition due to a greater relative abundance of larger, older spawning females (due to less fishing pressure), and may benefit from habitat conditions including the colder, low salinity characteristics of Pacific Subarctic Upper Water (Miller et al. 2014, Schroeder et al. 2019, Fennie et al. 2024). Our analyses identified where larvae were both more likely to be born in good condition (farther from shore) and more likely to be retained (higher retention). The intersection of locations that are both far from the coast and have high retention suggest a mesoscale hotspot location within the SCB (high values in Figure 2.5c), where larvae are likely to be in better condition and also remain inshore of the 2000 m isobath (Fennie et al. 2024). This hotspot slightly overlaps with the CCAs, although the core of the hotspot is south of the designated protected areas (Figure 2.5c). Our analyses also revealed the larger CCA as a high retention area, given its proximity to both the coast and the 2000 m isobath (Figure 2.5c and 2.5e). These findings have important management implications, as conserving quality habitat relies on understanding the location and size of optimal areas from a number of different perspectives, including but not limited to, retention and quality of larvae (Caselle et al. 2003, White et al. 2014).

Our analyses underscore Point Conception as a topographic feature that defines a significant transition in the flow and the resulting larval transport. Point Conception has been recognized as a major biogeographic boundary that separates the region into distinct circulation patterns (Gaylord and Gaines 2000, Checkley and Barth 2009, Gottscho 2016). Dispersal, growth, and connectivity of many planktonic organisms are affected by this oceanographic feature (Gaylord and Gaines 2000, Blanchette et al. 2007). The southward-flowing California Current separates from the coastline as it passes Point Conception (Hickey 1979). This divergence of flow forms the semi-persistent cyclonic Southern California Eddy (Owen 1980).

We found that larvae originating north of Point Conception were unlikely to be transported into the CCAs within the SCB (Figure 2.7b). Similarly, Field et al. (2021) found that pelagic YOY rockfish abundance in the SCB varied out of phase from abundance trends between Point Conception and Cape Mendocino to the north. Moreover, Nishimoto et al. (2019) conducted particle tracking simulations of larvae released from oil platform sites in the SCB and found that the potential for larvae to travel from southern locations to northern locations was greater than the potential for larvae to move from north to south. The CCAs, therefore, are sources of larvae that likely remain primarily within the SCB. Ideally, marine reserves should be strategically placed in locations where larvae are produced and dispersed to other nearby regions, while also reseeding the reserves with new adults (Pelc et al. 2010, Hitchman et al. 2012, Andrews et al. 2021). While our analyses cannot reveal where more mobile pelagic YOY rockfish will settle, the transport patterns show that larvae seeded in the CCAs are primarily retained inshore of the 2000 m isobath and transported to regions adjacent to the CCAs (Figure 2.7a). These findings suggest that the placement of the CCAs was favorable from a spatial management perspective, as larvae born in the CCAs would seed surrounding regions, including coastal areas more accessible to fishing. Previous work has illustrated the effectiveness of the CCAs by showing that these marine protected areas are associated with higher abundances, species richness, and enhanced diversity of rockfish species (Hitchman et al. 2012, Thompson et al. 2016, Freeman et al. 2022). The effectiveness of the CCAs is likely a function of both habitat and circulation, as well as reduced fishery removals due to their distance from port (Miller et al. 2014). Lagrangian particle tracking simulations provide a new source of evidence supporting the placement of these spatial management areas, adding context to their success in both maintaining and rebuilding rockfish

populations in this region by virtue of their role in reseeding both the CCAs as well as adjacent areas that remained open to fishing during the period of rockfish rebuilding.

Relationship between retention and recruitment

Density-independent environmental processes drive most of the variability in year-class strength of marine fishes, including rockfish, during the first 30 days of their life (Johnson 2006, Houde 2008, Field et al. 2010, Ralston et al. 2013), and these processes likely include ocean circulation patterns (Hjort 1926). Pelagic YOY abundances in central and southern California increased beginning in 2013 and remained high throughout the marine heatwave of 2014-2016 (Wells et al. 2017, Schroeder et al. 2019, Field et al. 2021). We hypothesized that retention of larvae, driven by ocean circulation, would be positively correlated with recruitment to the pelagic juvenile stage. If more larvae were retained, the abundance of larvae surviving to the juvenile stage would likely be higher. We tested this hypothesis by comparing interannual retention probabilities to abundances of YOY rockfish collected on the continental shelf 3-4 months after being born. In our study, there was not a single high abundance year during years of low retention. Low abundances that occurred during years of high retention were very likely due to other factors, such as greater starvation or predation mortality, poor temperature regimes, or factors related to food availability (Houde 2008, Hare 2014, Morales 2023, Swalethorp et al. 2023). In other words, retention appears to be an important factor in determining the potential for high juvenile abundances several months later. While other works have illustrated the importance of the environment and physical flow to rockfish juvenile abundances (e.g., Ralston et al. 2013; Schroeder et al. 2019), our simulations of larval transport directly link larval retention and juvenile abundances by identifying the mechanism responsible.

Recruitment is a complex function of hydrodynamic and trophodynamic factors that operate at various spatial and temporal scales (Houde 2008, Caselle et al 2010). Even if rockfish larvae are advected offshore, pelagic juveniles are competent swimmers and may be capable of returning shoreward by moving deeper in the water column where flow is directed onshore (Lenarz et al. 1991). Indeed, this likely occurred in 1999 when pelagic YOY abundance in central California was low but very large year classes were observed in the fisheries for nearly all rockfish species a few years later (Field et al. 2010, Ralston et al. 2013, Stachura et al. 2014). Therefore, while it is unlikely that juvenile abundance is solely a function of larval retention, our results suggest that retention is often a critical prerequisite to successful recruitment.

Limitations

Our analyses provide insight into larval transport and retention, with larvae randomly seeded throughout the entire study region to investigate potential transport. However, to comprehensively understand transport, we require a finer scale understanding of the spatial distributions and variability of larval rockfish spawning areas. If locations that we identified as having large fractions of larvae retained do not have a high number of larvae being produced there, these locations will not necessarily be important hotspots of retention or recruitment. Future work should take into account spatial variations in larval production to gain a better understanding of hotspots for production and associated retention (Taylor et al. 2004).

Future work would also benefit from a greater exploration of how larval transport and retention vary seasonally. Although the winter months are the peak of spawning activity for most winter-spawning rockfish, spawning can take place from mid-fall through the spring for most species, with many of the winter spawning rockfish in this region spawning multiple times

during favorable environmental conditions (Lefebvre et al. 2018, Holder and Field 2019, Beyer et al. 2021). Other work has shown that particle dispersal patterns show strong seasonality in the SCB, and releases of particles just weeks apart can lead to different trajectories (Mitarai et al. 2009). A greater understanding of the extent to which the advection and retention patterns observed in the SCB represent the entire spawning season would be beneficial in developing quantitative metrics to inform future recruitment studies; however, this was beyond the scope of this research effort.

We used satellite-derived velocity products to force our particle tracking simulations. For the mesoscale motions that we are interested in, satellite-derived velocities enable a synoptic understanding of the mesoscale patterns of flow (Parrish et al. 1981). Additionally, because rockfish larvae tend to be found in the upper layer of the ocean, and, importantly, show no evidence of vertical migration (Sakuma et al. 1999), they are well suited for simulations that use satellite-derived geostrophic and Ekman velocities, which resolve the upper water column. Petersen et al. (2010) conducted numerical simulations to investigate rockfish transport along the central California coast. They used the Regional Ocean Modeling System and tracked particles along five different isobaths, from 1 m to 70 m. The particles tracked in the winter showed coherent patterns of transport at all depths and aligned with our observations of northward particle transport of particles released in central California (Petersen et al. 2010).

A limitation of satellite-derived current velocities is they do not accurately reproduce near-coastal dynamics. Smaller-scale components of flow which likely affect larval transport, such as nearshore and tidal processes (Pineda 1991), are not examined here. Nearshore flows are more complex than the open-ocean currents that we use here and are influenced by a number of different processes such as buoyancy-driven flows, boundary-layer effects, bathymetry, and

surface gravity waves (Pineda et al. 2007). We focused our analyses on large spatial scales spanning southern and central California and from the coast to the 2000 m isobath. Thus, our analyses are applicable for understanding broad trends and patterns in retention and transport, but we caution against interpreting our results on a finer scale. Moreover, coarse velocity field resolutions, such as the resolution used here, have been shown to result in higher retention of particles nearshore (Dauhajre et al. 2019). Away from the coast, satellite-derived velocities may overestimate eddies and underestimate particle dispersal driven by submesoscale flows (Sinha et al. 2019). Additional work using higher-resolution velocity fields (e.g., SWOT; Morrow et al. 2019) should focus on disentangling the finer-scale dynamics of rockfish larval transport in specific regions, though even with higher resolution velocity fields, retention may still be overestimated (Sinha et al. 2019). Regions of interest to focus future studies on are the nearshore coastal region, the CCAs, and the recently created Groundfish Exclusion Areas (eight areas south of Point Conception implemented to protect sensitive habitats; PFMC 2023).

2.6 Conclusions

Disentangling the relationships between larval survival, hydrodynamic factors, and biological factors remains a primary challenge in fisheries oceanography (Hare 2014). The relative importance of physical and biological influences on larval survival has been a topic of debate for over a century, and the answers continue to be elusive (Hjort 1914, Houde 1987, Cury and Roy 1989, Houde 2008). Here, we provide novel insights into rockfish larval transport. Our simple Lagrangian simulations showed that larval retention varies spatially and temporally, driven by differing physical conditions. We found that the SCB is a highly retentive region, owing to its mesoscale circulation patterns and the presence of the Southern California Eddy. Our methods can be applied to species other than rockfishes that have similar passive pelagic

larval stages to understand larval retention and dispersal. Larval retention is a driving factor in setting recruitment strength, with higher retention acting as a prerequisite to high pelagic YOY abundance and ultimate year class strength within adult populations. Moreover, our analyses highlight the efficacy of the design of the CCAs, providing new supporting evidence that their geographic placement was effective for broad dispersal of successful recruits. While a broad array of additional biological and physical forcings play complex roles with respect to survival and dispersal of the early life stages of fishes, our work resolving transport pathways greatly enhances our understanding of the role of hydrodynamics on larval success and recruitment.

2.7 Acknowledgements

We would like to thank the captains, officers and crew of the NOAA ships and chartered survey vessels that made the pelagic juvenile rockfish data collections possible, as well as the many scientists and volunteers who participated and otherwise supported these surveys. We would also like to thank three anonymous reviewers for their insightful comments that improved the manuscript.

Chapter 2, in full, is a reprint of the material as it appears in: Quigley L.A., Franks, P.J.S., Thompson, A.R., Field, J.C., Santora J.A. (2024). Quantifying the fates and retention of larval rockfish through Lagrangian analyses. Marine Ecology Progress Series. The dissertation author was the primary investigator and author of this paper.

2.8 Supplemental Material

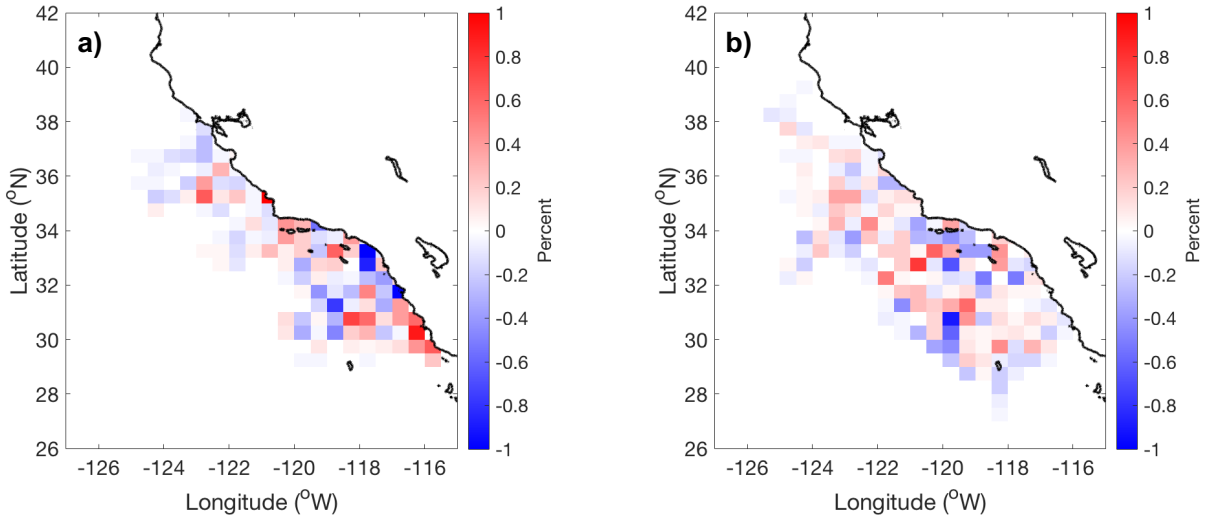

Supplemental Figure 2.1: Results of the sensitivity analysis for hourly vs. daily time steps. Hourly minus daily normalized distributions of final particle locations for 1998 (a) and 2022 (b). Color displays the percent difference between the distributions.

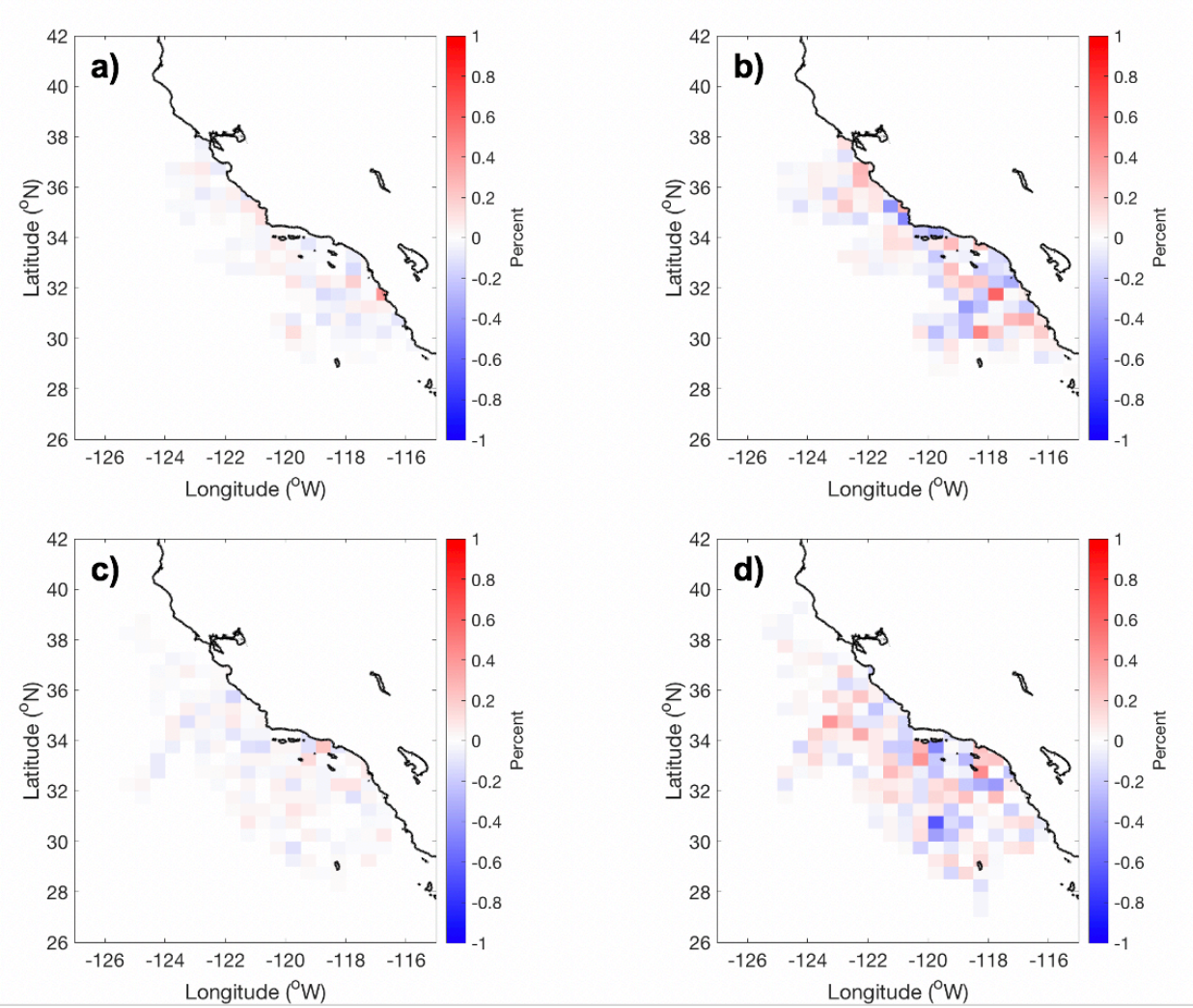

Supplemental Figure 2.2: Results of the sensitivity analysis for advecting 10,000, 1,000, and 100 particles. Normalized distributions of final particle locations for 10,000 minus 1,000 particles (a) and 1000 minus 100 particles (b) for the year 1998. Panels c and d are the same, for the year 2022. Color displays the percent difference between the distributions.

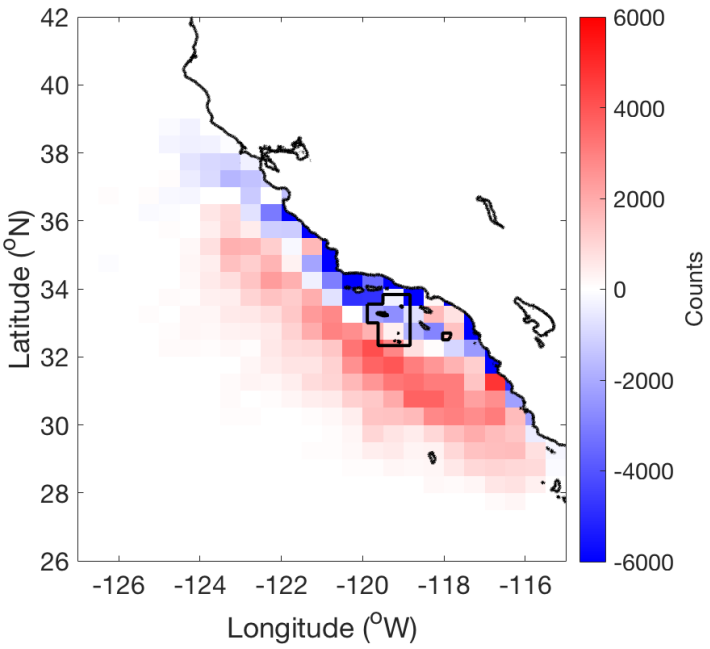

Supplemental Figure 2.3: Difference between final particle distributions of geostrophic + Ekman 15m simulations versus geostrophic simulations. Red values indicate a greater number of particles from the geostrophic + Ekman 15m simulations, and blue values indicate a greater number of particles from the geostrophic simulations

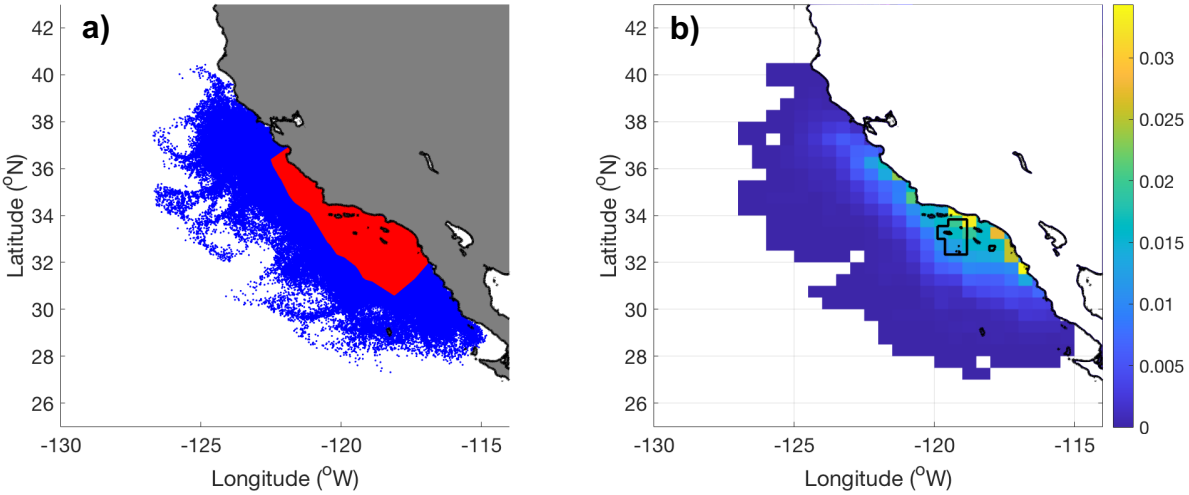

Supplemental Figure 2.4: a) Map of particle seed locations (red) and final locations (blue); b) Histogram of final locations, color corresponds to the percentage of total particles found in that grid cell. Particle simulations are forced by geostrophic velocities.

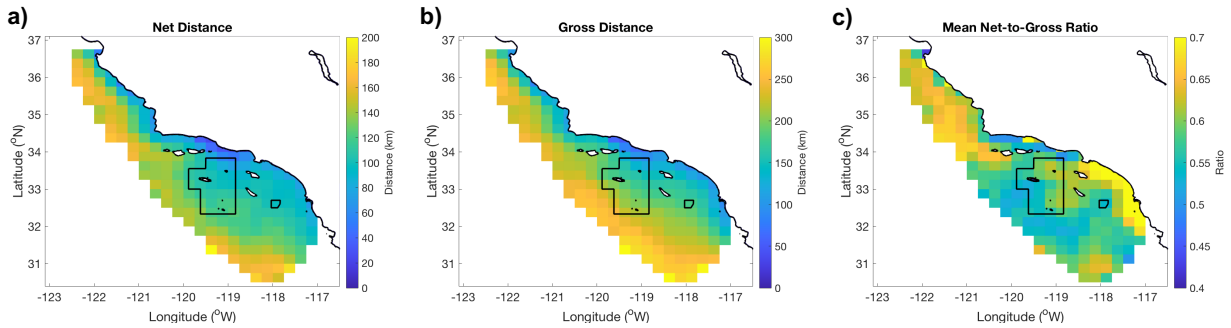

Supplemental Figure 2.5: a) Mean net distance traveled of particles seeded within each 0.25° x 0.25° grid cell; b) mean gross distance traveled of particles seeded within each 0.25° x 0.25° grid cell; c) mean net-to-gross ratio of particles seeded within each 0.25° x 0.25° grid cell. Particle simulations are forced by geostrophic velocities.

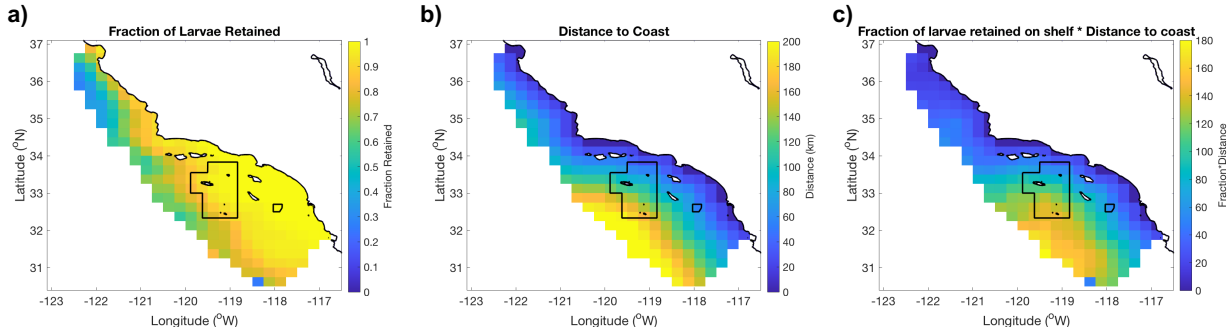

Supplemental Figure 2.6: a) Fraction of larvae seeded within each 0.25° x 0.25° grid cell that were retained on the shelf; b) distance to coast for each 0.25° x 0.25° grid cell; c) fraction of larvae retained on shelf multiplied by distance to coast. Particle simulations are forced by geostrophic velocities.

Supplemental Table 2.1: Fraction of larvae retained on the shelf for each year and all years combined. Geostrophic velocity fields were used to force the simulations.

Year	**Fraction Retained**
1998	0.85
1999	0.86
2000	0.86
2001	0.87
2002	0.87
2003	0.81
2004	0.86
2005	0.81
2006	0.84
2007	0.85
2008	0.84
2009	0.85
2010	0.77
2011	0.84
2012	0.84
2013	0.91
2014	0.88
2015	0.87
2016	0.85
2017	0.84
2018	0.90
2019	0.86
2020	0.83
2021	0.86
2022	0.86
All years	**0.85**

Chapter 3 : Larval transport pathways reveal critical habitat and benefits of a marine protected area to fisheries

3.1 Abstract

Quantifying where marine organisms are born and subsequently disperse to is essential for fisheries management. Many studies use hydrodynamic models to predict larval transport. However, few studies combine empirical data from collected larvae with particle tracking to investigate transport patterns. Here, we conducted Lagrangian particle tracking of rockfish (*Sebastes* spp.) larvae collected in the Southern California Bight over the course of 16 years. Particle tracking was performed forward and backward-in-time, to investigate birth locations and dispersal patterns, respectively. Otolith core width at extrusion was used as a proxy for larval condition at birth. We found that high quality larvae may have been born in offshore locations and subsequently advected throughout the region, including into large marine protected areas (e.g., Cowcod Conservation Areas). Additionally, 24% of larvae that were born in the Cowcod Conservations Areas remained within the reserve boundaries after 30 days, while the majority were advected to surrounding areas, confirming the importance of this source area. Our analyses illustrate the utility of coupling particle tracking methods with *in situ* collections to better identify areas that are hotspots for the production and growth of high quality larvae.

3.2 Introduction

In marine environments, dispersal of organisms with relatively sessile adult life stages is accomplished primarily by movement of larvae (Cowen et al. 2007, Cowen and Sponaugle 2009). When larvae are first born their swimming capacity is poor and dispersal is largely driven by currents (Fisher et al. 2000). Tracking larval movement between birth and either settlement to adult habitat for benthic species or recruitment into the adult population for pelagic species is

central to understanding population and metapopulation dynamics worldwide (Pelc et al. 2010, D'Aloia et al. 2015). In recent decades, the ability to investigate potential larval movement patterns has increased dramatically due to improvements in oceanographic modeling, and there are a multitude of studies following the path of virtual fish particles (Staaterman and Paris 2013). To increase the realism of particle tracking studies, it is helpful to couple models with observed larvae collected in the field; however, this type of research is rare due to logistical restraints and difficulty of organism collection (e.g. Hernandez et al. 2022, Rowe et al. 2022, Suca et al. 2022, Torri et al. 2023). Here, we use aged larvae collected in the field over 16 years to elucidate dispersal pathways of economically and ecologically important rockfish (genus *Sebastes*) species in the Southern California Bight (SCB; Figure 3.1).

Rockfish are a vital component of the marine economy off the west coast of the United States, contributing a significant portion of the approximately $319 million annual commercial and recreational groundfish fishery (Miller et al. 2014, Miller et al. 2017, National Marine Fisheries Service 2024). The SCB has the highest diversity of rockfish in the California Current System (Love et al. 2002). In the late 1990s, decades of high fishing pressure and low recruitment caused several populations to collapse, and multiple species were declared overfished (Berkeley et al. 2004a). In response, two spatial management areas, Cowcod Conservation Areas (CCAs), were established to help rebuild cowcod (*Sebastes levis*), and other species that live in similar habitats to cowcod, by prohibiting most bottom fishing at depths greater than 40 m, in an area approximately 11,130 km^2 (Butler et al. 2003, Dick and He, 2019). This management action, coupled with multiple years of high recruitment achieved the aim of recovering rockfish. In 2019, the cowcod stock was declared rebuilt, and as a result, Amendment 32 to the Pacific Coast Groundfish Fishery Management Plan passed in 2023 (Department of

Commerce 2023), removing most restrictions for recreational fisheries and non-trawl commercial groundfish fisheries in the CCAs.

The success of the CCAs benefited other rockfish species besides cowcod (Thompson et al. 2016, Thompson et al. 2017, Freeman et al. 2022). In theory, marine protected areas (MPAs) should benefit both individuals within the reserve boundaries, and fisheries adjacent to the reserves through the export of individuals to the surrounding region (Beukers-Stewart et al. 2005, Sale et al. 2005, Pelc et al. 2010). Larvae born in MPAs and subsequently transported to surrounding regions where they may settle, provide a recruitment subsidy and are one way of augmenting fisheries (Sale et al. 2005, Lenihan et al. 2021, Bode et al. 2025). Previous research indicates that the CCAs are an important region for rockfish, associated with high adult abundance and larval production (Hitchman et al. 2012, Thompson et al. 2016, Quigley et al. 2024). However, observing and quantifying the spillover of larvae is difficult: empirical evidence is lacking (Sale et al. 2005, Pelc et al. 2010), and there is limited work exploring whether the CCAs actually benefit fisheries through the production of larvae and associated recruitment subsidies to areas accessible to fishing (Thompson et al. 2017).

To understand whether the CCAs provide recruitment subsidies, we need to understand where larvae are born, where they settle, and the dispersal paths that connect these points. Previous studies have identified parturition (i.e. spawning) locations using locations of collected 1-2 day old rockfish larvae, assuming that the larvae had not traveled far from their locations of birth (Taylor et al. 2004, Hitchman et al. 2012, Thompson et al. 2016). However, the potentially strong influence of ocean currents driving larval transport is not typically taken into account. As larvae, rockfish are relatively weak swimmers and highly susceptible to passive dispersal from horizontal ocean currents (Kashef et al. 2014). Vertical shear of the water column may disperse

larvae either to or from habitat favorable to survival, however vertical migration behaviors are not fully understood (Sakuma et al. 1999, Bjorkstedt et al. 2002). Depth-stratified sampling has revealed rockfish larvae are rarely found beneath the upper mixed layer (>80 m depth, Ahlstrom 1959, Lenarz et al. 1991, Schonfeld et al. 2025), suggesting that upper ocean currents influence horizontal dispersal patterns (Petersen et al. 2010). The SCB is a dynamic region with prominent mesoscale circulation features (Checkley and Barth 2009, Bograd et al. 2019): larvae may be advected up to 70 km day^{-1} if entrained in a fast moving jet or filament (Zaba et al. 2021). Therefore, deriving parturition locations from 1-2 day old larvae may result in errors of over 100 km in estimates of where the larvae were born, and such error may be improved through integrating larvae observations with particle tracking studies.

Here, we use Lagrangian particle tracking of collected larval rockfishes to identify potential parturition locations and dispersal patterns through assessment of the influence of ocean currents on advecting larvae. Using a 16-year record of rockfish larvae collected in the SCB, we use backward and forward-in-time particle tracking of virtual particles representing collected rockfish. Additionally, we use growth metrics obtained from otoliths to further identify habitats that were associated with larger larvae. Finally, we analyze simulation patterns in the context of the CCAs and investigate the dispersal of rockfish born in the CCAs. Our methodology provides new insights into the parturition habitat of rockfish in the SCB, illustrates the efficacy of the CCAs, and provides information crucial for fisheries management.

3.3 Materials and Methods

Study area and sample collection

Larval rockfish specimens belonging to eight species were collected at California Cooperative Oceanic Fisheries Investigations (CalCOFI) stations throughout the SCB (Figure

3.1). The California Current flows equatorward along the coast of California, carrying cooler, fresh water from the north, and bifurcates at Point Conception, forming the cyclonic Southern California Eddy (Owen 1980). The interior of the SCB is characterized by complex bathymetry, high productivity, and retention (Nishimoto and Washburn 2002, Checkley and Barth 2009, Quigley et al. 2024).

Larvae were collected during winter (January-February) CalCOFI cruises from 1998-2013, as described in Thompson et al. (2017). Samples were collected using a 0.71 m diameter, 505 μm-mesh bongo net towed obliquely from a depth of 210 m to the surface at stations in the SCB and stored in 95% ethanol. Larvae were sorted and counted, and DNA barcoding of the mitochondrial cytochrome b gene was conducted on fish tissue to allow rockfish species identification as described in Thompson et al. (2017). Individual larvae were then stored in vials containing 95% ethanol.

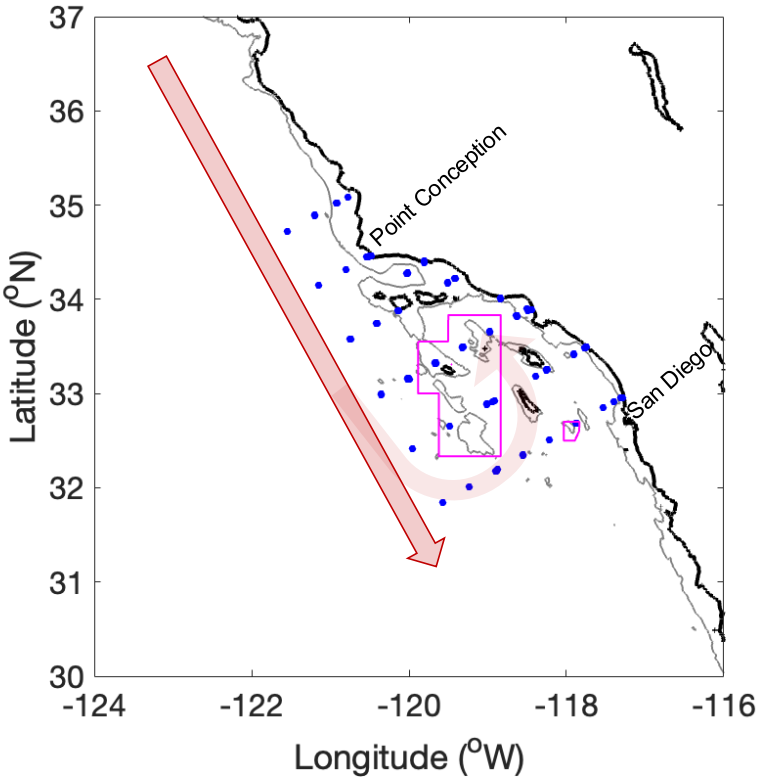

Figure 3.1: Study region off Southern California, depicting the collection locations of rockfish larvae (blue dots). The 400 m isobath is denoted by the thin gray contour line. The Cowcod Conservation Areas are shown outlined in pink. The California Current is illustrated by the red arrow; the Southern California Eddy denoted by the light red curved arrow.

Otolith preparation

Otoliths were extracted from collected rockfish as described in Fennie et al. (2024). Otoliths are calcareous structures found in teleosts, and are commonly used to quantify age and growth, as rings are laid down daily forming micro-increments (Campana and Neilson 1985). Micro-increment counts give reliable estimates of ages in days, and the width of increments is often used as a proxy for fish somatic growth, as otolith growth is typically coupled with fish growth (Morales-Nin 2000, Fennie et al. 2024). Briefly, sagittal otoliths from 2021 specimens belonging to eight species (*Sebastes goodei*, *S. mystinus*, *S. paucispinis*, *S. rufus*, *S. serranoides*,

S. hopkinsi, *S. jordani*, and *S. wilsoni*) were extracted and affixed to a microscope slide. Otoliths were photographed and analyzed using the R package RFishBC (v0.2.4; Ogle 2022). Otolith growth increments were assumed to be deposited daily, as daily increment validation has been conducted for a number of rockfish species (Laidig et al. 1991, Woodbury and Ralston 1991). Otolith core width and increment widths were measured, and the number of increments after the extrusion mark was counted to estimate age (in days). Quality control was performed by reading an otolith twice, and if the reads differed, a third read was performed. Samples with disagreement between the three reads were eliminated from further analyses. A total of 1497 samples within the study region were selected for further analysis. Fennie et al. (2024) found that otolith core width was significantly and positively related to larval size-at-extrusion for all eight species examined here, recent growth rate for five out of seven species tested, and survival for all eight species. Otolith core width thus was used here as an indicator of larval condition at parturition, with larger core widths indicating higher quality larvae.

The rockfish species used in this study differ in longevity and depth range and other life history characteristics (Fennie et al. 2024). With the exception of *S. jordani*, which tends to occupy mid-water habitats, all are demersal as adults and associate with rocky reef habitats, typically at bottom depths shallower than 400 m (Lenarz 1980, Love et al. 2002, Fennie et al. 2024). Importantly, all eight species were collected throughout the study region and likely have similar upper water column depth distributions during the pelagic larval stage (first 30 days of life) that we focus on here (Ahlstrom 1959, Lenarz et al. 1991), thus, individuals from all species were grouped together for further analyses. Core widths were significantly different between species (ANOVA, p-value < 0.001). To analyze all species together, we used a normalization to rescale individual core widths between 0 and 1. To calculate the normalized core width, we

subtracted the species' minimum core width and divided it by the range of the species' core widths. We used the normalized core width for all analyses.

Lagrangian particle tracking

We used forward and backward-in-time Lagrangian particle tracking of virtual particles representing rockfish larvae. To estimate parturition locations, particles were seeded at larval collection locations and advected backward in time. The number of otolith increments is a measure of the larval age since extrusion; thus, individual larvae have direct age estimates at their collection locations. The age (in days) estimated by the otolith readings determined the duration of the simulation, with backtracking ending when the larva reached age 0. To estimate final locations after 30 days, particles were seeded at larval collection locations and advected forward in time until each larva would have been 30 days old. Simulations were performed using a time step of 1 day. Previous work comparing time steps of 1 day and 1 hour in the same region showed no significant difference in particle advection, so we used daily time steps for computational efficiency (Quigley et al. 2024).

All larvae used in this study were 24 days old or younger, as determined by the number of otolith increments. Trajectories run backward in time were thus performed on rockfish that had limited swimming ability, no vertical migration, and were likely present in the upper 80 m (Love et al., 2002, Lenarz et al. 1991, Moser and Boehlert 1991, Sakuma et al. 1999). Thirty days was chosen as the rockfish pelagic larval duration (Petersen et al. 2010, Nishimoto et al. 2019, Quigley et al. 2024), after which, we assume that rockfish larvae begin to develop pelagic juvenile characteristics and are capable of outswimming horizontal currents (Kashef et al. 2014).

We use the same particle tracking algorithm described in Quigley et al. (2024). A first-order Euler scheme was used to resolve advection, with bilinear interpolation of velocity fields in space to estimate the particle's velocity at any arbitrary location. We added a stochastic term to represent horizontal diffusivity and ran particle simulations 100 times, so each larva was associated with 100 advective pathways, resulting in a total of 149,700 particle trajectories both forward and backward-in-time.

Velocity product

We used geostrophic velocities to force the Lagrangian particle tracking, obtained from the Copernicus Marine Environment Monitoring Service (https://doi.org/10.48670/mds-00327). Daily geostrophic velocities with a wind-driven Ekman component at 15 m were used, with Ekman currents modeled using European Centre for Medium-Range Weather Forecasts ERA5 wind stress (Rio et al. 2014). This data is available at a 1/4° (~28 km) resolution.

We also performed Lagrangian particle tracking simulations forced by the California Current System Short-term State Estimation (CASE), a regional, data-assimilating model based on the Massachusetts Institute of Technology general circulation model (MITgcm; Marshall et al. 1997a,b). The model domain ranges from 28°N to 40°N and from 130°W to 114°W, with a 1/16° horizontal resolution (~7 km) and 72 vertical levels. CASE uses an iterative adjoint method to assimilate available data from Spray glider profiles, High-Resolution XBT profiles, Argo profiles, and satellite SSH and SST, with an assimilation window of three months. The CASE model is available from 2007-2023, so we used daily surface currents from 12/1/2007 - 4/1/2013 to allow direct comparison with particle trajectories forced by the satellite-derived velocities. All other details of the particle tracking simulation were kept the same, with the

exception of the horizontal diffusivity term, which was based on the spatial resolution of the velocity data. We forced only forward-in-time particle tracking with CASE velocities because the three-month trajectories of ocean velocities begin every January 1st, creating a flow field discontinuity between December 31 and January 1 (Zaba et al. 2018). Our forward-in-time trajectories all began after January 1st and ended before April 1, thus they fell within the 3-month assimilation period; conversely, our backward-in-time trajectories began in January and February and ended in December, spanning the potential discontinuity. Comparisons between the particle simulations forced by the two velocity data sources used here are available in the Supplemental Material (Supplemental Figures 3.1-3.3).

Spatial distributions of larvae

To visualize the spatial distributions of larvae, we used 2-dimensional heat maps illustrating the counts of larvae found within 0.25° x 0.25° grid cells. Sampling effort varied among years, so for our spatial analyses, we grouped particles from all years together to obtain sufficient spatial coverage of the sampling region. We quantified the relative area encompassed by particles using the "boundary" function in Matlab. We also used heat maps to visualize the spatial distributions of the mean, minimum and maximum otolith core widths of larvae. We identified the larvae that were backtracked into the CCAs and predicted final locations of those larvae after 30 days of advection. Lastly, we calculated the bottom depth of backtracked and collection locations using bathymetry from the ETOPO Global Relief Model (NOAA National Centers for Environmental Information 2022).

3.4 Results

Larval distributions

Particle backtracking showed that larvae could have come from a wide area surrounding the collection locations. Predicted parturition locations were located throughout the entire SCB (Figure 3.2a). Final locations of particles encompassed a wider area, including farther north, up to Monterey Bay; however, the greatest concentration of particles remained within the SCB (Figure 3.2c). Collection locations encompassed an area of 5.9 square degrees, while backward-in-time and forward-in-time particle distributions encompassed 10.4 square degrees and 36.1 square degrees, respectively.

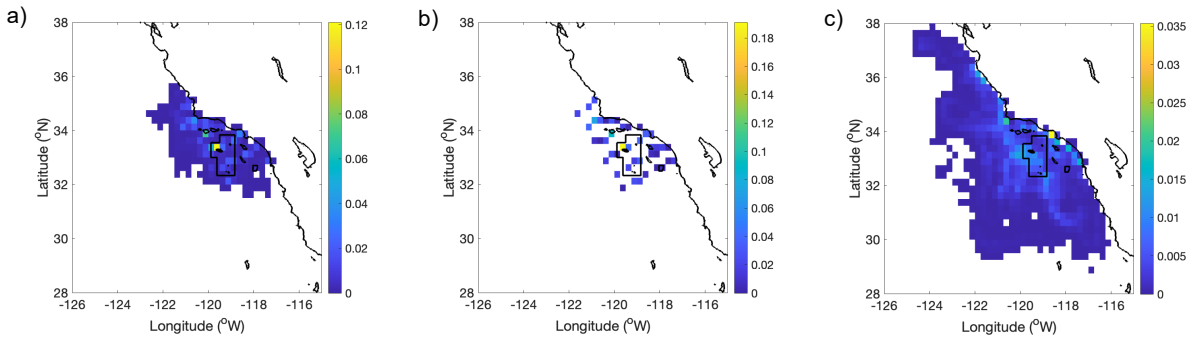

Figure 3.2: Locations of (a) backward-in-time, (b) collected, and (c) forward-in-time tracked larvae. Color corresponds to the percentage of total larvae found within each 0.25 x 0.25 grid cell. The Cowcod Conservation Areas are outlined in black.

Core width distributions

Particle backtracking revealed that offshore parturition locations had relatively high mean core widths (Figure 3.3a). The most distant offshore parturition locations in the northwest had no larvae with small core widths born there (Figure 3.3b). Parturition locations with large core widths were found throughout the region, near the Channel Islands, and in the large CCA. (Figure 3.3c). Mean otolith core width was significantly different between larvae born inside the CCAs (mean=0.34 normalized value), and larvae born outside of the CCAs (mean=0.40 normalized value; *t*-test: p=0, *t*=-61.2).

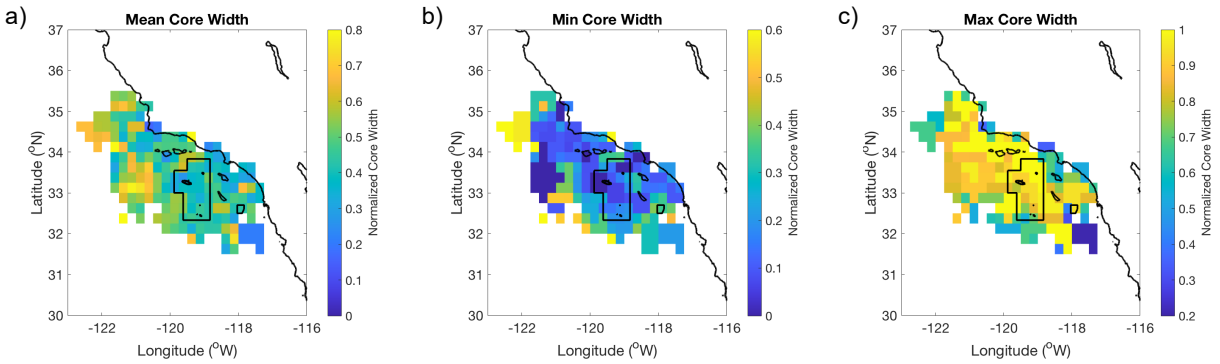

Figure 3.3: Spatial patterns of (a) mean, (b) minimum, and (c) maximum otolith core width of particles within each 0.25 x 0.25 grid cell, plotted on backward-in-time particle distributions.

Collection locations had similar mean otolith core widths throughout the region (Figure 3.4a). Particle backtracking revealed that the most distant offshore areas had no larvae with small core widths born there (Figure 3.3b), however, this finding is not apparent in the heat maps of collection locations (Figure 3.4b). Maximum otolith core widths plotted at the collection locations align with the results from the core width plotted on the parturition locations, with the largest core widths being found in the northern part of the domain, near Channel Islands and CCA (Figure 3.4c).

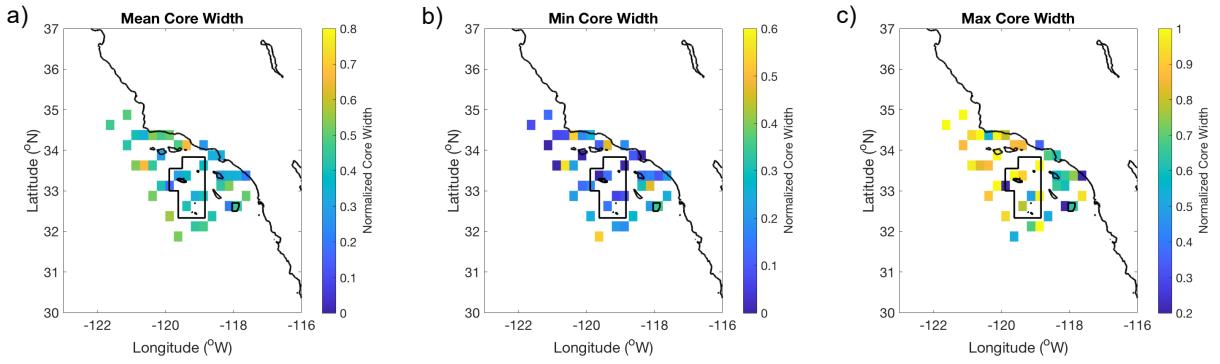

Figure 3.4: Spatial patterns of (a) mean, (b) minimum, and (c) maximum otolith core width of particles within each 0.25 x 0.25 grid cell, plotted on collection location particle distributions.

Forward-in-time particle tracking revealed spatial variability in mean otolith core width distributions (Figure 3.5a). The larvae with the largest core widths ended up in the large CCA and northwest of the CCA (Figure 3.5c). This trend is not visible in the mean core width heat map (Figure 3.5a), as larvae with particularly small core widths were also advected into the CCAs (Figure 3.5b).

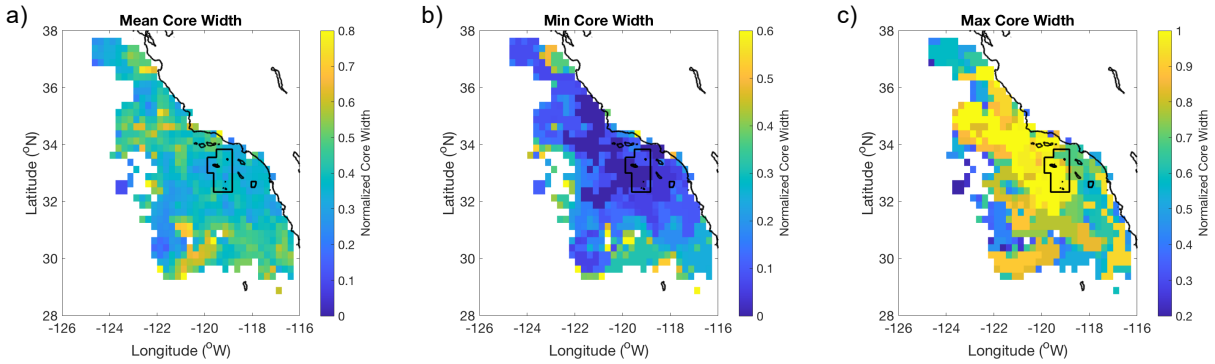

Figure 3.5: Spatial patterns of (a) mean, (b) minimum, and (c) maximum otolith core width of particles within each 0.25 x 0.25 grid cell, plotted on forward-in-time particle distributions.

Larvae that were born in the CCAs were collected at locations in an area encompassing approximately 4.0 square degrees (Figure 3.6a and 3.6b). Forward-in-time tracking showed that these larvae were advected to a wider area encompassing 15.2 square degrees after 30 days (Figure 3.6c). Of the larvae that were born in the CCAs, 24% remained in the CCAs after 30 days.

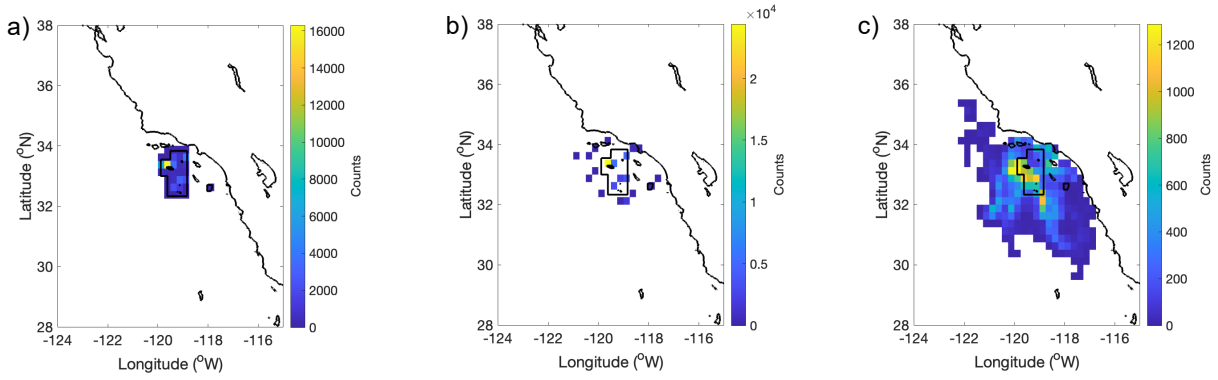

Figure 3.6: Heat maps of a) backtracked larvae located within the Cowcod Conservation Areas; b) collection locations of those larvae; c) forward-in-time locations of those larvae.

We found that 42.5% of all backward-in-time tracked larvae began life in waters shallower than 400 m (Figure 3.7). The deepest bottom depth of the collection locations was 2336 m, while the deepest backward-in-time location was 4160 m. We repeated these analyses with only one-day old larvae and with *Sebastes jordani* removed, as adults of this rockfish species are found in the midwater more often than the other demersal species (Lenarz 1980). With *Sebastes jordani* removed, we found that 46% of one-day-old larvae were backtracked to locations deeper than 400 m.

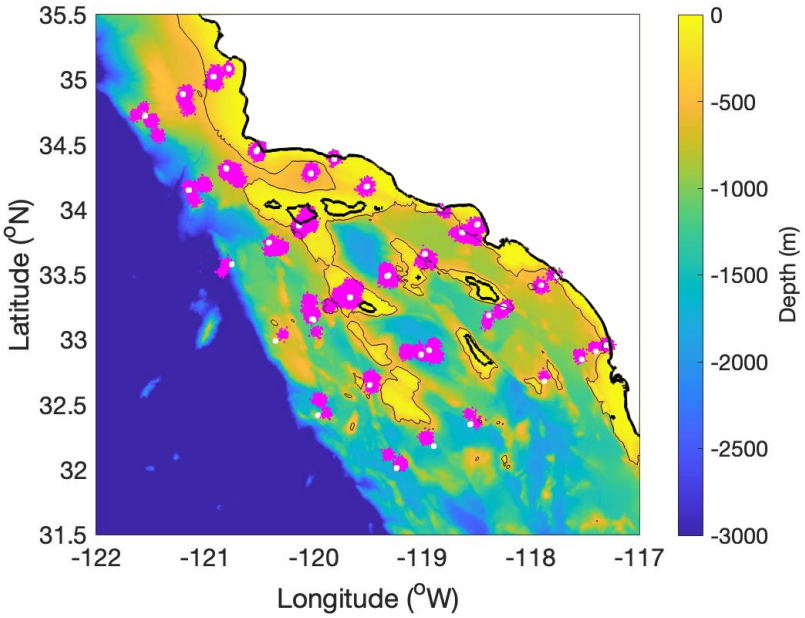

Figure 3.7: Collection locations (white dots) and estimated parturition locations (pink) of all 1 day old larvae, excluding *Sebastes jordani*. The 400 m isobath is denoted by the thin black contour line.

3.5 Discussion

Although there are myriad studies using simulated particles to track larval fish distributions (reviews by Staaterman and Paris 2013, Leis 2021), those that combine tracking with real, aged larvae are less frequent in the literature. Combining backward and forward particle tracking with larval otolith measurements provides a novel approach for understanding rockfish birth areas and dispersal patterns. The use of Lagrangian particle tracking of collected larvae has the potential to support fisheries management by providing robust predictions of spatial areas that are important for conservation and includes an element of realism not inherent to most modeling studies. Otolith data has been used in conjunction with particle tracking to effectively identify spawning locations for a number of different species, including bluefin tuna (*Thunnus thynnus*), sand lance (*Ammodytes dubius*), and round sardinella (*Sardinella aurita*)

(Hernandez et al. 2022, Suca et al. 2022, Torri et al. 2023). Combined with long-term sampling, our work applied these methods to rockfish larvae in the SCB, which is a hotspot of rockfish species richness and larval abundance (Love et al. 2002), and thus an ideal location to develop a framework to inform critical habitat for conservation and potential fishery management.

Backward-in-time trajectories

Particle backtracking revealed previously unrecognized locations where high quality larvae are produced that were not apparent from just analyzing collection locations. For example, backward-in-time simulations revealed that areas offshore Point Conception had no larvae with small core widths born there (Figure 3.3b). However, analyzing only the collection locations, and assuming the collection locations are indicative of parturition locations, this pattern of large core widths offshore is not apparent (Figure 3.4b). Fennie et al. (2024) suggested that offshore areas with high quality larvae are associated with the presence of Pacific Subarctic Upper Water (PSUW) at the depths gestating mothers occupied during the fall months prior to parturition. The California Current brings cool, fresh, PSUW equatorward; the contribution of PSUW to the inshore region of the SCB remains minimal throughout the year (Bograd et al. 2019). Our analyses support these findings: offshore parturition locations estimated through particle backtracking had high mean core widths (Figure 3.3a). Cooler, fresher waters (i.e. minty waters) such as PSUW have been shown to be associated with higher abundances of juvenile rockfish, suggesting the importance of water mass characteristics for rockfish survival (Schroeder et al. 2019).

Using backward-in-time simulations to estimate parturition locations, we identified an area 1.8 times larger than the region encompassing the collection locations. Our work suggests

that rockfish larvae are born in areas extending beyond the collection locations in all directions. Including these areas in future analyses of rockfish parturition is essential; ignoring these areas may lead to inaccurate conclusions about essential rockfish habitat.

Forward-in time trajectories

Density-independent processes such as the transport of larvae are important in determining survival and recruitment of rockfish (Ralston et al. 2013, Schroeder et al. 2019, Morales et al. 2023, Quigley et al. 2024). Forward-in-time particle tracking revealed spatial variability in the mean otolith core width of larvae after 30 days. High mean core width regions were found southwest and northwest of the large CCA, with other smaller hotspots scattered throughout the region (Figure 3.5a). This spatial heterogeneity of otolith core widths reveals the importance of ocean circulation patterns in determining larval survival. If larvae that are born in good condition (large core widths) are subsequently advected to unfavorable areas, it is unlikely that they will survive. Offshore areas may be unfavorable due to their deep bottom depth, oligotrophic characteristics, poor larval and pelagic juvenile growth potential, and unsuitable for rockfish adult habitats (Nieto et al. 2014, Morales et al. 2023, 2024). Alternatively, offshore areas associated with minty waters may facilitate higher recruitment and the production of high quality larvae (Schroeder et al. 2019, Fennie et al. 2024). Thus, there are ecological trade offs, and the extent to which advection of rockfish to offshore habitats has a negative impact on survival and subsequent recruitment remains an unanswered question.

In the spring, higher levels of PSUW driven by stronger equatorward transport of the California Current are found off Point Conception (Bograd et al. 2019, Figure 3.1). Our forward-in-time trajectories revealed areas with high mean and maximum core widths off Point

Conception. Taking into account the positive effect of minty waters on juvenile recruitment (Schroeder et al. 2019), this region off Point Conception may represent a recruitment hotspot, given the presence of PSUW in the spring and that high quality larvae are advected into the region. Spatial distributions of rockfish juvenile abundances show similarities with our estimates of transport of high quality larvae (Field et al. 2021). High juvenile abundances of *S. jordani, S. paucispinis, S. hopkinsi*, and *S. goodei* in the SCB were found off Point Conception and south, near the Channel Islands, aligning with our analyses of the transport of high quality larvae to this region (Figure 3.5c; Field et al. 2021). These results emphasize the potential for the transport of high quality larvae into this region to translate to high juvenile abundances.

Cowcod Conservation Areas

Forward-in-time particle tracking revealed that high quality larvae were advected into the large CCA (Figure 3.5c). Larvae that were born in the CCAs were advected to areas outside of the CCAs in all directions, likely making them accessible to fishing. Nearly 25% of larvae that were born in the CCAs remained in the CCAs after 30 days, but the majority were dispersed to areas outside of the MPA boundaries. This is evidence that the CCAs potentially generate recruitment subsidies to nearby regions through the dispersal of larvae. Similarly, Legrand et al. (2019) used Lagrangian modelling methods to show that larvae are exported from MPAs in the Adriatic Sea to surrounding areas, illustrating the utility of particle tracking methods for management and conservation.

Reserve size is an important factor to consider when determining MPA placement. However, defining marine reserve success is often based on two distinct foci: conservation, measured by the rebuilding of a population, and fisheries, determined by high fishing yields

(Kaplan and Botsford 2005). Botsford et al. (2001) showed that sustaining a species within a reserve requires the reserve size to be larger than the average dispersal distance of larvae. Rockfish larvae in the SCB may be transported a net distance of up to 200 km in the first 30 days of their lives (Quigley et al. 2024). The large CCA is approximately 90 km by 200 km. Based on reserve size theory, larvae born in the large CCA may disperse to areas surrounding the CCA in the cross shore direction, while larvae are more likely to remain within CCA boundaries if they are advected in the alongshore direction. Ocean currents in this region advect larvae in all directions (Figure 3.5c). The multidirectional dispersal in this region combined with the large size of the reserve relative to dispersal distances contributes to the CCA's success in both conservation and rebuilding fisheries.

Downstream effects of expanded fishing within CCAs

The entirety of the Southern California Bight is fished both recreationally and commercially for a variety of benthic and pelagic species. In the summer and fall months (June – October), the SCB's offshore waters are consistently fished by recreational anglers aboard both private and Commercial Passenger Fishing Vessels (CPFV) targeting bluefin tuna (*Thunnus orientalis*) and yellowtail (*Seriola dorsalis*). Due to the successful rebuilding of rockfish stocks earlier than originally forecasted, the Pacific Fishery Management Council repealed the CCAs in 2024 and replaced them with 8, smaller, Groundfish Exclusion Areas (50 CFR § 300,660). The remaining area was opened to bottom fishing several months of the year. Once the CCAs were opened to bottom fishing, many of the aforementioned CPFV trips targeting pelagic fishes expanded their targets to include rockfish, mainly as a secondary option if tuna are either absent or if catch limits of tuna are reached early in the trip, leaving anglers with extra time with which

to target other species. This increased exploitation is leading to the removal of many large female rockfish from areas long protected from fishing pressure.

Modeled historical catches of rockfish also reveal how geographic expansion of fishing has occurred in the SCB (Miller et al. 2014). Bellquist and Semmens (2016) showed that one consequence of enhanced fishing pressure in nearshore regions is that larger rockfish are found further from fishing ports. Keller et al. (2019) showed that a majority of rockfish species were larger in the CCA than in non-MPA locations that tended to be closer to shore. Given that larger, healthier, females contribute disproportionately to overall recruitment (Barneche et al. 2018), and that increased fishing often leads to the removal of the largest individuals from a population (Barnett et al. 2017), it is important to highlight the potential negative implications to rockfish recruitment throughout the SCB due to increased fishing pressure in waters previously protected by the CCAs. This potential for negative impacts to larval survivorship and subsequent recruitment is not unfounded, since both maternal size/condition as well as parental environmental experience during gestation drive variability in the quality of rockfish larvae (Berkeley et al. 2004b, Sogard et al. 2008, Rodgveller et al. 2012, Fennie et al. 2024).

Bathymetry of parturition and collection locations

As adults, most rockfishes are commonly demersal and remain primarily in one location (Love et al. 1990, Taylor et al. 2004). The eight rockfish species in this study occupy adult habitats on the shallow shelf, deep shelf, and slope, with depth ranges from 0-360 m (Love et al. 2002, Fennie et al. 2024). Estimates of adult habitat depths vary among species, but most of the adult rockfish in this study likely inhabit depths shallower than 400 m. The bathymetry of the SCB is complex, with steep slopes and basins that can cause the bottom depth to vary rapidly

over short distances, which allows adults to find suitable habitats throughout the region. However, we found that both our backward-in-time particle tracking locations and the collection locations place larvae at locations with waters deeper than 400 m (Figure 3.7).

Love et al. (2002) suggested that midwater and demersal rockfish species may release their larvae high in the water column. However, there has been limited work on identifying where adult rockfish actually release larvae, and thus, it remains an unanswered question. Previous work has examined the distributions of young rockfish larvae compared to adult depth habitats. Hitchman et al. (2012) found 60% of recently born larvae (mean age 0.6 days) were collected at stations within the CCA that were less than 300 m bottom depth. Similar to our work, this suggests that there are still a large proportion of young larvae that were born in areas with deeper bottom depths. Taylor et al. (2004) investigated whether 1-day old Sebastes spp. larvae were found within potential adult habitat, defined by the bottom depth associated with adult maximum depth distributions. They found associations of 1-day old larvae with their potential adult habitat for some species but not all, with some 1-day old larvae observed outside of the potential adult habitat (Taylor et al. 2004).

Our particle tracking simulations do not solve the spatial mismatch between young larval locations and adult rockfish habitat. Rather, our Lagrangian tracking simulations build on previous work in demonstrating that even when we account for the influence of ocean currents, most young larvae cannot have been born in areas with bottom depths shallower than 400 m. Indeed, we found that a majority of the youngest larvae – one-day olds – that would be advected minimally by ocean currents over the course of one day, were collected at locations with bottoms depths greater than 400 m. Even with Sebastes jordani removed and only focusing on one-day olds, we still found a significant portion of larvae predicted to be born in locations deeper than

400 m. It is possible adult rockfish inhabit deeper depths, or some species are more mobile than previously thought as some work suggests (Stanley et al. 1994, Starr et al. 2002). Alternatively, these results could suggest that the intensity of advection and diffusion in this region is significantly higher than modeled here by geostrophic and Ekman currents. Testing these hypotheses is beyond the scope of this work; however, our results warrant a more comprehensive investigation into the parturition locations of rockfish larvae, as we demonstrate that young larvae are found in deep waters, too far to have been advected to from shallower areas.

Limitations and future directions

We found differences between the spatial patterns of forward-in-time trajectories when forcing the particle tracking with CASE and Geostrophic + Ekman 15 m flow fields. The CASE model resulted in greater advection offshore: 65% of larvae were retained inshore of the 2000 m isobath using the CASE velocities, while 74% of larvae were retained using the Geostrophic + Ekman 15 m velocities. Despite differences in particle final locations, the main conclusions regarding distributions of high quality larvae remained the same (Supplemental Figure 3.3). Comparisons of the spatial distributions of otolith core widths revealed the largest larvae were advected to the Channel Islands area and north of Point Conception for both models during the years 2008-2013 (Supplemental Figure 3.3).

Our conclusions here are based on Lagrangian particle tracking simulations. Given this, it is imperative to assess how the velocity product chosen to force the simulations affects our conclusions. One limitation of the satellite-derived velocities is the spatial scale. General circulation models such as CASE can provide a finer velocity resolution, as well as resolve smaller submesoscale features. This resolution is evident in CASE particle tracking results,

where particle final locations appear in distinct patterns resembling Lagrangian coherent structures (Supplemental Figure 3.2). Ocean circulation models are often used to investigate larval transport (Petersen et al. 2010, Lilly et al. 2022). These models have proven to be useful for reproducing average ocean properties, but they can perform poorly in reproducing specific observed historical particle trajectories – the focus of this work. Modeled velocities have been shown to recreate small-scale physical features in the wrong space or time. Satellite altimetry-derived ocean currents can only be used to describe present or historical currents, while models can forecast future ocean properties (Liu et al. 2014). For simulations predicting a future position of a particle, a numerical model is a strong choice, but for recreating specific particle pathways from a known previous location and time, observation-based currents may be a more appropriate choice (Dagestad and Röhrs 2019). Strub et al. (2024) found that satellite altimeter-derived geostrophic currents contained the relevant large-scale circulation patterns necessary to realistically recreate copepod transport pathways from waters off Oregon to the SCB.

Comparisons between float trajectories and modeled and satellite-derived velocities suggest that both velocity products have a relatively low skill in predicting submerged float trajectories, and satellite-derived velocities perform nearly as well as assimilated velocity models despite the coarser resolution (Liu et al. 2014, Dagestad and Röhrs 2019). The CASE data is not available prior to 2007, so we used the available satellite-derived velocities, which represent the upper water column, and cover the entire time period of our data. Future work should be devoted to understanding the extent to which velocity data used in particle tracking simulations affect outputs, specifically for fisheries applications, including spawning and dispersal of larvae. Additionally, a greater understanding of the vertical distribution and behavior of larval rockfish in the water column would also enhance our ability to realistically model their transport and

understand their susceptibility to transport by strong surface currents (Briseño-Avena et al. 2020, Choukroun et al. 2025).

Our spatial distributions of predicted parturition locations are inherently a function of the ages and quality of the larvae that we collected. Estimated parturition locations of older larvae are associated with more uncertainty due to longer advection by particle tracking. These older larvae are also more likely to have larger core widths, as larval quality (core width) and survival (age) are positively correlated (r^2=0.22, p-value<0.001; Supplemental Figure 3.4; Fennie et al. 2024). However, we note that the largest normalized core widths in this study came from intermediate-aged larvae (Supplemental Figure 3.4). The uncertainty of estimated parturition locations of older larvae is likely to be higher than for younger larvae due to cumulative error in the particle tracking scheme. However, most of the larvae used in this study were young: fifty percent of the larvae were 1 day old, while only 10% of the larvae were 10 days or older. The potential influence of size-selective mortality should be considered when interpreting our results, especially with respect to the spatial distribution of inferred source locations of larvae in relation to larval quality. To address this potential bias, future particle tracking efforts should focus on analyzing the same range of age classes and size classes at each station throughout the region.

3.6 Conclusions

Conventional fisheries research often focuses on correlating spatially and temporally averaged environmental properties with averaged fish distributions and abundances (Bakun 2006). However, this approach limits our ability to discern the smaller-scale, shorter time scale physical-biological interactions that underlie the observations. Satellite altimetry enables us to resolve the spatial structures and temporal fluctuations of mesoscale physical dynamics and horizontal currents (Strub et al. 2024). Combining measured ichthyoplankton distributions with

Lagrangian techniques provides novel insights into birth locations and ichthyoplankton transport pathways (Diaz-Barroso et al. 2022). Through forward and backward-in-time particle tracking, we identified hotspots important to the production and dispersal of high quality larvae and illustrated the benefits of the CCAs for fisheries and conservation. We found that offshore locations were associated with the production of large sized larvae, and that large larvae were also advected into the CCAs. We illustrated how the CCAs proved a recruitment subsidy to adjacent areas accessible to fishing through the advection of larvae that were born in the CCAs. Finally, our analyses provide insight into the habitats of adult rockfish, as we showed that the majority of larvae were likely to have been born in locations previously thought to be unsuitable adult habitat. We built on previous work that demonstrated the utility of numerical simulations for resolving rockfish transport pathways (Petersen et al. 2010, Quigley et al. 2024), and work that investigated spatial distributions and biology of rockfish through collected larvae and otolith analyses (Taylor et al. 2004, Hitchman et al. 2012, Thompson et al. 2016, Thompson et al. 2017, Fennie et al. 2024). Combining these two lines of investigation enabled a more comprehensive understanding of rockfish early life histories and provided information critical for fisheries management.

3.7 Acknowledgements

This study has been conducted using E.U. Copernicus Marine Service Information; https://doi.org/10.48670/mds-00327. This publication uses results from the CASE project, operated by Scripps Institution of Oceanography and funded by the Climate Observations and Monitoring Program, National Oceanic and Atmospheric Administration, U.S. Department of Commerce. The authors thank Ganesh Gopalakrishnan for assistance with the CASE model data, and John Field for valuable feedback. The authors declare no conflicts of interest.

Chapter 3, in full, has been submitted for publication of the material as it may appear in: Quigley L. A., Franks, P. J. S., Thompson, A. R., Ben-Aderet, N., Fennie, H. W., Morales, M. M., Santora J.A., Bjorkstedt, E. P. (2025). Larval transport pathways reveal critical habitat and benefits of a marine protected area to fisheries. Fisheries Oceanography. The dissertation author was the primary investigator and author of this paper.

3.8 Supplemental Material

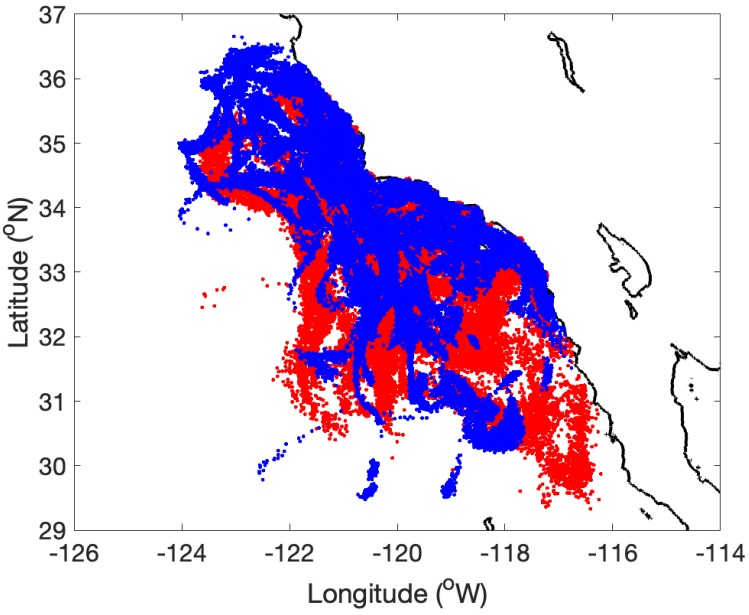

Supplemental Figure 3.1: Forward-in-time locations of particles 2008-2013 forced by CASE (blue), and Geostrophic + Ekman 15 m (red).

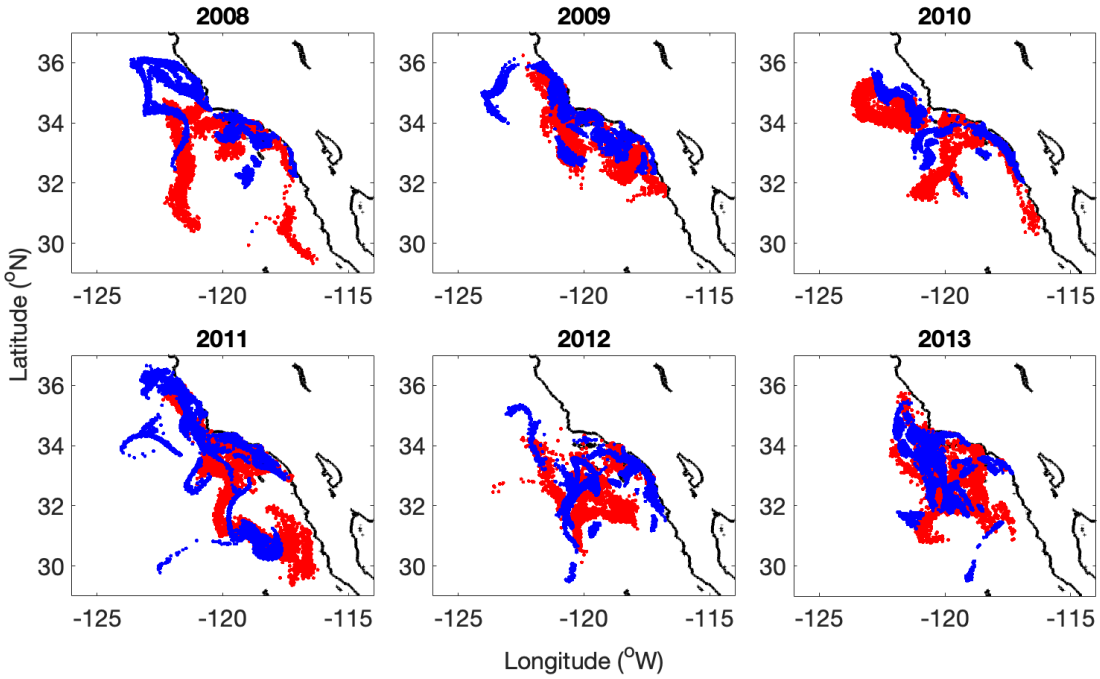

Supplemental Figure 3.2: Yearly comparisons of forward-in-time final locations of particles after 30 days. CASE (blue), Geostrophic + Ekman 15 m (red).

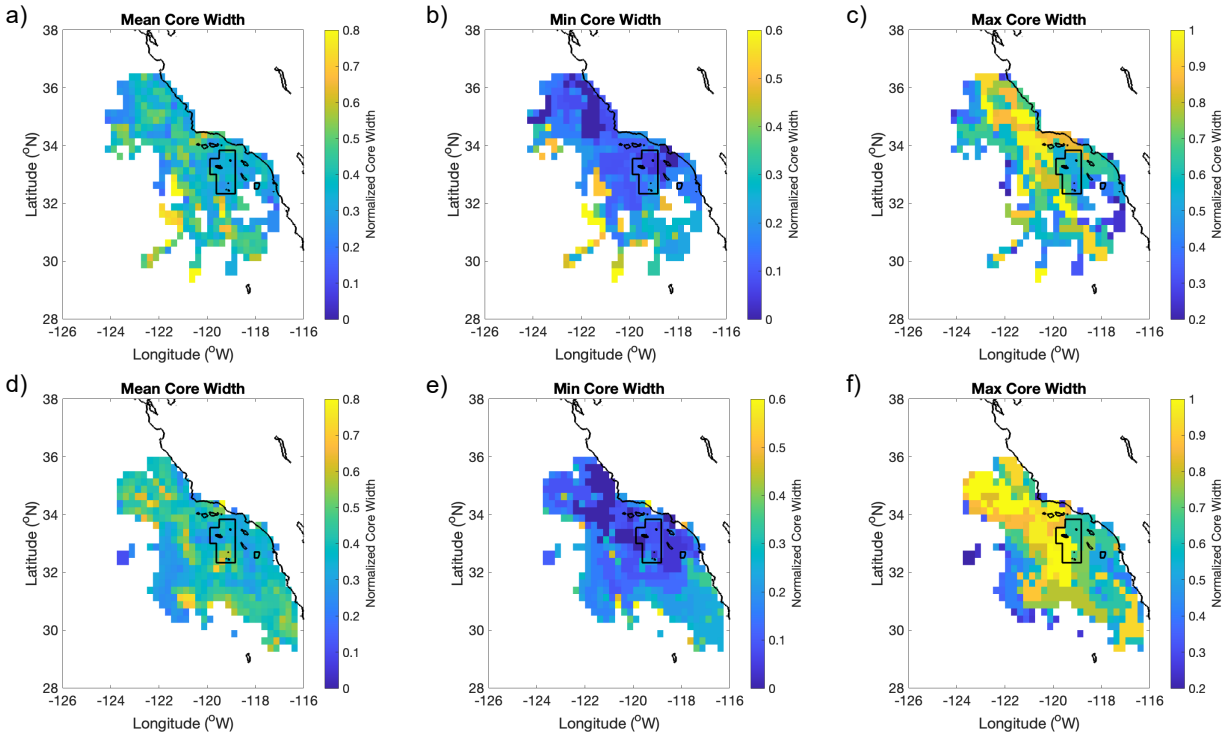

Supplemental Figure 3.3: Spatial patterns of mean, minimum, and maximum otolith core width of particles within each 0.25 x 0.25 grid cell, plotted on forward-in-time particle distributions. Particles were forced by CASE velocities (a-c) and Geostrophic + Ekman 15 m velocities (d-f).

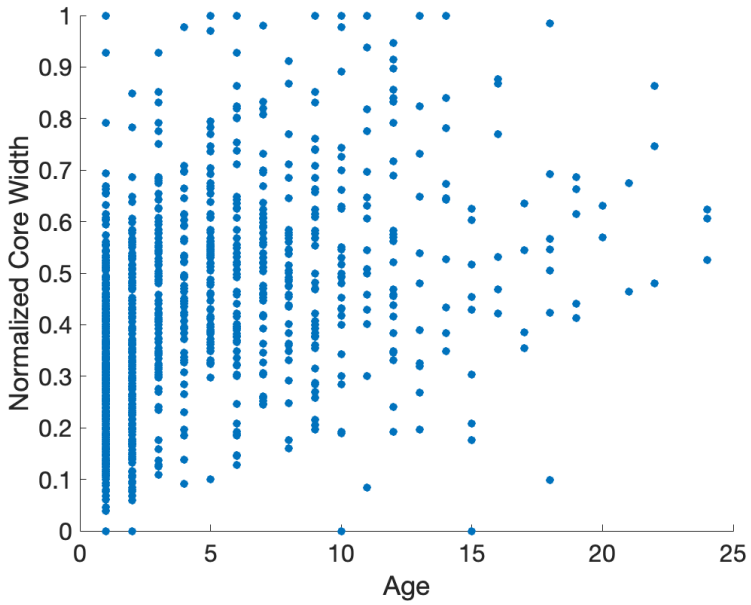

Supplemental Figure 3.4: Normalized otolith core width as a function of larval age. $R^2 = 0.22$, p-value<0.001.

CONCLUSIONS

In this dissertation, I leveraged empirical data to investigate the transport and retention of rockfish in the SCB. This work illustrates the utility of geostrophic velocities for understanding processes central to the early life stages of fishes, including identifying birth regions, quantifying dispersal, and assessing temporal fluctuations in retention.

In Chapter 1, I addressed an underlying existing question in the literature: what depths do satellite-derived geostrophic velocities represent? Comparisons between satellite-derived geostrophic velocities and high-resolution *in situ* velocities measured by gliders enabled a comprehensive understanding of the subsurface dynamics that influence altimetry-derived velocities. I demonstrated that satellite-derived geostrophic velocities are highly correlated with velocities within the upper 200 m, influenced by horizontal density gradients at the pycnocline in the CCS. These results are consistent with the theories of Ekman flow and geostrophy, but they are novel in their illustration of these dynamics and implications for research that use altimetry-derived velocities. Importantly, this work lays the foundation for the application of geostrophic velocities to assess larval transport processes in the upper 200 m of the water column, which I build on in the following two chapters.

In Chapter 2, I used satellite-derived geostrophic velocities to simulate forward-in-time trajectories of virtual particles representing rockfish larvae. In Chapter 3, I built upon these analyses further by conducting Lagrangian particle tracking both forward and backward-in-time and using biological data from *in situ* collections of rockfish larvae. In Chapter 2, yearly values of predicted larval retention in the SCB were found to be correlated with measured rockfish pelagic juvenile abundances collected later that same year. Similarly, in Chapter 3, spatial patterns of high quality larvae showed strong correspondence with mean distributions of juvenile

abundances. These results underscore the importance of physical processes in driving recruitment success and highlight the effectiveness of the Lagrangian approach. This work also illustrated the utility of numerical simulations for identifying and assessing the efficacy of conservation areas. Moving forward, these methods should be considered for analyses of optimal marine reserve design.

Assessing dispersal and connectivity of larvae is a common goal in fisheries oceanography. Most studies use high-resolution numerical models to force particle tracking schemes. Numerical models are valuable tools for predicting and reproducing mean patterns and statistics but may not reproduce specific, observed circulation features spatially or temporally. Here, I have illustrated the ability for measured altimeter-derived velocities to provide useful insight into transport processes, underscoring the utility of data-driven analyses to resolve larval dynamics. The methods I employ in this dissertation are widely applicable – geostrophic velocities are available globally, many organisms have pelagic larval stages similar to rockfish, and these analyses can be performed in any region.

As high-resolution satellite altimetry becomes available in the future, finer-scale analyses may enable a more comprehensive understanding of the influence of circulation patterns on larval transport processes. Specifically, submesoscale features that are not resolved by most satellite altimetry, may play a significant role in retention and advection of larvae. Future work should leverage high-resolution satellite altimetry and other measured velocities (e.g. High-Frequency radar) to understand dispersal patterns and to assess how different estimates of ocean velocities provide unique insight into larval transport processes.

REFERENCES

Ahlstrom, E.H. (1959). Vertical distribution of pelagic fish eggs and larvae off California and Baja California. Fish. Bull. US, 60, pp.106-146.

Amos, C. M., Castelao, R. M., and Medeiros, P. M. (2019). Offshore transport of particulate organic carbon in the California Current System by mesoscale eddies. Nature Communications, 10(1), 4940. https://doi.org/10.1038/s41467-019-12783-5

Andrews, K., Bartos, B., Harvey, C., Tonnes, D., Bhuthimethee, M., and MacCready, P. (2021). Testing the potential for larval dispersal to explain connectivity and population structure of threatened rockfish species in Puget Sound. Mar Ecol Prog Ser, 677, 95–113. https://doi.org/10.3354/meps13858

Bakun, A. (2006). Fronts and eddies as key structures in the habitat of marine fish larvae: opportunity, adaptive response and competitive advantage. Scientia Marina, 70(S2), 105–122. https://doi.org/10.3989/scimar.2006.70s2105

Barceló-Llull B., Pascual A., Sánchez-Román A,. Cutolo E., d'Ovidio F., Fifani G., Ser-Giacomi E., Ruiz S., Mason E., Cyr F., Doglioli A., Mourre B., Allen J. T., Alou-Font E., Casas B., Díaz-Barroso L., Dumas F., Gómez-Navarro L. and Muñoz C. (2021) Fine-Scale Ocean Currents Derived From in situ Observations in Anticipation of the Upcoming SWOT Altimetric Mission. Front. Mar. Sci. 8:679844. doi: 10.3389/fmars.2021.679844

Barneche, D. R., Robertson, D. R., White, C. R., Marshall, D. J. (2018). Fish reproductive-energy output increases disproportionately with body size. Science 360, 642–645. DOI: 10.1126/science.aao6868

Barnett, L. A. K., Branch, T. A., Ranasinghe, R. A., Essington, T. E. (2017). Old-growth fishes become scarce under fishing. Curr. Biol. 27, 2843–2848.e2. https://doi.org/10.1016/j.cub.2017.07.069

Batchelder, H. P. (2006). Forward-in-Time-/Backward-in-Time-Trajectory (FITT/BITT) Modeling of Particles and Organisms in the Coastal Ocean. J Atmos Ocean Technol, 23(5), 727–741. https://doi.org/10.1175/JTECH1874.1

Bellquist, L., and Semmens, B. X. (2016). Temporal and spatial dynamics of 'trophy'-sized demersal fishes off the California (USA) coast, 1966 to 2013. Marine Ecology Progress Series, 547, 1–18 https://doi.org/10.3354/meps11667

Berkeley, S. A., Chapman, C., and Sogard, S. M. (2004b). Maternal age as a determinant of larval growth and survival in a marine fish, *Sebastes melanops*. Ecology, 85(5), 1258–1264. https://doi.org/10.1890/03-0706

Berkeley, S. A., Hixon, M. A., Larson, R. J. and Love, M. S. (2004a). Fisheries sustainability via protection of age structure and spatial distribution of fish populations. Fisheries, 29(8), pp.23-32. https://doi.org/10.1577/1548-8446(2004)29[23:FSVPOA]2.0.CO;2

Beukers-Stewart B.D., Vause B.J., Mosley M.W.J., Rossetti H.L., Brand, A.R. (2005). Benefits of closed area protection for a population of scallops. Marine Ecology Progress Series. 298. 189-204. 10.3354/meps298189.

Beyer, S., Alonzo, S., and Sogard, S. (2021). Zero, one or more broods: reproductive plasticity in response to temperature, food, and body size in the live-bearing rosy rockfish *Sebastes rosaceus*. Mar Ecol Prog Ser, 669, 151–173. https://doi.org/10.3354/meps13718

Bjorkstedt, E. P., Rosenfeld, L. K., Grantham, B. A., Shkedy, Y., and Roughgarden, J. (2002). Distributions of larval rockfishes Sebastes spp. across nearshore fronts in a coastal upwelling region. Marine Ecology Progress Series, 242, 215–228. https://doi.org/10.3354/MEPS242215

Blanchette, C. A., Helmuth, B., and Gaines, S. D. (2007). Spatial patterns of growth in the mussel, *Mytilus californianus*, across a major oceanographic and biogeographic boundary at Point Conception, California, USA. J Exp Mar Biol Ecol, 340(2), 126–148. https://doi.org/10.1016/J.JEMBE.2006.09.022

Bode, M., Choukroun, S., Emslie, M. J., Harrison, H. B., Leis, J. M., Mason, L. B., Srinivasan, M., Williamson, D. H., Jones, G. P. (2025). Marine reserves contribute half of the larval supply to a coral reef fishery. Sci. Adv. 11, eadv5639. DOI: 10.1126/sciadv.adt0216

Bograd, S. J., Schroeder, I. D., and Jacox, M. G. (2019). A water mass history of the Southern California current system. Geophys Res Lett, *46*(12), 6690–6698. https://doi.org/10.1029/2019GL082685

Borrione, I., Oddo, P., Russo, A., and Coelho, E. (2019). Understanding altimetry signals in the Northeastern Ligurian sea using a multi-platform approach, Deep Sea Res. Pt. I, 145, 83–96, https://doi.org/10.1016/j.dsr.2019.02.003.

Botsford L.W., Hastings A., Gaines, S.D. (2001). Dependence of sustainability on the configuration of marine reserves and larval dispersal distance. Ecology Letters, 4: 144-150. https://doi.org/10.1046/j.1461-0248.2001.00208.x

Briseño-Avena, C., Schmid, M. S., Swieca, K., Sponaugle, S., Brodeur, R. D., and Cowen, R. K. (2020). Three-dimensional cross-shelf zooplankton distributions off the Central Oregon Coast during anomalous oceanographic conditions. Progress in Oceanography, 188, 102436. https://doi.org/10.1016/j.pocean.2020.102436

Butler JL, Jacobson LD, Barnes JT, Moser HG (2003) Biology and population dynamics of cowcod (*Sebastes levis*) in the southern California Bight. Fishery Bulletin, 101(2): 260–280.

Caldeira, R. M. A., Marchesiello, P., Nezlin, N. P., DiGiacomo, P. M., McWilliams, J. C. (2005). Island wakes in the Southern California Bight. J Geophys Res 110(C11):C11012. https://doi.org/10.1029/2004JC002675

Campana, S. E., and Neilson, J. D. (1985). Microstructure of Fish Otoliths. Canadian Journal of Fisheries and Aquatic Sciences, 42(5), 1014–1032. https://doi.org/10.1139/f85-127

Caselle, J. E., Hamilton, S. L., and Warner, R. R. (2003). The Interaction of Retention, Recruitment, and Density-Dependent Mortality in the Spatial Placement of Marine Reserves. Gulf Caribb Res, 14. https://doi.org/10.18785/gcr.1402.08

Caselle, J. E., Kinlan, B. P. and Warner, R. R. (2010). Temporal and spatial scales of influence on nearshore fish settlement in the Southern California Bight. Bull Mar Sci, 86(2), pp. 355-385.

Castelao, R. M., Oliver, H., and Medeiros, P. M. (2023). Satellite-Derived Lagrangian Transport Pathways in the Labrador Sea. Remote Sensing, 15(23), 5545. https://doi.org/10.3390/rs15235545

Chabert, P., d'Ovidio, F., Echevin, V., Stukel, M. R., and Ohman, M. D. (2021). Cross-Shore Flow and Implications for Carbon Export in the California Current Ecosystem: A Lagrangian Analysis. Journal of Geophysical Research: Oceans, 126(2). https://doi.org/10.1029/2020JC016611

Chavanne, C. P., and Klein, P. (2010). Can oceanic submesoscale processes be observed with satellite altimetry? Geophys. Res. Lett., 37, L22602, doi:10.1029/2010GL045057.

Checkley, D. M., and Barth, J. A. (2009). Patterns and processes in the California Current System. Progress in Oceanography 83:49-64. https://doi.org/10.1016/j.pocean.2009.07.028

Chelton, D. B., Schlax, M. G., and Samelson, R. M. (2007). Summertime coupling between sea surface temperature and wind stress in the California current system. J Phys Oceanogr, 37(3), 495–517. https://doi.org/10.1175/JPO3025.1

Chenillat, F., Franks, P. J. S., Rivière, P., Capet, X., Grima, N., and Blanke, B. (2015). Plankton dynamics in a cyclonic eddy in the Southern California Current System. Journal of Geophysical Research: Oceans, 120(8), 5566–5588. https://doi.org/10.1002/2015JC010826

Chereskin, T. K. (1995). Direct evidence for an Ekman balance in the California Current, J. Geophys. Res., 100(C9), 18261–18269, doi:10.1029/95JC02182.

Choukroun, S., Stewart, O. B., Mason, L. B., and Bode, M. (2025). Larval dispersal predictions are highly sensitive to hydrodynamic modelling choices. Coral Reefs, 44(1), 1-13. https://doi.org/10.1007/s00338-024-02563-z

Cowen, R. K. and Sponaugle, S. (2009). Larval Dispersal and Marine Population Connectivity. Annual Review of Marine Science 1:443-466. https://doi.org/10.1146/annurev.marine.010908.163757

Cowen, R. K., Gawarkiewicz, G., Pineda, J., Thorrold, S. R., and Werner, F. E. (2007). Population connectivity in marine systems an overview. Oceanography 20:14-21. https://doi.org/10.5670/oceanog.2007.26

Cury, P., and Roy, C. (1989). Optimal Environmental Window and Pelagic Fish Recruitment Success in Upwelling Areas. Can J Fish Aquat Sci, 46(4), 670–680. https://doi.org/10.1139/f89-086

D'Aloia, C. C., Bogdanowicz, S. M., Francis, R. K., Majoris, J. E., Harrison, R. G. and Buston, P. M. (2015). Patterns, causes, and consequences of marine larval dispersal. Proceedings of the National Academy of Sciences 112:13940-13945. https://doi.org/10.1073/pnas.1513754112

d'Ovidio, F., De Monte, S., Alvain, S., Dandonneau, Y., and Lévy, M. (2010). Fluid dynamical niches of phytoplankton types, Proc. Natl. Acad. Sci. U.S.A. 107 (43) 18366-18370, https://doi.org/10.1073/pnas.1004620107

Dagestad, K. F., and Röhrs, J. (2019). Prediction of ocean surface trajectories using satellite derived vs. modeled ocean currents. Remote sensing of environment, 223, 130-142. https://doi.org/10.1016/j.rse.2019.01.001

Dauhajre, D. P., McWilliams, J. C., and Renault, L. (2019). Nearshore Lagrangian Connectivity: Submesoscale Influence and Resolution Sensitivity. Journal of Geophysical Research: Oceans, 124(7), 5180–5204. https://doi.org/10.1029/2019JC014943

Della Penna, A., De Monte, S., Kestenare, E. Guinet, C., d'Ovidio, F. (2015). Quasi-planktonic behavior of foraging top marine predators. Sci Rep 5, 18063. https://doi.org/10.1038/srep18063

Department of Commerce (2023) Magnuson-Stevens Act Provisions; Fisheries Off West Coast States; Pacific Coast Groundfish Fishery; Pacific Coast Groundfish Fishery Management Plan; Amendment 32; Modifications to Non-Trawl Sector Area Management Measures. Federal Register 88:83830-83860

Desbruyères, D., Chafik, L. and Maze, G. (2021). A shift in the ocean circulation has warmed the subpolar North Atlantic Ocean since 2016. Commun Earth Environ 2, 48. https://doi.org/10.1038/s43247-021-00120-y

Díaz-Barroso, L., Hernández-Carrasco, I., Orfila, A., Reglero P., Balbín, R., Hidalgo, M., Tintoré, J., Alemany, F., and Alvarez-Berastegui, D. (2022). Singularities of surface mixing activity in the Western Mediterranean influence bluefin tuna larval habitats. Marine Ecology Progress Series, 685, 69–84. https://doi.org/10.3354/meps13979

Dick, E. J., and He, X. (2019). Status of Cowcod (*Sebastes levis*). Pacific Fishery Management Council, Portland, OR.

Doglioni, F., Ricker, R., Rabe, B., Barth, A., Troupin, C., and Kanzow, T. (2023). Sea surface height anomaly and geostrophic current velocity from altimetry measurements over the Arctic Ocean (2011–2020), Earth Syst. Sci. Data, 15, 225–263, https://doi.org/10.5194/essd-15-225-2023.

Dong, C., Idica, E. Y., McWilliams, J. C. (2009) Circulation and multiple-scale variability in the Southern California Bight. Prog Oceanogr 82(3):168–190. https://doi.org/10.1016/j.pocean.2009.07.005

Dong, H., Zhou, M., Hu, Z., Zhang, Z., Zhong, Y., Basedow, S. L., and Smith, W. O. (2021). Transport Barriers and the Retention of *Calanus finmarchicus* on the Lofoten Shelf in Early

Spring. Journal of Geophysical Research: Oceans, 126(8), e2021JC017408. https://doi.org/10.1029/2021JC017408

Fennie, H. W., Ben-Aderet, N., Bograd, S. J., Kwan, G. T., Santora, J. A., Schroeder, I. D., and Thompson, A. R. (2024). Momma's larvae: Maternal oceanographic experience and larval size influence early survival of rockfishes. Fisheries Oceanography, 33(2), e12658. https://doi.org/10.1111/fog.12658

Fiedler, P. C. (1986). Offshore entrainment of anchovy spawning habitat, eggs, and larvae by a displaced eddy in 1985. California Cooperative Oceanic Fisheries Investigation Reports, 27, pp. 144-152.

Field J. C., MacCall A. D., Ralston S., Love M. S., Miller E. F. (2010) Bocaccionomics:the effectiveness of pre-recruit indices for assessment and management of bocaccio. Calif Coop Ocean Fish Invest Rep 51: 77−90

Field, J. C., Miller, R. R., Santora, J. A., Tolimieri, N., Haltuch, M. A., Brodeur, R. D., Auth, T. D., Dick, E. J., Monk, M. H., Sakuma, K. M., and Wells, B. K. (2021). Spatiotemporal patterns of variability in the abundance and distribution of winter-spawned pelagic juvenile rockfish in the California Current. PLOS ONE, 16(5), e0251638. https://doi.org/10.1371/journal.pone.0251638

Fisher, R., D. R. Bellwood, and S. D. Job. (2000). Development of swimming abilities in reef fish larvae. Marine Ecology Progress Series 202:163-173.

Freeman, J., Semmens, B., and Thompson, A. (2022). Impacts of marine protected areas and the environment on larval rockfish species richness and assemblage structure in the Southern California Bight. Mar Ecol Prog Ser, 698, 125–137. https://doi.org/10.3354/meps14161

Furey, H. H., Foukal, N. P., Anderson, A., and Bower, A. S. (2023). Investigation of the Source of Iceland Basin Freshening: Virtual Particle Tracking with Satellite-Derived Geostrophic Surface Velocities. Remote Sensing, 15(24), 5711. https://doi.org/10.3390/rs15245711

Gangrade, S., and Franks, P. J. S. (2023). Phytoplankton patches at oceanic fronts are linked to coastal upwelling pulses: Observations and implications in the California Current System. Journal of Geophysical Research: Oceans, 128, e2022JC019095. https://doi.org/10.1029/2022JC019095

Gaspar, P., Georges, J. Y., Fossette, S., Lenoble, A., Ferraroli, S., and Le Maho, Y. (2006). Marine animal behaviour: neglecting ocean currents can lead us up the wrong track. Proceedings. Biological sciences, 273(1602), 2697–2702. https://doi.org/10.1098/rspb.2006.3623

Gaylord, B., and Gaines, S. D. (2000). Temperature or Transport? Range Limits in Marine Species Mediated Solely by Flow. The American Naturalist, 155(6), 769–789. https://doi.org/10.1086/303357

Giddings, A., Franks, P. J. S., and Baumann-Pickering, S. (2022). Monthly to Decadal Variability of Mesoscale Stirring in the California Current System: Links to Upwelling, Climate

Forcing, and Chlorophyll Transport. Journal of Geophysical Research: Oceans, 127(6). https://doi.org/10.1029/2021JC018180

Gottscho, A. D. (2016). Zoogeography of the San Andreas Fault system: Great Pacific Fracture Zones correspond with spatially concordant phylogeographic boundaries in western North America. Biological Reviews, 91(1), 235–254. https://doi.org/10.1111/brv.12167

Hare, J. A. (2014). The future of fisheries oceanography lies in the pursuit of multiple hypotheses. ICES J Mar Sci, *71*(8), 2343–2356. https://doi.org/10.1093/icesjms/fsu018

Hart-Davis, M. G., Backeberg, B. C., Halo, I., van Sebille, E., and Johannessen, J. A. (2018). Assessing the accuracy of satellite derived ocean currents by comparing observed and virtual buoys in the greater Agulhas region. Remote Sensing of Environment, 216, 735–746.

Hernández, C. M., Richardson, D. E., Rypina, I. I., Chen, K., Marancik, K. E., Shulzitski, K., and Llopiz, J. K. (2022). Support for the Slope Sea as a major spawning ground for Atlantic bluefin tuna: evidence from larval abundance, growth rates, and particle-tracking simulations. Canadian Journal of Fisheries and Aquatic Sciences, 79(5), 814-824. https://doi.org/10.1139/cjfas-2020-0444

Hersbach, H., Bell, B., Berrisford, P., Biavati, G., Horányi, A., Muñoz Sabater, J., Nicolas, J., Peubey, C., Radu, R., Rozum, I., Schepers, D., Simmons, A., Soci, C., Dee, D., Thépaut, J-N. (2023). ERA5 monthly averaged data on pressure levels from 1940 to present. Copernicus Climate Change Service (C3S) Climate Data Store (CDS), DOI: 10.24381/cds.6860a573. Accessed on October 5, 2023.

Hickey, B. M. (1979). The California current system—hypotheses and facts. Prog Oceanogr, 8(4), 191–279. https://doi.org/10.1016/0079-6611(79)90002-8

Hitchman, S. M., Reyns, N. B., and Thompson, A. R. (2012). Larvae define spawning habitat of bocaccio rockfish *Sebastes paucispinis* within and around a large southern California marine reserve. Mar Ecol Prog Ser, 465, 227–242. https://doi.org/10.3354/MEPS09926

Hjort, J. (1914). Fluctuations in the great fisheries of northern Europe viewed in the light of biological research. *Conseil Permanent International pour l'Exploration de la Mer*, 20: 1–228.

Hjort, J. (1926). Fluctuations in the year classes of important food fishes. *Journal Du Conseil International Pour l'Exploration de La Mer*, *1*(1), 5–38.

Holder, A. M., and Field, J. C. (2019). An exploration of factors that relate to the occurrence of multiple brooding in rockfishes (*Sebastes spp.*). Fishery Bulletin, 117(3), 56–64. https://doi.org/10.7755/FB.117.3.5

Houde, E. D. (2008). Emerging from Hjort's Shadow. J Northw Atl Fish Sci, 41, 53–70. https://doi.org/10.2960/J.v41.m634

Houde, E.D. (1987) Fish Early Life Dynamics Recruitment Variability. American Fisheries Society Symposium, 2, 17-29.

Johnson, D. W. (2006). Predation, habitat complexity, and variation in density-dependent mortality of temperate reef fishes. Ecology, 87(5), pp.1179-1188.

Kaplan, D. M. and Botsford, L. W. (2005). Effects of variability in spacing of coastal marine reserves on fisheries yield and sustainability. Canadian Journal of Fisheries and Aquatic Sciences. 62(4): 905-912. https://doi.org/10.1139/f04-243

Kara, A. B., Rochford, P. A., and Hurlburt, H. E. (2000). An optimal definition for ocean mixed layer depth, J. Geophys. Res., 105(C7), 16803–16821, doi:10.1029/2000JC900072.

Kashef, N. S., Sogard, S. M., Fisher, R., and Largier, J. L. (2014). Ontogeny of critical swimming speeds for larval and pelagic juvenile rockfishes (*Sebastes* spp., family Scorpaenidae). Marine Ecology Progress Series, 500, 231–243. https://doi.org/10.3354/MEPS10669

Kataoka, T., Hinata, H., and Nihei, Y. (2013). Numerical estimation of inflow flux of floating natural macro-debris into Tokyo Bay. Estuar Coast Shelf Sci, 134, 69–79. https://doi.org/10.1016/J.ECSS.2013.09.005

Keller, A. A., Harms, J. H., Wallace, J. R., Jones, C., Benante, J. A., and Chappell, A. (2019). Changes in long-lived rockfishes after more than a decade of protection within California's largest marine reserve. Marine Ecology Progress Series, 623, 175–193. https://doi.org/10.3354/meps13019

Kosempa, M., and Chambers, D. P. (2014). Southern Ocean velocity and geostrophic transport fields estimated by combining Jason altimetry and Argo data. Journal of Geophysical Research: Oceans, 119(8), 4761–4776. https://doi.org/10.1002/2014JC009853

Laidig, T. E., Ralston, S., and Bence, J. R. (1991). Dynamics of Growth in the Early Life History of Shortbelly Rockfish *Sebastes jordani*. Fishery Bulletin, US, 89, 611–621.

Lefebvre, L. S., Beyer, S. G., Stafford, D. M., Kashef, N. S., Dick, E. J., Sogard, S. M., and Field, J. C. (2018). Double or nothing: Plasticity in reproductive output in the chilipepper rockfish (*Sebastes goodei*). Fish Res, 204, 258–268. https://doi.org/10.1016/j.fishres.2018.03.002

Legrand, T., di Franco, A., Ser-Giacomi, E., Caló, A., and Rossi, V. (2019). A multidisciplinary analytical framework to delineate spawning areas and quantify larval dispersal in coastal fish. Marine Environmental Research, 151, 104761.https://doi.org/10.1016/J.MARENVRES.2019.104761

Leis, J. M. (2021). Perspectives on Larval Behaviour in Biophysical Modelling of Larval Dispersal in Marine, Demersal Fishes. Oceans 2:1-25. doi:10.3390/oceans2010001

Lenarz, W.H. (1980). Shortbelly rockfish, *Sebastes jordani*: A large unfished resource in waters off California. Mar. Fish. Rev. 42:34-40.

Lenarz, W.H., Larson, R.J. and Ralston, S. (1991). Depth distributions of late larvae and pelagic juveniles of some fishes of the California Current. Cal. Coop. Fish. Invest. Rpt, 32, pp.41-46.

Lenihan, H.S., Gallagher, J.P., Peters, J.R., Stier, A.S., Hofmeister, J. K. K., and Reed, D. C. (2021). Evidence that spillover from Marine Protected Areas benefits the spiny lobster (*Panulirus interruptus*) fishery in southern California. Sci Rep 11, 2663. https://doi.org/10.1038/s41598-021-82371-5

Lett, C., Roy, C., Levasseur, A., Van Der Lingen, C. D., and Mullon, C. (2006). Simulation and quantification of enrichment and retention processes in the southern Benguela upwelling ecosystem. Fish Oceanogr 15(5), 363–372. https://doi.org/10.1111/J.1365-2419.2005.00392.X

Lilly L. E., Cornuelle B. D., Ohman M. D. (2022) Using a Lagrangian particle tracking model to evaluate impacts of El Niño-related advection on euphausiids in the southern California Current System. Deep Sea Res I 187: 103835. https://doi.org/10.1016/j.dsr.2022.103835

Lin L. I. (1989). A concordance correlation coefficient to evaluate reproducibility. Biometrics, 45(1), 255–268.

Liu, Y., Weisberg, R. H., Vignudelli, S. and Mitchum, G. T. (2014) Evaluation of altimetry-derived surface current products using Lagrangian drifter trajectories in the eastern Gulf of Mexico, J. Geophys. Res. Oceans, 119, 2827–2842, doi:10.1002/2013JC009710.

Love, M. S., Morris, P., McCrae, M., and Collins, R. (1990). Life History Aspects of 19 Rockfish Species (Scorpaenidae: *Sebastes*) from the Southern California Bight. U.S. Department of Commerce. NOAA Technical Report NMFS 87: 38 pp

Love, M.S., Yoklavich, M.M., and Thorsteinson, L. (2002). The rockfishes of the Northeast Pacific. University of California Press, Berkeley, Calif.

Luschi P., Sale A., Mencacci R., Hughes G. R., Lutjeharms J. R. E. and Papi F. (2003). Current transport of leatherback sea turtles (*Dermochelys coriacea*) in the oceanProc. R. Soc. Lond. B.270S129–S132. http://doi.org/10.1098/rsbl.2003.0036

Lynn R. J. and Simpson J. J. (1987) The California Current System: The seasonal variability of its physical characteristics. Journal of Geophysical Research 92:12947-12966

Marshall, J., Adcroft, A., Hill, C., Perelman, L. and Heisey, C. (1997a): A finite-volume, incompressible Navier Stokes model for studies of the ocean on parallel computers. J. Geophys. Res., 102, 5753–5766, https://doi.org/10.1029/96JC02775.

Marshall, J., Hill, C., Perelman, L. and Adcroft, A. (1997b): Hydrostatic, quasi-hydrostatic, and nonhydrostatic ocean modeling. J. Geophys. Res., 102, 5733–5752, https://doi.org/10.1029/96JC02776.

Matsuzaki, Y., and Fujita, I. (2017). In situ estimates of horizontal turbulent diffusivity at the sea surface for oil transport simulation. Mar Pollut Bull, 117(1–2), 34–40. https://doi.org/10.1016/J.MARPOLBUL.2016.10.026

McClatchie, S. (2014). Introduction to the Fisheries and the Surveys. In: Regional Fisheries Oceanography of the California Current System. Springer, Dordrecht. https://doi.org/10.1007/978-94-007-7223-6_1

McGillicuddy, D. J. (2016). Mechanisms of Physical-Biological-Biogeochemical Interaction at the Oceanic Mesoscale. Annu. Rev. Mar. Sci. 8, 125–159.

Miller R. R., Field J. C., Santora J. A., Monk, M. H., Kosaka R., and Thomson, C. (2017). Spatial valuation of California marine fisheries as an ecosystem service. Canadian Journal of Fisheries and Aquatic Sciences. 74(11): 1732-1748. https://doi.org/10.1139/cjfas-2016-0228

Miller, R. R., Field, J. C., Santora, J. A., Schroeder, I. D., Huff, D. D., Key, M., Pearson, D. E. and MacCall, A. D. (2014). A spatially distinct history of the development of California groundfish fisheries. PLOS ONE, 9(6), p.e99758. https://doi.org/10.1371/journal.pone.0099758

Mitarai, S., Siegel, D. A., Watson, J. R., Dong, C., and McWilliams, J. C. (2009). Quantifying connectivity in the coastal ocean with application to the Southern California Bight. Journal of Geophysical Research: Oceans, 114(10), 1–21. https://doi.org/10.1029/2008JC005166

Morales-Nin, B. (2000). Review of the growth regulation processes of otolith daily increment formation. Fisheries Research, 46(1–3), 53–67. https://doi.org/10.1016/S0165-7836(00)00133-8

Morales, M. M. (2023) Physical-biological drivers of population replenishment for an ecologically important fish species of the California Current. PhD Dissertation, University of California, Santa Cruz, CA.

Morales, M. M., Fiechter, J., Field, J.C., Kashef, N.S., Hazen, E.L. and Carr, M.H. (2024). Development and application of a bioenergetics growth model for multiple early life stages of an ecologically important marine fish. Ecological Modelling, 488, p.110575. https://doi.org/10.1016/j.ecolmodel.2023.110575

Mori, M., Mizobata, K., Ichii, T., Ziegler, P., and Okuda, T. (2022). Modeling the egg and larval transport pathways of the Antarctic toothfish (*Dissostichus mawsoni*) in the East Antarctic region: New insights into successful transport connections. Fish Oceanogr, 31(1), 19–39. https://doi.org/10.1111/FOG.12560

Mork, K. A. and Skagseth, Ø. (2010). A quantitative description of the Norwegian Atlantic Current by combining altimetry and hydrography, Ocean Sci., 6, 901–911, https://doi.org/10.5194/os-6-901-2010

Morrow, R., Carret, A., Birol, F., Nino, F., Valladeau, G., Boy, F., Bachelier, C., and Zakardjian, B. (2017). Observability of fine-scale ocean dynamics in the northwestern Mediterranean Sea, Ocean Sci., 13, 13–29, https://doi.org/10.5194/os-13-13-2017

Morrow, R., Fu, L-L., Ardhuin, F., Benkiran, M., Chapron, B., Cosme, E., d'Ovidio, F., Farrar, J. T., Gille, S. T., Lapeyre, G., Le Traon, P-Y., Pascual, A., Ponte, A., Qiu, B., Rascle, N., Ubelmann, C., Wang, J., and Zaron, E. D. (2019). Global Observations of Fine-Scale Ocean

Surface Topography With the Surface Water and Ocean Topography (SWOT) Mission. Front. Mar. Sci. 6:232. doi: 10.3389/fmars.2019.00232

Moser, H. G., and Boehlert, G. W. (1991). Ecology of pelagic larvae and juveniles of the genus *Sebastes*. Environ Biol Fishes, 30(1–2), 203–224. https://doi.org/10.1007/978-94-011-3792-8_20

Nagai, T., Gruber, N., Frenzel, H., Lachkar, Z., McWilliams, J. C., and Plattner, G.-K. (2015). Dominant role of eddies and filaments in the offshore transport of carbon and nutrients in the California Current System. Journal of Geophysical Research: Oceans, 120(8), 5318–5341. https://doi.org/10.1002/2015JC010889

National Marine Fisheries Service (2024). Fisheries Economics of the United States, 2021. U.S. Dept. of Commerce, NOAA Tech. Memo. NMFS-F/SPO-247, 188 p.

Nieto, K., McClatchie, S., Weber, E. D., and Lennert-Cody, C. E. (2014). Effect of mesoscale eddies and streamers on sardine spawning habitat and recruitment success off Southern and central California. Journal of Geophysical Research: Oceans, 119(9), 6330–6339. https://doi.org/10.1002/2014JC010251

Nishimoto, M. M., Simons, R. D., and Love, M. S. (2019). Offshore oil production platforms as potential sources of larvae to coastal shelf regions off southern California. Bulletin of Marine Science, 95(4), 535–558. https://doi.org/10.5343/bms.2019.0033

Nishimoto, M., and Washburn, L. (2002). Patterns of coastal eddy circulation and abundance of pelagic juvenile fish in the Santa Barbara Channel, California, USA. Mar Ecol Prog Ser, 241, 183–199. https://doi.org/10.3354/meps241183

NOAA National Centers for Environmental Information. (2022). ETOPO 2022 30 Arc-Second Global Relief Model. NOAA National Centers for Environmental Information. DOI: 10.25921/fd45-gt74. Accessed August 7, 2023.

Ogle, D.H. (2022). RFishBC. R package version 0.2.4, https://derekogle.com/RFishBC/

Okubo, A. (1970). Horizontal dispersion of floatable particles in the vicinity of velocity singularities such as convergences. Deep Sea Research and Oceanographic Abstracts, 17(3), 445–454. https://doi.org/10.1016/0011-7471(70)90059-8

Onink, V., Wichmann, D., Delandmeter, P., and van Sebille, E. (2019). The Role of Ekman Currents, Geostrophy, and Stokes Drift in the Accumulation of Floating Microplastic. Journal of geophysical research. Oceans, 124(3), 1474–1490. https://doi.org/10.1029/2018JC014547

Owen R. (1980). Eddies of the California Current System: physical and ecological characteristics. In: Power D (ed) The California islands: proceedings of a multidisciplinary symposium. Santa Barbara Museum of Natural History, Santa Barbara, CA, p 237– 263

Pacific Fishery Management Council 2023. Pacific Coast Groundfish Fisheries Management Plan for the California, Oregon and Washington Groundfish Fishery. Pacific Fishery Management Council. Portland, Oregon, USA.

Parrish, R. H., Nelson, C. S. and Bakun, A. (1981). Transport Mechanisms and Reproductive Success of Fishes in the California Current, Biol Oceanogr, 1:2, 175-203.

Pelc, R. A., Warner, R. R., Gaines, S. D., and Paris, C. B. (2010). Detecting larval export from marine reserves. Proc Natl Acad Sci USA, *107*(43), 18266–18271. https://doi.org/10.1073/pnas.0907368107

Petersen, C. H., Drake, P. T., Edwards, C. A., and Ralston, S. (2010). A numerical study of inferred rockfish (*Sebastes spp.*) larval dispersal along the central California coast. Fish Oceanogr, 19(1), 21–41. https://doi.org/10.1111/j.1365-2419.2009.00526.x

Pickett, M. H., and Paduan, J. D. (2003). Ekman transport and pumping in the California Current based on the U.S. Navy's high-resolution atmospheric model (COAMPS), J. Geophys. Res., 108, 3327, doi:10.1029/2003JC001902, C10.

Pineda J., Hare J. A., Sponaugle S. (2007). Larval transport and dispersal in the coastal ocean and consequences for population connectivity. Oceanography 20(3):22–39

Pineda, J. (1991). Predictable Upwelling and the Shoreward Transport of Planktonic Larvae by Internal Tidal Bores. Science, 253(5019), 548–549. https://doi.org/10.1126/SCIENCE.253.5019.548

Quigley, L. A., Franks, P. J. S., Thompson, A. R., Field, J. C., Santora, J. A. (2024). Quantifying the fates and retention of larval rockfish through Lagrangian analyses. Marine Ecology Progress Series. https://doi.org/10.3354/meps14718

Raj, R.P.; Nilsen, J.E.Ø.; Johannessen, J.A.; Furevik, T.; Andersen, O.B.; Bertino, L. (2018). Quantifying Atlantic Water transport to the Nordic Seas by remote sensing. Remote Sens. Environ. 216, 758–769. https://doi.org/10.1016/j.rse.2018.04.055

Ralston, S., Sakuma, K. M., and Field, J. C. (2013). Interannual variation in pelagic juvenile rockfish (*Sebastes spp*.) abundance – going with the flow. Fish Oceanogr, 22(4), 288–308. https://doi.org/10.1111/FOG.12022

Rio, M. H., Mulet, S., and Picot, N. (2014) Beyond GOCE for the ocean circulation estimate: synergetic use of altimetry, gravimetry, and in situ data provides new insight into geostrophic and Ekman currents. Geophys Res Lett 41: 8918–8925. doi:10.1002/2014GL061773

Rodgveller, C. J., Lunsford, C. R., and Fujioka, J. T. (2012). Effects of maternal age and size on embryonic energy reserves, developmental timing, and fecundity in quillback rockfish (*Sebastes maliger).* Fishery Bulletin, 110, 36–45.

Rowe, M.D., Prendergast, S.E., Alofs, K.M., Bunnell, D.B., Rutherford, E.S. and Anderson, E.J. (2022). Predicting larval alewife transport in Lake Michigan using hydrodynamic and Lagrangian particle dispersion models. Limnol Oceanogr, 67: 2042-2058. https://doi.org/10.1002/lno.12186

Rudnick, D. (2016). California Underwater Glider Network [Data set]. Scripps Institution of Oceanography, Instrument Development Group. doi: 10.21238/S8SPRAY1618

Rudnick, D. L., and Cole, S. T. (2011). On sampling the ocean using underwater gliders, J. Geophys. Res., 116, C08010, doi:10.1029/2010JC006849.

Rudnick, D. L., Zaba, K. D., Todd, R. E., and Davis, R. E. (2017a). A climatology of the California current system from a network of underwater gliders. Prog. Oceanogr. 154, 64–106. doi: 10.1016/j.pocean.2017.03.002

Rudnick, D. L., Zaba, K. D., Todd, R. E., and Davis, R. E. (2017b). A climatology using data from the California Underwater Glider Network - Dataset [Downloaded 05-11-25]. Scripps Institution of Oceanography, Instrument Development Group. doi: 10.21238/S8SPRAY7292

Sakuma, K.M., Ralston, S. and Roberts, D.A. (1999). Diel vertical distribution of postflexion larval *Citharichthys* spp. and *Sebastes* spp. off central California. Fisheries Oceanography, 8, 68-76.

Sale, P.F., Cowen, R. K., Danilowicz, B. S., Jones, G. P., Kritzer, J. P., Lindeman, K. C., Planes, S., Polunin, N. V.C., Russ, G. R., Sadovy, Y. J., and Steneck, R. S. (2005) Critical science gaps impede use of no-take fishery reserves. Trends Ecol Evol 20:74–80. https://doi.org/10.1016/j.tree.2004.11.007

Santora, J. A., Rogers, T. L., Cimino, M. A., Sakuma, K. M., Hanson, K. D., Dick, E. J., Jahncke, J., Warzybok, P., and Field, J. C. (2021). Diverse integrated ecosystem approach overcomes pandemic-related fisheries monitoring challenges. Nat Commun, 12(1), 6492. https://doi.org/10.1038/s41467-021-26484-5

Schonfeld, A., Gasbarro, R. P., Cimino, M. A., Field, J. C., Bograd, S. J., Hazen, E. L., Santora, J. A. (2025). Water column structure influences variability of micronekton distribution and biodiversity in the California Current. Manuscript submitted for publication

Schroeder, I. D., Santora, J. A., Bograd, S. J., Hazen, E. L., Sakuma, K. M., Moore, A. M., Edwards, C. A., Wells, B. K., and Field, J. C. (2019). Source water variability as a driver of rockfish recruitment in the California Current Ecosystem: implications for climate change and fisheries management. Can J Fish Aquat Sci, 76(6), 950–960. https://doi.org/10.1139/cjfas-2017-0480

Shen, S. G., Thompson, A. R., Correa, J., Fietzek, P., Ayón, P. and Checkley, D. M. (2017). Spatial patterns of Anchoveta (*Engraulis ringens*) eggs and larvae in relation to $p\,CO_2$ in the Peruvian upwelling system. Proc R Soc B, *284*(1855), 20170509. https://doi.org/10.1098/rspb.2017.0509

Sherman, J., Davis, R. E., Owens, W. B., and Valdes, J. (2001). The autonomous underwater glider “Spray,”, IEEE J. Oceanic Eng., 26, 437–446, doi:10.1109/48.972076.

Sinha, A., Balwada, D., Tarshish, N., and Abernathey, R. (2019). Modulation of Lateral Transport by Submesoscale Flows and Inertia-Gravity Waves. Journal of Advances in Modeling Earth Systems, 11(4), 1039–1065. https://doi.org/10.1029/2018MS001508

Sogard, S. M., Berkeley, S. A., and Fisher, R. (2008). Maternal effects in rockfishes *Sebastes* spp.: A comparison among species. Marine Ecology Progress Series, 360, 227–236. https://doi.org/10.3354/meps07468

Staaterman, E., and Paris, C. B. (2013). Modelling larval fish navigation: the way forward. ICES Journal of Marine Science 71:918-924. 10.1093/icesjms/fst103

Stachura, M.M., Essington, T.E., Mantua, N.J., Hollowed, A.B., Haltuch, M.A., Spencer, P.D., Branch, T.A. and Doyle, M.J. (2014), Linking Northeast Pacific recruitment synchrony to environmental variability. Fish Oceanogr, 23: 389-408. https://doi.org/10.1111/fog.12066

Stanley, R.D., Leaman, B. M., Haldorson, L., O'Connell, V. M. (1994). Movements of tagged adult yellowtail rockfish, *Sebaste flavidus*, off the west coast of North Americas. Fishery Bulletin, 92(3), pp.655-663.

Starr, R.M., Heine, J.N., Felton, J.M. and Cailliet, G.M. (2002). Movements of bocaccio (*Sebastes paucispinis*) and greenspotted (*S. chlorostictus*) rockfishes in a Monterey submarine canyon: implications for the design of marine reserves. Fishery Bulletin, 100(2), pp.324-3

Stockhausen W. T., and Hermann A. J. (2007) Modeling larval dispersion of rockfish: a tool for marine reserve design? In: Heifetz J, DiCosimo J, Gharrett AJ, Love MS, O'Connell T, Stanley R (eds) Biology, assessment, and management of North Pacific rockfishes. Alaska Sea Grant College Program AK-SG-07-01. University of Alaska, Fairbanks, AK, p 251–273

Strub, P. T., James, C., Fisher, J. L., Fewings, M. R., Zeman, S. M., Combes, V., Garwood, J. C., Bolm, A. E., Scherer, A. (2024). Altimeter-derived poleward Lagrangian pathways in the California Current system: Part 1. Progress in Oceanography, 229, 103353. https://doi.org/10.1016/j.pocean.2024.103353

Suca, J. J., Ji, R., Baumann, H., Pham, K., Silva, T. L., Wiley, D. N., Feng, Z., Llopiz, J. K. (2022). Larval transport pathways from three prominent sand lance habitats in the Gulf of Maine. Fisheries Oceanography, 31(3), 333–352. https://doi.org/10.1111/fog.12580

Sudre, J., Morrow, R.A. (2008). Global surface currents: a high-resolution product for investigating ocean dynamics. Ocean Dynamics 58, 101–118. https://doi.org/10.1007/s10236-008-0134-9

Swalethorp, R., Landry, M.R., Semmens, B.X., Ohman, M.D., Aluwihare, L., Chargualaf, D. and Thompson, A.R. (2023) Anchovy boom and bust linked to trophic shifts in larval diet. Nature Communications, 14, 7412.

Taylor C. A., Watson W., Chereskin T., Hyde J., Vetter R. (2004) Retention of larval rockfishes, Sebastes, near natal habitat in the Southern California Bight, as indicated by molecular

identification methods. California Cooperative Oceanic Fisheries Investigations Reports 45: 152-166.

Thompson, A. R., Chen, D. C., Guo, L. W., Hyde, J. R., and Watson, W. (2017). Larval abundances of rockfishes that were historically targeted by fishing increased over 16 years in association with a large marine protected area. Royal Society Open Science, 4(9). https://doi.org/10.1098/RSOS.170639

Thompson, A. R., Hyde, J. R., Watson, W., Chen, D. C., and Guo, L. W. (2016). Rockfish assemblage structure and spawning locations in southern California identified through larval sampling. Mar Ecol Prog Ser, 547, 177–192. https://doi.org/10.3354/MEPS11633

Todd, R. E., Rudnick, D. L., Mazloff, M. R., Davis, R. E., and Cornuelle, B. D. (2011). Poleward flows in the southern California Current System: Glider observations and numerical simulation, J. Geophys. Res., 116, C02026, doi:10.1029/2010JC006536.

Todd, R. E., Rudnick, D. L., Sherman, J. T., Owens, W. B., and George, L. (2017). Absolute velocity estimates from autonomous underwater gliders equipped with Doppler current profilers. Journal of Atmospheric and Oceanic Technology, 34, 309-333, doi: 10.1175/JTECH-D-16-0156.1.

Torri, M., Russo, S., Falcini, F., De Luca, B., Colella, S., Volpe, G., Corrado, R., Placenti, F., Giaramita, L., Musco, M., Masullo, T., Bennici, C., Di Natale, M. V., Patti, B., Lacorata, G., Arculeo, M., and Cuttitta, A. (2023) Coupling Lagrangian simulation models and remote sensing to explore the environmental effect on larval growth rate: The Mediterranean case study of round sardinella (*Sardinella aurita*) early life stages. Front. Mar. Sci. 9:1065514. doi: 10.3389/fmars.2022.1065514

Vinogradova, N. T., Ponte, R. M., and Stammer, D. (2007). Relation between sea level and bottom pressure and the vertical dependence of oceanic variability. Geophysical Research Letters, 34(3). https://doi.org/10.1029/2006gl028588

Walker, N., Pilley, C., Raghunathan, V., D'Sa, E., Leben, R., Hoffmann, N., Brickley, P., Coholan, P., Sharma, N., Graber, H., and Turner, R. (2011). Impacts of loop current frontal cyclonic eddies and wind forcing on the 2010 Gulf of Mexico oil spill. In monitoring and modeling the deepwater horizon oil spill: A record-breaking enterprise. American Geophysical Union, 195, 103–116. 10.1029/2011GM001120

Wells, B. K., Schroeder, I. D., Bograd, S. J., Hazen, E. L., Jacox, M. G., Leising, A., Mantua, N., Santora, J. A., Fisher, J., Peterson, W. T., Bjorkstedt, E., Robertson, R. R., Chavez, F. P., Goericke, R., Kudela, R., Anderson, C., Lavaniegos, B. E., Gomez-Valdes, J., Brodeur, R. D., Daly, E. A., Morgan, C. A., Auth, T. D., Field, J. C., Sakuma, K., McClatchie, S., Thomspon, A. R., Weber, E. D., Watson, W., Suryan, R. M., Parrish, J., Dolliver, J., Loredo, S., Porquez, J M., Zamon, J. E., Schneider, S. R., Golightly, R. T., Warzybok, P., Bradley, R., Jahncke, J., Sydeman, W., Melin, S. R., Hildebrand, J. A., Debich, A. J., Thayre, B. (2017). State of the California current 2016-2017: still anything but “Normal” in the North. Calif Cooperat Ocean Fish Investig Rep. 58, 1–55.

White, J. W., Schroeger, J., Drake, P. T., and Edwards, C. A. (2014). The Value of Larval Connectivity Information in the Static Optimization of Marine Reserve Design. Conserv Lett, 7(6), 533–544. https://doi.org/10.1111/conl.12097

Woodbury, D., and Ralston, S. (1991). Interannual variation in growth-rates and back-calculated birthdate distributions of pelagic juvenile rockfishes (Sebastes spp.) of the central California coast. Fishery Bulletin 89:523–533.

Wunsch, C. (1997). The Vertical Partition of Oceanic Horizontal Kinetic Energy. Journal of Physical Oceanography, 27(8), 1770-1794. https://doi.org/10.1175/1520-0485(1997)027<1770:TVPOOH>2.0.CO;2

Wunsch, C., and Gaposchkin, E. M. (1980). On using satellite altimetry to determine the general circulation of the oceans with application to geoid improvement, Rev. Geophys., 18(4), 725–745.

Zaba K. D., Franks P. J. S., and Ohman M. D. (2021) The California undercurrent as a source of upwelled waters in a coastal filament. J Geophys Res Oceans 126:e2020JC016602. https://doi.org/10.1029/2020JC016602

Zaba, K. D., Rudnick, D. L., Cornuelle, B. D., Gopalakrishnan, G., and Mazloff, M. R. (2018). Annual and Interannual Variability in the California Current System: Comparison of an Ocean State Estimate with a Network of Underwater Gliders. Journal of Physical Oceanography, 48(12), 2965-2988. https://doi.org/10.1175/JPO-D-18-0037.1